Norwegian Univeristy of Science and Technology
Faculty of Information Technology and Electrical Engineering
Department of Mathematical Sciences

and

University of Pavia
Department of Mathematics

ANALYTICAL AND NUMERICAL BIFURCATION METHODS FOR NONLOCAL WAVE EQUATIONS

PhD Thesis

Filippo Remonato

Supervisor at NTNU: Prof. Mats Ehrnström
Supervisor at UniPV: Prof. Giancarlo Sangalli

Alla nonna Angelica

Acknowledgements

I get by with a little help from
my friends.

Helge Holden,
Tools from the Toolbox
(Original text by the Beatles)

Be it with important mathematical knowledge, a creative solution to a problem, or simply sharing a laugh, a number of people have helped me in the course of the doctoral studies. It is my pleasure to acknowledge here these many contributions.

First and foremost, the expert guidance of my two supervisors, Prof. Mats Ehrnström and Prof. Giancarlo Sangalli, has been paramount. I owe a profound debt of gratitude to Mats, who gave me a position when I did not have one, investing in the training and scientific growth of a student who was not even specialised in his field. His door has always been open, and the possibility to leverage my research through his vast expertise in several fields of Mathematics has been invaluable. Giancarlo's extensive numerical knowledge and formidable intuition, and his enthusiasm for a project out of his area, have been an inspiration and the foundations upon which the numerical code for the Euler equations is built. I could not have asked for a better management of a long-distance supervision, or support during my visiting semester in Pavia.

I am thankful to my senior collaborators, Prof. Mathew A. Johnson of the University of Kansas and Prof. Henrik Kalisch of the University of Bergen, for their excellent job co-authoring our papers, their contagious energy and positive mindset, and very friendly attitude. Working with them not only built a great network, but expanded my scientific field of vision and helped developing my profile as a mathematician.

The friends and colleagues I met in Trondheim have been the pillars of the last four years. I am not ashamed in saying I would not have made it through without them. Mathias Nikolai Arnesen is a truly brilliant guy and one of the first Norwegian friends I got. Together we shared many a laugh and an arbitrarily large number of hamburgers and beers. I cannot overstate my opinion of Kristoffer Varholm's sheer brainpower. His patiently offered explanations helped me more than once when I was stuck, and his calm and reflective attitude always made for interesting conversations on the most different subjects. If Mathias and Kristoffer have been my colleague-brothers, Gabriele Brüll has been the mother. Besides being an extremely skilled mathematician, with kind heart and caring attitude she listened to my complains and worries. The "coffee breaks team" with her and Katrin Grunert has been the arena where we laughed about the grotesquely ironic events my life seems abundant of. Their friendship is something I hold dear. I have found truly akin souls in Ola Isaac Høgåsen Mæhlen and Audun Reigstad, who share so

much of my own character and humour. Together we spent countless hours having fun or discussing life as a PhD student, developing internal jokes that will forever be great memories. Yuexun Wang and his permanently cheerful attitude gave me new insight on what being a foreigner means, enriching my own experience as an outsider. Fredrik Hildrum is one of the most educated persons I know and taught me the value of small polite acts, even as simple as dressing with a shirt at the right time. Together with the above, Raj Narayan Dhara contributed in making "Team Mats" one of the best research teams I could hope to work with.

The quality of the work environment would have not been the same without a nice group of fellow PhD students. My thanks go to Jacopo Paglia, Paul André Dillon Trygsland, Sondre Tesdal Galtung, Markus Grasmair, Ingeborg Gullikstad Hem, Susanne Solem, Jon Vegard Venås, and everyone who joined the common lunches and made for a friendly atmosphere.

I have to give thanks to my friend and fellow researcher Kjetil André Johannessen. With his exceptional coding skills he has been my Norwegian reference to anything IGA or supercomputing related. The biologists' group of Nicola Montaldo, Synnøve Ræder, and Rossana Aprigliano contributed in making my time in Trondheim great, with many koselig evenings and expertly homemade pizzas. Cesilie Welle's pragmatism and sharp sarcastic humour have been essential in several moments. Flora Anna Crocker Ångman suggested and shared with me many films, with impeccable taste for the art of cinema. Throughout my master and PhD the friendship with Marius "the bro" Münch resulted in lots of fun and interesting cross-discipline transfer of knowledge. Sometimes in life you meet people with the power to brighten your whole day with a simple smile. Margrethe Kvale Loe is one such splendid person, and I could not be happier I met her on my path.

At NTNU I have always felt welcomed in knocking at a professor's door, and the friendliness of the permanent staff made the whole department feel to me like a big family of scientists. A special thank you goes to Prof. Peter Lindqvist, Prof. Helge Holden, and the head of department Prof. Einar Rønquist. Too often the importance of the administrative staff goes unrecognised. Stian Tamlagsrønning is the reason 6 years ago I have been able to stay in Norway, as he helped me getting my first paid job as a teaching assistant. Without that I would have had to interrupt my studies and go back to Italy. Anne Margrethe Kajander and Tanja Helene Opheim offered tremendous support and made a fantastic job in helping me navigate the regulations and bureaucracy. In the age of technology my work would not have been possible without the skillful IT computer wizards: Per Kristian Hove, Torstein Fiskvik, and Hallvard Norheim Bø.

Of the people at the University of Pavia I would like to thank Rafael Vázquez for the enormous help in using the GeoPDEs package for Matlab, and Monica Montardini for having endured long working days to make the Euler code run smoothly. Barbara Giunti has given me indispensable support both during and after my visit in Pavia, providing straightforward, unbiased opinions I knew I could rely on. If there is one good thing Italians are known for, is their social and friendly attitude, and the whole group of PhD students at Pavia kept this attitude well alive.

I would like to take the time here to mention two persons who exerted a big influence on the development of my persona, and therefore indirectly but noticeably also on the

results of my studies: Caterina Parolin and Erika Brugnoli. Over the course of many years, Caterina thought me how to stay connected with the inner child we all have, and see the beauty even in the small things, like an earthworm. I cannot express how much I find this important in my everyday life as a scientist. Erika's strength and sense of duty is something I have always looked up to. If this thesis has been delivered in time I have to thank also her example. Without their teachings I would probably be in a very different place in life now.

Last, but by no means least, the support of my family must be acknowledged. My parents provided me with top class education and etiquette, which made it easy for me to fit into a different society. They have been patient toward a not always easy son living thousands of kilometres away while remaining available at all times. My father pushed me to invest in my own education. My mother has always been there for me, for anything I could have needed. I have moreover been lucky enough to have a brother who is, among many other qualities, a talented designer with a great aesthetic mind. He passed his love for clear visual communication onto me and essentially single-handedly created the graphical layouts I use in my presentations. Given that even the most important mathematical result can be rendered useless by poor communication, I believe my brother's help improved the quality of my scientific work immeasurably.

Filippo Remonato
Trondheim, May 2018

Contents

There appears to be no single precise definition of what exactly constitutes a wave.

Gerald B. Whitham

0

Introduction

Introduction

0.1 Waves in water

This thesis deals with the analysis of waves in a homogeneous fluid of finite depth, a layer of water being the prime example, and in particular with waves which are described through bifurcation theory.

The motion of an inviscid, incompressible fluid over a flat, rigid, impermeable bottom $\mathcal{B}$ is described by the Euler equations with suitable boundary conditions. The resulting mathematical model is called the *water wave problem*. In two dimensions, letting Ω indicate the interior of a fluid domain of depth d, and assuming its *free boundary* $\mathcal{S}$ can be represented by the graph of a function with vertical coordinate $y = d + \eta(x,t)$, the Euler system reads

$$\begin{aligned} u_t + uu_x + vu_y &= -P_x && \text{in } \Omega \\ v_t + uv_x + vv_y &= -P_y - g && \\ u_x + v_y &= 0 && \text{in } \Omega \\ v &= \eta_t + u\eta_x && \text{on } \mathcal{S} \\ v &= 0 && \text{on } \mathcal{B} \\ P &= P_{\text{atm}} && \text{on } \mathcal{S}. \end{aligned} \tag{0.1.1}$$

Here (u, v) is the velocity field of the fluid, P is the pressure, and g is the acceleration due to gravity. Note that since Ω, or actually η, is to be found as part of the solution this is a free boundary problem. Albeit being a special case of the Navier-Stokes equations, the Euler equations are still arduous for both analytical and numerical approaches. Their great complexity has thus pushed the scientific community to develop, throughout the years, several simplified models for the description of the fluid's surface.

Even if waves on Earth can reach amplitudes of over 30 metres [33], smaller waves are much more common and easily observable in a laboratory. For this reason, and for sheer mathematical convenience, several model equations to approximate the behaviour of the surface given by the system (0.1.1) have been proposed in the small amplitude - long wavelength regime. The first topic presented in this thesis is the *Whitham equation*,

a model closely-related to the famous Korteweg-de Vries (KdV) equation. Presented in 1967 [38] by the British-born American mathematician Gerald B. Whitham, the equation - in two physical dimensions and after a scaling - can be written as

$$u_t + uu_x + Mu_x = 0. \tag{0.1.2}$$

The real function u represents the fluid's surface, and the convolution operator M is defined by

$$\widehat{Mf}(\xi) = m(\xi)\widehat{f}(\xi) = \sqrt{\frac{\tanh(\xi)}{\xi}}\ \widehat{f}(\xi). \tag{0.1.3}$$

The important feature of the Whitham equation lies precisely in the choice of symbol above: The quantity $m(\xi)$ in (0.1.3) coincides with the dispersion relation of the linearised water wave problem for purely gravitational waves. In contrast, while having the same structure as (0.1.2), the KdV equation features a dispersion relation of the form

$$m_{KdV}(\xi) = 1 - \tfrac{1}{6}\xi^2,$$

which is only a second order approximation to the symbol in (0.1.3). As a result the KdV model is too strongly dispersive to capture phenomena such as wave breaking and waves with singular points (cusps), which are instead known to exist in the full water wave problem. Recognising these issues, Whitham conjectured that using the same phase speed as the linearised Euler equations would enable the model to describe the waves' behaviours that were lost to the KdV equation. Yet, the new convolution kernel was nonetheless too difficult to treat due to its singularity at the origin, and Whitham resorted to investigate a kernel with a different symbol [38, 39], leaving his claims intuitively plausible, but mathematically unproven. It did not take long, however. In [5] wave breaking for solutions of the Whitham equation was proven, albeit the authors apply their method to the case of a continuous kernel (but state that the same approach works also for the singular one). A more recent proof where the singular kernel given by (0.1.3) is considered is given in [17], and wave breaking has been numerically studied in [22]. The existence of a highest cusped wave was instead numerically observed in [11] and analytically confirmed in [14].

0.2 The capillary Whitham equation

In this thesis we analyse the bifurcation branches of travelling wave solutions of the Whitham equation when capillary forces are taken into account. The travelling waves assumption allows to integrate Equation (0.1.2) once, and using a Galilean shift to set the integration constant to zero, one can write the equation in the form

$$-cu + u^2 + Mu = 0, \tag{0.2.1}$$

with $c > 0$ being the speed of the wave. The operator M as described by (0.1.3) accounts only for the presence of gravitational forces. The inclusion of surface tension is done, in

the spirit of Whitham, by using as symbol for the convolution kernel the phase speed coming from the linearised Euler equations with capillarity. That is, one uses

$$m_T(\xi) = \sqrt{\frac{(1 + T\xi^2)\tanh(\xi)}{\xi}} \tag{0.2.2}$$

where $T \geqslant 0$ represents the strength of the capillary effects. Note that for $T = 0$ the above symbol agrees with the gravitational one in (0.1.3), but for $T > 0$ its asymptotic behaviour changes drastically: From $|\xi|^{-1/2}$ to $|\xi|^{1/2}$. This means in particular that m_T is no longer bounded and decreasing on $\mathbb{R}$, and as a consequence the corresponding operator M_T will no longer be smoothing. This issue prompted us to rewrite the equation through the use of the operator $L_T = (M_T)^{-1}$, to recover the boundedness and smoothing properties. On the other hand, this change leads Equation (0.2.1) to assume the more complicated form

$$u + L_T\left(u^2 - cu\right) = 0. \tag{0.2.3}$$

The analysis of the branches of solutions of the capillary Whitham equation, either in the form (0.2.1) or (0.2.3), is the topic of the first two works included in this thesis.

0.2.1 Paper I: Simple and double bifurcations in the capillary Whitham equation

This paper provides the first analytical investigation of the bifurcation branches of the capillary Whitham equation (0.2.3). The general approach mimics the one used in other works such as [10, 11], with important differences concerning the three main areas of the paper: The theory for the operator L_T, the simple bifurcations, and the double bifurcations.

First, respect to the work in [11], Equation (0.2.3) has the additional difficulty that the nonlocal operator here acts also on the nonlinear term. This required a thorough study of the new convolution kernel which we accomplish using complex analysis techniques and the theory of Stieltjes functions. The many properties of L_T recorded in the first part of the paper constitute the first step on the way to develop the theory for more general types of equations featuring nonlinear-nonlocal terms.

The second main result is the existence of branches of solutions at points where the bifurcation kernel is one-dimensional. The branches are shown to locally contain only unimodal solutions and we furthermore prove that they can be globally extended. Similar results were already obtained for the Whitham equation but in the purely gravitational setting: The local bifurcation branches found in [12] were extended to global ones in [11], and, with techniques similar to those applied here, the authors of [14] were able to give a complete description of the main global branch, terminating with a highest cusped wave (thereby also proving Whitham's conjecture). In this work, while we expect no loops to occur for large surface tension, due to the higher complexity of both the equation and the convolution operator at play here a complete proof is currently in progress. Numerical evidence coming from the code developed in **Paper II** suggests that for large surface tension the branches are unbounded, with the solutions satisfying $|u - c + 1| \to 0$ pointwise as $c \to \infty$.

Third, the new form of the phase speed (0.2.2), being not monotone in its argument, allows for two families of waves to bifurcate at the same speed - something that is precluded in the purely-gravitational case. For any choice of two distinct wavenumbers k_1 and k_2 we show that there are points where the bifurcation kernel is two-dimensional, and at those points we prove the existence of local sheets of solutions containing unimodal waves or bimodal waves featuring the prescribed wavenumbers, also called Wilton Ripples. Additionally, we point out that for the particular choice $k_2/k_1 \in \mathbb{N}_0$ purely k_1-mode solutions might not exist, and only the k_2-mode and the mixed-mode solutions appear to occur, pointing toward resonance phenomena between the two wavenumbers. This matches the observations made for the Euler equations in [29] for double bifurcations of $(1, 2)$-modes: There the authors noted that also their technique failed to prove the existence of the lower mode branch at the double bifurcation point, and instead a curve of mixed-mode solutions appeared. The same situation for bimodal waves was additionally found, also for the Euler equations but including vorticity effects, in [10]. In that work the authors further wonder whether there might be cases of the bifurcation kernel having dimension greater than two. That has been answered in the positive by some of the same authors in [13], where examples of trimodal waves are presented. The question has been further settled in the work [1], where bifurcation kernels with arbitrary dimension have been proved to exist in the Euler equations with vorticity. Using a different approach, based on the roots of the dispersion relation, the authors of [23] also proved the existence of waves with an arbitrary number of modes.

We list here some additional related works: The existence of solitary wave solutions for, among others, the capillary Whitham equation was proved in [2]. In the same work the (conditional) stability of such solutions was analysed, while the (modulational) (in)stability of the periodic solutions has been treated in [16]. Regarding multimodal waves in the capillary Euler equations, the stability of Wilton ripples has been the topic of [34], while bimodal waves in the presence of both capillarity and (constant) vorticity have been studied in [25]. Lastly, the relevance of the capillary Whitham equation as a model for water waves has been the subject of the study [26], which shows that it gives a valid description of surface waves short enough for capillary effect to play a role. There it is also formally shown that the Whitham equation can be derived from the Euler equations via an exponential scaling.

0.2.2 Paper II: Numerical bifurcation for the capillary Whitham equation

This work is the numerical counterpart of **Paper I** and uncovers the rich bifurcation structure of the capillary Whitham equation, finding and describing a number of solution curves in both the one- and two-dimensional bifurcation settings. In the case of one-dimensional bifurcations, we show that the global branches contain purely unimodal waves, with possible subharmonic, frequency-doubling components appearing for large amplitudes. In the case of two-dimensional bifurcations with wavenumbers k_1 and k_2, we present cases of curves of solutions featuring *crossings* in the speed-height diagram (the curves meet at a point but do not share the same solution) or *connections* (the curves

actually share the same wave solution), and present examples of branches featuring self-crossings without self-connections. In the cases where two branches connect we discover that for particular resonances, i.e. specific multiplicities between two wavenumbers, one of the branches terminates after connecting with the other, while for different multiplicities it continues after the connection giving rise to a secondary bifurcation. In any two-dimensional bifurcation case with $k_2 = nk_1$, $n \in \mathbb{N}$, however, no purely k_1-mode curve of solutions is found, but only curves of purely k_2 or mixed modes, in accordance with the observations in **Paper I**. Moreover, for all configurations of parameters no end of the branches has been reached, and waves with amplitude well over 1 have been computed; this supports the idea expressed in **Paper I** that the branches are unbounded.

The tool of the analysis is a spectral Fourier-collocation scheme built on the technique presented in [11, 12], where the study of travelling waves for the gravitational Whitham equation was in focus. Spectral collocation schemes have been proved to be convergent on similar nonlocal equation in, for instance, [19, 28]. Here we substantially modify and extend the numerical approach of the earlier works to include the effect of surface tension and allow following branches of any (smooth) shape. This is particularly important: Already in the case of no surface tension the branches were shown to present features, like turning points, which are challenging for a numerical-continuation scheme. With the introduction of capillarity forces the shape of the branches can exhibit even more exotic behaviours, so that a robust method to follow them results to be essential to the analysis. To pursue a complete investigation, we additionally equipped the code with the capability of automatically detecting secondary bifurcation points, and locking on and resolving the secondary curves.

The analysis performed in this work is novel for the capillary Whitham equation, but similar investigations have been conducted, with a completely different method, for the capillary Euler equations in [3]. We here obtain matching global bifurcation diagrams for some configurations of wavenumber and surface tension, indicating that the Whitham equation may provide an interesting model for water waves even outside the small amplitude regime where it is originally defined. While we tested a great number of solution waves in a simple time integration scheme, especially large-amplitude ones, their evolution and stability has not been in focus in this work. Those topics have been analysed in [24] for the full-dispersion Kadomtsev-Petviashvli (FKDP) equation with capillarity, which reduces to the capillary Whitham when one considers two-dimensional waves. With a numerical scheme different to the one used here, it was shown that the FDKP features stable, large-amplitude lump solitary waves for large surface tension. It was moreover shown that the capillary Whitham equation features global-in-time solutions for small enough initial data.

0.3 The free boundary problem in the Euler equations

Having analysed the bifurcations of the (capillary) Whitham equation in detail, we have been interested to move our attention to the full water wave problem, for which the

Whitham equation is a simplified model.

When searching for travelling wave solutions, one can rewrite the Euler equations (0.1.1) in a steady form, which is known as the *stream function formulation* (see [6] for details):

$$\begin{aligned} \Delta\psi &= -\omega && \text{in } \Omega \\ \psi &= m_0 && \text{on } \mathcal{B} \\ \psi &= m_1 && \text{on } \mathcal{S} \\ \frac{1}{2}|\nabla\psi|^2 + \eta &= Q && \text{on } \mathcal{S}. \end{aligned} \tag{0.3.1}$$

Here ψ is the stream function, satisfying $\nabla\psi = [-v,\, u-c]$, $m_1 - m_0$ is the relative mass flux, and Q is a constant coming from the Bernoulli equation. Note also that the *vorticity* ω is defined in terms of the stream function: $\omega = \omega(\psi)$. Up until recently the majority of works on the Euler equations assumed either $\omega = 0$, corresponding to irrotational flows, or $\omega = a \in \mathbb{R}$, corresponding to flows with constant vorticity. Our aim is instead directed at the linear vorticity case, so that $\omega = a\psi + b$, for constants $a, b \in \mathbb{R}$.

If $Q - \eta$ does not change sign on $\mathcal{S}$, then thanks to the third equation in (0.3.1) we can rewrite the system in a more general form

$$\begin{aligned} -\Delta u &= f && \text{in } \Omega \\ u &= h && \text{on } \Gamma_D \\ \partial_n u &= g && \text{on } \mathcal{S} \end{aligned} \tag{0.3.2}$$

where $\Gamma_D = \mathcal{B} \cup \mathcal{S}$ is the part of the boundary where Dirichlet conditions are applied. Here $\partial_n u$ denotes the normal derivative, and f, h, and g are functions defined in a larger domain containing Ω and its deformations. The assumption on the sign of $Q - \eta$ is legitimate: if $\frac{\partial}{\partial y}\psi$ would change sign on $\mathcal{S}$ then a stagnation point would be present at the surface and no bifurcation could occur; see for instance the explanation in [37]. Rewriting the problem as in (0.3.2) is then justified, and is on systems of that form that we developed the free boundary isogeometric algorithms that are the topics of the third work in this thesis.

Those algorithms represent the core of a continuation-method for bifurcations of the steady Euler equations: Coupled with a quasi-Newton stepping scheme, they will be used to solve the Euler system of equations and provide the direction of the update of the free boundary. Through this process, the numerical method will then iteratively converge to the branch of solutions.

The algorithms we develop are based on isogeometric analysis (IGA) techniques. IGA is a fairly recent technique which can be seen as an enhancement of the standard finite element method (FEM) through the use of smooth B-splines basis functions, and has attracted a lot of attention from the research community ([4, 18, 36]). We refer to the book [7] for the details of this approach. The main advantages of IGA over standard FEM are the possibility to naturally describe curved geometries through the use of splines functions and the construction of discrete spaces with basis with C^p continuity. Both these features find perfect applications to free boundary problems involving waves, and

permit to achieve high accuracy in the description of both the surface and the internal streamlines.

0.3.1 Paper III: Isogeometric methods for free boundary problems

This work concerns numerical techniques for systems of the form (0.3.2), with the aim to apply such methods to the study of the bifurcation branches of solutions of the Euler equations (0.3.1). In particular, in this paper we review and extend two existing methods for free boundary problems, and develop a third scheme which is completely novel.

The first method is based on the one presented in [40] - the first application of IGA to a free boundary problem - which is here extended to the case of periodic boundary conditions. Our second algorithm uses the approach presented in [20, 21], based on the classical FEM, which in addition to a similar extension to periodic problems has here been recast in the IGA framework. The change from FEM to IGA is in this case especially advantageous: Since the finite element basis produces meshes with straight edges, the authors of those two earlier works needed to introduce an artificial regularisation of the free boundary to approximate its curvature. This can be completely avoided in an IGA framework, resulting in a much more accurate, and straightforward, description of the curvature-dependent terms. Both of our two first methods are based on an IGA-Galerkin approach. The third algorithm is instead a completely novel, efficient fast collocation method based on the superconvergent points presented in [15, 27], and represents the first application of IGA-collocation to free boundary problems. In all algorithms the treatment of the unknown free boundary is tackled with a superlinear quasi-Newton method based on the shape calculus techniques presented in [9, 32].

We compare the three numerical schemes on several benchmark tests, including either Dirichlet or periodic conditions on the vertical sides of the domain Ω, and for different free-boundary solutions cases. The main conclusion is that the three methods are overall comparable in terms of accuracy, but display more marked differences in runtime. While the two Galerkin-based methods converged to the correct solution faster in terms of number of iterations respect to the collocation scheme, the latter is decisively more efficient in the use of machine resources and reached tolerance in half the processing time. In addition, our algorithms obtain significantly improved results respect to [40] when applied to the same test case: We do not see a plateau in the error quantities and convergence is instead reached for any meshsize.

As mentioned, while the Euler equations are not the focus of this work our interest in such methods lies in a future application to the study of the branches of periodic solutions of the system of equations (0.3.1). Numerical experiments in this direction have so far used finite differences methods [8], boundary-integral formulations [31, 35], or finite elements [30]. The application of IGA to the Euler equations with affine vorticity is then a promising novel approach, in view of the accurate description of the curved surface enabled by the use of splines functions.

References

[1] A. Aasen and K. Varholm. "Traveling Gravity Water Waves with Critical Layers". In: *Journal of Mathematical Fluid Mechanics* 20.1 (2018), pp. 161–187.

[2] M.N. Arnesen. "Existence of solitary-wave solutions to nonlocal equations". In: *arXiv* (2015). arXiv:1506.05256v1.

[3] P.J. Aston. "Local and global aspects of the (1,n) more interaction for capillary-gravity waves". In: *Physica D* 52 (1991), pp. 415–428.

[4] Y. Bazilevs, L. Beirao de Veiga, J.A. Cottrell, T.J.R. Hughes, and G. Sangalli. "Isogeometric analysis: approximation, stability and error estimates for h-refined meshes". In: *Mathematical Models and Methods in Applied Sciences* 16 (2006), pp. 1031–1090.

[5] A. Constantin and J. Escher. "Wave breaking for nonlinear nonlocal shallow water equations". In: *Acta Mathematica* 181.2 (1998), pp. 229–243.

[6] A. Constantin and W. Strauss. "Exact Steady Periodic Water Waves with Vorticity". In: *Comm. on Pure and Applied Mathematics* 57 (2004), pp. 481–527.

[7] J.A. Cottrell, T.J.R. Hughes, and Y. Bazilevs. *Isogeometric Analysis, Toward Integration of CAD and FEA*. Wiley, 2009.

[8] Robert A Dalrymple. "A numerical model for periodic finite amplitude waves on a rotational fluid". In: *Journal of Computational Physics* 24.1 (1977), pp. 29–42.

[9] M.C. Delfour and J.P. Zolésio. *Shapes and Geometries: Metrics, analysis, differential calculus, and optimization*. Society for Industrial and Applied Mathematics (SIAM), Philadelphia, PA, 2011.

[10] M. Ehrnström, J. Escher, and E. Wahlén. "Steady Water Waves with Multiple Critical Layers". In: *SIAM J. Math. Anal.* 43.3 (2011), pp. 1436–1456.

[11] M. Ehrnström and H. Kalisch. "Global Bifurcation for the Whitham Equation". In: *Mathematical Modelling of Natural Phenomena* 8 (5 2013), pp. 13–30.

[12] M. Ehrnström and H. Kalisch. "Traveling Waves for the Whitham Equation". In: *Differential and Integral Equations* 22.11-12 (2009), pp. 1193–1210.

[13] M. Ehrnström and E. Wahlén. "Trimodal Steady Water Waves". In: *Archive for Rational Mechanics and Analysis* 216.2 (2015), pp. 449–471.

[14] M. Ehrnström and E. Wahlèn. "On Whitham's conjecture of a highest cusped wave for a nonlocal dispersive equation". In: *arXiv* (2016). arXiv:1602.05384.

[15] Hector Gomez and Laura De Lorenzis. "The variational collocation method". In: *Computer Methods in Applied Mechanics and Engineering* 309 (2016), pp. 152–181.

[16] V. M. Hur and M. A. Johnson. "Modulational instability in the Whitham equation with surface tension and vorticity". In: *Nonlinear Anal.* 129 (2015), pp. 104–118.

[17] V.M. Hur. "Breaking in the Whitham equation for shallow water waves". In: *arXiv* (2015). arXiv:1506.04075v3.

[18] K. A. Johannessen, F. Remonato, and T. Kvamsdal. “On the similarities and differences between Classical Hierarchical, Truncated Hierarchical and LR B-splines”. In: *Computer Methods in Applied Mechanics and Engineering* 291 (2015), pp. 64–101.

[19] H. Kalisch. “Error Analysis of a Spectral Projection of the Regularized Benjamin–Ono Equation”. In: *BIT Numerical Mathematics* 45.1 (2005), pp. 69–89.

[20] K. T. Kärkkäinen and T. Tiihonen. “Free surfaces: Shape sensitivity analysis and numerical methods”. In: *International Journal for Numerical Methods in Engineering* 44 (1999), pp. 1079–1098.

[21] K. T. Kärkkäinen and T. Tiihonen. “Shape calculus and free boundary problems”. In: *European Congress on Computational Methods in Applied Sciences and Engineering ECCOMAS*. 2004.

[22] C. Klein and J.-C. Saut. “A numerical approach to blow-up issues for dispersive perturbations of Burgers’ equation”. In: *Physica D* 295–296 (2015), pp. 46–65.

[23] V. Kozlov and E. Lokharu. “N-Modal Steady Water Waves with Vorticity”. In: *Journal of Mathematical Fluid Mechanics* (2017), pp. 1–15.

[24] D. Lannes and J.-C. Saut. “Remarks on the full dispersion Kadomtsev-Petviashvli equation”. In: *Kinet. Relat. Models* 6.4 (2013), pp. 989–1009.

[25] C.I. Martin and B.-V. Matioc. “Existence of Wilton Ripples for Water Waves with Constant Vorticity and Capillary Effects”. In: *SIAM Journal on Applied Mathematics* 73.4 (2013), pp. 1582–1595.

[26] D. Moldabayev, H. Kalisch, and D. Dutykh. “The Whitham equation as a model for surface water waves”. In: *Phys. D* 309 (2015), pp. 99–107.

[27] M. Montardini, G. Sangalli, and L. Tamellini. “Optimal-order isogeometric collocation at Galerkin superconvergent points”. In: *Comput. Methods Appl. Mech. Engrg.* 316 (2017), pp. 741–757.

[28] Beatrice Pelloni and Vassilios A. Dougalis. “Error estimates for a fully discrete spectral scheme for a class of nonlinear, nonlocal dispersive wave equations”. In: *Applied Numerical Mathematics* 37.1 (2001), pp. 95–107.

[29] J. Reeder and M. Shinbrot. “On Wilton ripples, II: Rigorous results”. In: 77 (Dec. 1981), pp. 321–347.

[30] C. H. Rycroft and J. Wilkening. “Computation of three-dimensional standing water waves”. In: *Journal of Computational Physics* 255 (2013), pp. 612–638.

[31] J. A. Simmen and P. G. Saffman. “Steady Deep-Water Waves on a Linear Shear Current”. In: *Studies in Applied Mathematics* 73.1 (1985), pp. 35–57.

[32] J. Sokolowski and J.P. Zolésio. *Introduction to shape optimization: shape sensitivity analysis*. Springer, Berlin: Springer series in computational mathematics, 1992.

[33] H. L. Tolman. “Practical Wind Wave Modeling”. In: *Proceedings of the Conference Water Waves: Theory and Experiment*. World Scientific, 2012, pp. 79–92.

[34] O. Trichtchenko, B. Deconinck, and J. Wilkening. “The instability of Wilton ripples”. In: *Wave Motion* 66 (2016), pp. 147–155.

[35] J.-M. Vanden-Broeck. *Gravity-Capillary Free-Surface Flows*. Cambridge University Press, 2010.

[36] A.V. Vuong, C. Giannelli, B. Jüttler, and B. Simeon. "A hierarchical approach to adaptive local refinement in isogeometric analysis". In: *Computer Methods in Applied Mechanics and Engineering* 200.49–52 (2011), pp. 3554–3567.

[37] E. Wahlén. "Steady water waves with a critical layer". In: *Journal of Differential Equations* 246.6 (2009), pp. 2468–2483.

[38] G. B. Whitham. "Variational methods and applications to water waves". In: *Proc. of the Royal Society of London Series A* 299.1456 (1967), pp. 6–25.

[39] G.B. Whitham. *Linear and Nonlinear Waves*. Pure and Applied Mathematics. John Wiley & Sons Inc., New York, 1974.

[40] K.G. van der Zee, G.J. van Zwieten, C.V. Verhoosel, and E.H. van Brummelen. "Shape-Newton Method for Isogeometric Discretization of Free-Boundary Problems". In: *MARINE 2011, IV International Conference on Computational Methods in Marine Engineering : selected papers : part III*. Springer, 2013, pp. 85–102.

Quelli che s'innamorano della pratica senza la scienza, sono come i nocchieri che entrano in naviglio senza timone o bussola, che mai hanno certezza dove si vadano. Sempre la pratica dev'essere edificata sopra la buona teorica, della quale la prospettiva è guida e porta, e senza questa nulla si fa bene.*

Leonardo da Vinci,
Trattato della Pittura

*Those who fall in love with practice without theory, are like those who go sailing without rudder or compass, such that they never know where they are going. At all times should practice be built upon good theory, its perspective is guide and gate, and without it none is done well.

Paper I

Simple and double bifurcations in the capillary Whitham equation

Mats Ehrnström, Mathew A. Johnson, Ola Isaac Høgåsen Mæhlen,
and Filippo Remonato

Simple and double bifurcations in the capillary Whitham equation

Mats Ehrnström[1], Mathew A. Johnson[2], Ola Isaac Høgåsen Mæhlen[1], and Filippo Remonato[1,3]

[1] Department of Mathematical Sciences, NTNU, Trondheim, Norway
[2] Department of Mathematics, Kansas University, Lawrence, Kansas
[3] Department of Mathematics, University of Pavia, Pavia, Italy

Abstract

We consider the bifurcation of periodic travelling waves of a generalized Whitham equation that incorporates the effects of capillarity into the dispersion relation. In particular, we consider a nonlinear pseudo-differential equation that combines the canonical shallow water nonlinearity together with the exact (unidirectional) dispersion for finite-depth gravity-capillary waves. We prove several properties of the new operator arising from the inclusion of surface tension, and show that in almost all cases of one-dimensional bifurcation, the curves of solutions can be extended globally. At points where the bifurcation kernel is two-dimensional, we show the local existence of sheets of solutions containing bimodal waves.

I.1 Introduction

We consider periodic travelling wave solutions of the capillary-gravity Whitham equation

$$u_t + M_T u_x + 2uu_x = 0 \tag{I.1.1}$$

where M_T is a Fourier multiplier operator defined via its symbol m_T as

$$\widehat{M_T f}(\xi) = m_T(\xi)\widehat{f}(\xi) = \left(\frac{(1+T\xi^2)\tanh(\xi)}{\xi}\right)^{\frac{1}{2}} \widehat{f}(\xi), \tag{I.1.2}$$

and the coefficient $T > 0$ denotes the strength of the surface tension. The symbol m_T arises as the linear dispersion relation for capillary-gravity water waves over a finite depth described by the Euler equations [27, 13]. In the purely gravitational case, i.e. with $T = 0$, the use of this symbol was proposed by Whitham as a way to generalise the KdV

equation and remedy its strong dispersion [26]. Bifurcation in the gravitational setting has been investigated by some of the authors in [7, 8]. We are here interested in completely characterising the local theory for travelling wave solutions of (I.1.1), and understanding their global extensions.

The overarching technique follows an approach similar to that used for the gravity Whitham equation in [7] or the Euler equations in [6], where a Lyapunov-Schmidt reduction is used to prove the existence of wave solutions through the application of the implicit function theorem. Here, however, the symbol significantly changes its asymptotic behaviour: From $|\xi|^{-1/2}$ for the gravity case to $|\xi|^{1/2}$ when capillarity is present. This introduces several mathematical challenges, which are tackled by rewriting the equation in an equivalent form (I.1.5) through the inverse of the convolution operator. While doing so recovers the boundedness and smoothing properties of the symbol, it has the effect of applying a nonlocal operator to the nonlinear part of the equation. This required the development of much of the theory for the new convolution operator, which is here presented.

Our main results are the following: We show that the inverted convolution operator is integrable, completely monotone for strong enough surface tension, and that the symbol allows for two-dimensional bifurcation kernels. With the application of the reduction described above we prove the existence of small-amplitude solutions, and later extend those local branches to global ones. Lastly, in the case of a two-dimensional kernel, the existence of small-amplitude, two-dimensional manifolds of solutions is shown; these sets contain bimodal waves with profiles featuring first order terms with two different wavenumbers. Respect to earlier works on the gravitational Whitham equation, the present investigation has several important differences, which we now bring forward and comment on.

The technical challenges arising in the present work are multiple. The new operator appearing in (I.1.5) is investigated in a fashion similar to the approach of [10] in the water waves problem. We apply complex analysis techniques and the theory of Stieltjes functions to show the properties of the convolution kernel, among others its regularity, smoothing and Fredholm properties, and when surface tension is large enough also complete monotonicity. This analysis sets the foundations for the development of more general theory for similar classes of equations featuring nonlocal-nonlinear terms. The properties of the operator here recorded provide the mathematical basis upon which the existence of the bifurcation branches, and later their global extensions, is based. Another challenge is that the increased complexity in the problem makes it harder to rule out alternatives arising from the global extension of branches. With the presence of surface tension two-dimensional *transcritical* bifurcation can occur, as we will show. Numerical calculations furthermore suggest that for very large waves the profile converges pointwise to a constant solution of positive height, but with a strong steepening of the slope. This complicates the analysis of the alternatives as carried out, for example, in [10]. For these reasons, while at least for strong surface tension we expect that no loops can be present, and the branches would therefore be unbounded, a rigorous proof is still in preparation.

The existence of multimodal waves, not possible in the purely gravitational setting, is given in Theorem I.4.1, where we show that for any two wavenumbers k_1 and k_2 there are values of the parameters which allow for solutions with first-order terms of the form

$\cos(k_1 x)$ and $\cos(k_2 x)$. These waves, also called *Wilton ripples*, have been shown by Reeder and Shinbot in [21] to exist for the Euler equations with surface tension, albeit only in the case with $k_1 = 1$, $k_2 = 2$, and their spectral stability has been recently numerically investigated in [25]. Additionally, the work [19] showed the existence of Wilton ripples for the Euler equations with both (constant) vorticity and capillarity. In addition to the existence result, Theorem I.4.1 brings forward two main points: First, it is possible to have branches with different wavenumbers connect. This result matches the observations made in [22], which is the numerical counterpart of the present work, and was also found and analysed in the water wave problem given by the Euler equations in [2]. Second, when the bifurcation kernel is two-dimensional and k_2 is a multiple of k_1, our method fails at finding any branch containing pure k_1-mode solutions. The same situation has been encountered in [21], where their proof of existence of the lower-mode branch also failed in this case. Indeed, the k_1-mode waves' branch ceases to exist and is instead replaced by a branch of solutions with mixed (k_1, k_2)-wavenumber. Numerical confirmation of this is again given in [22]. Multimodal solutions of the Euler equations have additionally been studied in [1, 16], where it is in particular proven, with two different approaches, that bifurcations with arbitrarily large kernels can occur.

The relevance of the Whitham equation as a model for water waves has been studied for instance in [20], where it is formally shown that it follows from the full Euler equations via an exponential scaling. There it is also found that the Whitham equation performs better than the KdV or BBM equations in describing the surface of waves in the intermediate or short waves regime. The performance of the full-dispersion Kadomtsev-Petviashvli equation (FDKP) with capillarity is instead analysed in [17], where it is shown that it provides a better approximation of surface waves than the standard KP equation. The FKDP equation reduces to the Whitham equation when the waves are two-dimensional. The local solvability of the Cauchy problem for a family of dispersive equations, including KdV, Benjamin-Ono, Burgers, and capillary Whitham, has instead been proved in [18], while the stability of the waves described by the capillary Whitham equation has been the subject of the investigation in [12], showing that they can be modulationally unstable, depending on the wavenumber and strength of the capillarity. As said above, out interest in this work is to prove the existence of periodic travelling waves for the capillary Whitham equation.

Traveling-wave solutions of the form $u(x - ct)$ satisfy the (profile) equation

$$-cu + M_T u + u^2 = 0, \tag{I.1.3}$$

where we have integrated once and used Galilean invariance to set the constant of integration to zero. Since m_T is strictly positive on $\mathbb{R}$, the operator M_T is invertible (for example in an L^2-based Fourier space) with inverse L_T defined via

$$\widehat{L_T f}(\xi) = l_T(\xi)\widehat{f}(\xi), \qquad l_T(\xi) = (m_T(\xi))^{-1}. \tag{I.1.4}$$

In particular, the capillary-gravity Whitham equation (I.1.3) can be rewritten in the "smoothing" form

$$u - cL_T(u) + L_T(u^2) = 0, \tag{I.1.5}$$

with $L_T = K_T*$ where K_T is the convolution kernel corresponding to the symbol l_T, and will be analysed in the forthcoming section. The form (I.1.5) is resemblant of the Whitham equation itself, but with a nonlocal nonlinearity. In fact, we view this paper as a part of a larger programme to understand and quantify how the precise balance between dispersion and nonlinearities interact to large and largest waves and determine their regularity. The equation (I.1.5) fits into this scheme as it is a first step, in a simple model, to treat the case of a nonlocal nonlinearity when the linear dispersion is understood.

This paper is organised as follows: In Section I.2 we establish several properties of the convolution kernel K_T which will be useful in the treatment of the bifurcations. In particular, we show that K_T is completely monotone when $T \geqslant 4/\pi^2$. Section I.3 contains the analysis of the bifurcations in the case of a one-dimensional bifurcation kernel; the main result is the existence of global branch of solutions bifurcating from the trivial line. The case of two-dimensional bifurcation kernels is instead treated in Section I.4, where the existence of small-amplitude, two-dimensional sheets of solution is proved.

I.2 Properties of the convolution kernel K_T

In the rest of this work we shall make heavy use of the properties of the convolution kernel K_T and its symbol. To start, note that $K_T = \mathcal{F}^{-1} l_T$ is smooth away from the origin with

$$\int_{\mathbb{R}} K_T(x)\,\mathrm{d}x = \lim_{\xi\to 0} l_T(\xi) = 1 \tag{I.2.1}$$

and

$$\lim_{x\to 0} K_T(x) = \int_{\mathbb{R}} l_T(\xi)\,\mathrm{d}\xi = +\infty.$$

Moreover, since l_T is analytic, K_T has rapid decay at $\pm\infty$, whence $K_T \in L^1(\mathbb{R})$ provided that the blow-up at $x = 0$ is not too fast. We will show that the singularity at the origin is of order $|x|^{-\frac{1}{2}}$ (there is a lower-order singularity appearing as well), and that the convolution kernel is completely monotone for strong enough surface tension.

I.2.1 Complete monotonicity

A function $g : (0,\infty) \to [0,\infty)$ is called *completely monotone* if g is infinitely differentiable with

$$(-1)^n g^{(n)}(\lambda) \geqslant 0$$

for $n = 0, 1, 2, \ldots$ and all $\lambda > 0$. If it can furthermore be written in the form

$$g(\lambda) = \frac{a}{\lambda} + b + \int_{(0,\infty)} \frac{1}{\lambda + t}\,\mathrm{d}\sigma(t)$$

for some constants $a, b > 0$, with σ a Borel measure satisfying $\int_{(0,\infty)} \frac{1}{1+t}\,\mathrm{d}\sigma(t) < \infty$, then it is called *Stieltjes*. Our interest in such functions is motivated by the following two results, taken from [10] and [23].

Lemma I.2.1. [10] *Let* $f : \mathbb{R} \to \mathbb{R}$ *and* $g : (0,\infty) \to \mathbb{R}$ *be two functions satisfying* $f(\xi) = g(\xi^2)$ *for* $\xi \neq 0$. *Then* f *is the Fourier transform of an even, integrable, and completely monotone function if and only if* g *is Stieltjes with* $\lim_{\lambda \searrow 0} g(\lambda) < \infty$ *and* $\lim_{\lambda \to \infty} g(\lambda) = 0$.

Lemma I.2.2. [23] *Let* g *be a positive function on* $(0,\infty)$. *Then* g *is Stieltjes if and only if* $\lim_{\lambda \searrow 0} g(\lambda)$ *exists in* $[0,\infty]$ *and* g *extends analytically to* $\mathbb{C} \setminus (-\infty, 0]$ *such that* $\operatorname{Im}(z) \cdot \operatorname{Im}(g(z)) \leqslant 0$.

With $f(\xi) = l_T(\xi)$ and $g(\xi) = l_T(\sqrt{\xi})$ we want to employ the two above results to conclude that $K_T = \mathcal{F}^{-1}(l_T(\xi))$ is completely monotone. Since l_T has a unit limit at the origin and a vanshing limit at infinity, it only remains to prove that $l_T \circ \sqrt{\cdot}$ is Stieltjes. To this end, define

$$\varrho_T(\zeta) = \frac{\zeta}{(1 + T\zeta^2)\tanh(\zeta)}, \tag{I.2.2}$$

with ζ a complex number. We are interested in $l_T = \sqrt{\varrho_T}$, $\sqrt{\cdot}$ denoting the principal branch of the square root, and thus want to determine the pre-image of $(-\infty, 0)$ together with the singularities of ϱ_T. Let furthermore

$$\begin{aligned} Z_c &= \left\{\pi(k - \tfrac{1}{2}) \colon k \in \mathbb{Z}\right\}, \\ Z_s &= \left\{\pi k \colon k \in \mathbb{Z} \setminus \{0\}\right\}, \\ Z_T &= \left\{-\tfrac{1}{\sqrt{T}}, \tfrac{1}{\sqrt{T}}\right\}, \end{aligned}$$

be the set of zeros of cos, sinc and $\zeta \mapsto 1 - T\zeta^2$, respectively. Finally, recall that the *symmetric difference* between two sets A and B is the set $A \triangle B$ of elements either in A and not B, or contrariwise.

Lemma I.2.3. *Let* $\zeta = \xi + i\eta$. *Then* ϱ_T *takes a zero or infinite value exactly if* $\xi = 0$ *and* $\eta \in Z_s \cup (Z_c \triangle Z_T)$*; and it is negative exactly if* $\xi = 0$, $\eta \notin Z_s \cup (Z_c \triangle Z_T)$ *and the intersection* $(0, |\eta|) \cap \big((Z_c \cup Z_s) \triangle Z_T\big)$ *contains an odd number of elements.*

Proof. By the infinite product formulas for $\sinh\zeta$ and $\cosh\zeta$ we obtain

$$\varrho_T(\zeta) = \frac{1}{1 + T\zeta^2} \prod_{n=1}^{\infty} \frac{1 + \frac{\zeta^2}{\pi^2(n-\frac{1}{2})^2}}{1 + \frac{\zeta^2}{\pi^2 n^2}}. \tag{I.2.3}$$

The first part of the lemma now follows immediately, where the symmetric difference accounts for removable singularities should the term $(1 + T\zeta^2)$ coincide with a term of the form $1 + \frac{\zeta^2}{\pi^2(n-\frac{1}{2})^2}$. For the second part we start by showing that ϱ_T is never negative away from the imaginary axis. As ϱ_T is symmetric about zero, we restrict our attention to $\xi > 0$. We have

$$\begin{aligned} \operatorname{Re}\Big[\cosh(\zeta)\overline{\sinh(\zeta)}\Big] &= \frac{1}{2}\sinh(2\xi) > 0, \\ \operatorname{Re}\Big[\zeta\,\overline{(1 + T\zeta^2)}\Big] &= \xi + \xi T(\xi^2 + \eta^2) > 0, \end{aligned}$$

and consequently $|\arg(\frac{\zeta}{1+T\zeta^2})|, |\arg(\frac{1}{\tanh(\zeta)})| < \frac{\pi}{2}$. This in turn implies that $|\arg(\varrho_T)| < \pi$, and so ϱ_T cannot be negative. Restricting our attention to the imaginary axis ($\zeta = i\eta$) and away from zeroes and singularities, it is clear from (I.2.3) that ϱ_T is real valued and satisfies

$$\operatorname{sgn}(\varrho_T) = \operatorname{sgn}(1 - T\eta^2) \prod_{n=1}^{\infty} \operatorname{sgn}\Big(1 - \frac{\eta^2}{\pi^2(n-\frac{1}{2})^2}\Big)\operatorname{sgn}\Big(1 - \frac{\eta^2}{\pi^2 n^2}\Big).$$

As ϱ_T is positive for $\eta = 0$, it is negative exactly when an odd number of factors in the expression above has swapped sign. This is equivalent to the last part of the lemma. ■

According to Lemma I.2.3 the real-valued function l_T can be extended analytically as $l_T = \sqrt{\varrho_T}$ outside of its singularities on the imaginary axis. With $\zeta = \xi + i\eta$, since furthermore $\sqrt{\mathbb{C} \setminus (-\infty, 0]} = \mathbb{C}_{\xi>0}$ we can record the following result.

Corollary I.2.4. *The symbol l_T extends analytically onto the strip $\mathbb{R} \times i(-\delta^*, \delta^*)$, where*

$$\delta^* = \begin{cases} \min\{\frac{1}{\sqrt{T}}, \frac{\pi}{2}\}, & T \neq 4/\pi^2, \\ \pi & T = 4/\pi^2. \end{cases}$$

Hence, the function $\zeta \mapsto \sqrt{\varrho_T(\sqrt{\zeta})}$ is the unique analytic extension of $l_T \circ \sqrt{\cdot}$ to $\mathbb{C} \setminus (-\infty, 0]$.

We may now use Lemma I.2.2 to determine a critical value of the surface tension T for the Stieltjes property of $l_T \circ \sqrt{\cdot}$. Note that this value *does not* correspond to the, likewise critical, Bond number $T = \frac{1}{3}$ that separates strong from weak surface tension.

Theorem I.2.5. *The function $l_T \circ \sqrt{\cdot}$ is Stieltjes exactly if $T \geq \frac{4}{\pi^2}$. These are the values for which the convolution kernel K_T is completely monotone.*

Proof. By positivity of $l_T \circ \sqrt{\cdot}$, the limit $\lim_{\lambda \searrow 0} l_T(\sqrt{\lambda}) = 1$ and the second part of Corollary I.2.4, it follows from Lemma I.2.2, that $l_T \circ \sqrt{\cdot}$ is Stjeltjes exactly if $\operatorname{Im}(\zeta) \cdot \operatorname{Im}\sqrt{\varrho_T(\sqrt{\zeta})} \leqslant 0$ for $\zeta \in \mathbb{C} \setminus (-\infty, 0]$. This last property is satisfied if and only if it is satisfied for $\varrho_T \circ \sqrt{\cdot}$, which we now prove is the case exactly when $T \geq \frac{4}{\pi^2}$. Assume first that $T < \frac{4}{\pi^2}$, then $\varrho_T(i\frac{\pi}{2}) = 0$ and

$$\frac{d\varrho_T}{d\zeta}\Big(i\frac{\pi}{2}\Big) = \frac{i\frac{\pi}{2}}{1 + T(i\frac{\pi}{2})^2} \frac{d\coth}{d\zeta}\Big(i\frac{\pi}{2}\Big) = \frac{i\frac{\pi}{2}}{1 - T(\frac{\pi}{2})^2},$$

demonstrating that for $\epsilon > 0$ small enough we have $\operatorname{Im}\big[\varrho_T(\varepsilon + i\frac{\pi}{2})\big] > 0$. For such an ϵ, we can set $\zeta = (\varepsilon + i\frac{\pi}{2})^2$ to also obtain $\operatorname{Im}(\zeta) > 0$. We turn to the case $T \geq \frac{4}{\pi^2}$. Moving the first factor of $\cosh\zeta$ out of the infinite product in (I.2.3) and taking the argument of both sides we obtain

$$\begin{aligned} \arg\big(\varrho_T\big(\sqrt{\zeta}\big)\big) = &\Big[\arg\Big(1 + \frac{4}{\pi^2}\zeta\Big) - \arg(1 + T\zeta)\Big] \\ &+ \sum_{n=1}^{\infty} \Big[\arg\Big(1 + \frac{\zeta}{\pi^2(n+\frac{1}{2})^2}\Big) - \arg\Big(1 + \frac{\zeta}{\pi^2 n^2}\Big)\Big]. \end{aligned} \tag{I.2.4}$$

This equation is valid whenever the right hand side takes values in $(-\pi, \pi)$, which in turn is always true in $\zeta \in \mathbb{C}\setminus(-\infty, 0]$ as it is continuous in ζ, zero for $\zeta > 0$ and prevented from taking a value in $\{-\pi, \pi\}$ as $\varrho_T(\sqrt{\zeta})$ is never negative (Lemma I.2.3). When $\mathrm{Im}(\zeta) > 0$, it is easy to see that $\alpha \mapsto \arg(1 + \alpha\zeta)$ is increasing for $\alpha > 0$, and so each square bracket in (I.2.4) is negative, which again implies $\mathrm{Im}(\zeta) \cdot \mathrm{Im}\sqrt{\varrho_T(\sqrt{\zeta})} < 0$. After a similar argument for $\mathrm{Im}(\zeta) < 0$, we obtain the first part of the theorem. The last part is a direct consequence of Lemma I.2.1 and the discussion thereafter. ■

I.2.2 Regularity properties and decay

In this subsection we split K_T according to its singularities, and determine the precise regularity of these (there are two of them, both at the origin). We also record the rapid decay and smoothing properties of K_T. Write

$$l_T = l_{-\frac{1}{2}} + l_{\frac{3}{2}} + l_\omega,$$

with $l_{-\frac{1}{2}} = \frac{1}{\sqrt{T|\xi|}}$, $l_{\frac{3}{2}}(\xi) = \sqrt{\frac{|\xi|}{1+T\xi^2}} - \frac{1}{\sqrt{T|\xi|}}$ and $l_\omega(\xi) = l_T(\xi) - \sqrt{\frac{|\xi|}{1+T\xi^2}}$. The subscripts represent the regularity of each corresponding term of K_T, as will be seen. The decay of $l_{-\frac{1}{2}} \eqsim |\xi|^{-\frac{1}{2}}$ is clear, and for any fixed $T > 0$, it is readily seen that

$$l_{\frac{3}{2}}(\xi) \eqsim |\xi|^{-\frac{5}{2}},$$

and

$$l_\omega(\xi) = \sqrt{\frac{\xi}{1+T\xi^2}}\left(\sqrt{\coth(\xi)} - 1\right) \eqsim \xi^{-\frac{1}{2}}\, e^{-2\xi},$$

both for $|\xi| \gg 1$.

To establish the regularity of the corresponding parts of K_T we shall use Zygmund spaces. Let $\{\psi_j^2\}_{j=0}^\infty$ be a partition of unity with $\psi_0(\xi)$ supported in $|\xi| \leq 1$, $\psi_1(\xi)$ supported in $\frac{1}{2} \leq |\xi| \leq 2$, and $\psi_j(\xi) = \psi_1(2^{1-j}\xi)$ for $j \geq 2$. Then the support of each ψ_j is concentrated around $\xi \eqsim 2^j$. With $D = -i\partial_x$, the Fourier multiplier operators $\psi_j(D)\colon f \mapsto \mathcal{F}^{-1}(\psi_j \hat{f})$ characterises the Zygmund spaces: we say $u \in \mathcal{C}^s(\mathbb{R})$ if

$$||u||_{\mathcal{C}^\alpha(\mathbb{R})} = \sup_j\, 2^{j\alpha}\, ||\psi_j^2(D)u||_{L^\infty} \tag{I.2.5}$$

is finite. For non-integer values of $s \geq 0$ the Zygmund spaces coincide with the standard (inhomogeneous) Hölder spaces,

$$\mathcal{C}^s(\mathbb{R}) \cong C^s(\mathbb{R}), \qquad s \in \mathbb{R}_+ \setminus \mathbb{N}_0,$$

and one furthermore has the embedding $C^k(\mathbb{R}) \hookrightarrow \mathcal{C}^k(\mathbb{R})$ for integer values of k. We refer the reader to [24, Section 13.8] and [11, Section 1.4].

Now, the symbols $l_{-\frac{1}{2}}$, $l_{\frac{3}{2}}$ and l_ω all have well-defined Fourier transforms, and we let

$$\begin{aligned} K_{-\frac{1}{2}}(x) &= \mathcal{F}^{-1}(1/\sqrt{T|\xi|}), \\ K_{\frac{3}{2}}(x) &= \mathcal{F}^{-1}(l_{\frac{3}{2}}), \\ K_\omega(x) &= \mathcal{F}^{-1}(l_\omega), \end{aligned}$$

so that

$$K_T(x) = \mathcal{F}^{-1}(l_T) = K_{-\frac{1}{2}}(x) + K_{\frac{3}{2}}(x) + K_\omega(x)$$

where we know that $K_{-\frac{1}{2}} = \sqrt{\frac{2\pi}{T|\cdot|}} \in \mathcal{C}^{\frac{1}{2}}(\mathbb{R})$, as it is an eigenfunction of the Fourier transform. Note also that K_ω is real-analytic by Paley–Wiener's theorem, as $l_\omega \in L^1(\mathbb{R})$ has exponential decay rate. The optimal regularity of $K_{\frac{3}{2}}$ follows from the following theorem about the integral kernel K_T.

Theorem I.2.6. *The integral kernel K_T may be written as*

$$K_T(x) = \sqrt{\frac{2\pi}{T|x|}} + K_{\frac{3}{2}}(x) + K_\omega(x),$$

where the second term belongs to the optimal Hölder class $C^{\frac{3}{2}}$ and the third is real-analytic. Consequently,

$$\lim_{x\to 0} \sqrt{|x|}\, K_T(x) = \sqrt{\frac{2\pi}{T}}$$

belongs to $L^1(\mathbb{R})$. Moreover,

$$K_T(x) \lesssim e^{-\delta|x|} \qquad \text{for } |\xi| \gtrsim 1,$$

with $\delta < \delta^*$ as given in Corollary I.2.4.

Proof. It only remains to determine the regularity of $K_{\frac{3}{2}}$. We have $\psi_j^2(D)K_{\frac{3}{2}} = \mathcal{F}^{-1}\left(\psi_j^2 l_{\frac{3}{2}}\right)$ and, using the L^1-norm to estimate the infinity norm, we have that

$$||\psi_j^2(D)K_{\frac{3}{2}}||_{L^\infty} \lesssim \int_{2^{j-2}}^{2^j} |l_{\frac{3}{2}}(\xi)|\, \mathrm{d}\xi \lesssim \int_{2^{j-2}}^{2^j} \xi^{-\frac{5}{2}}\, \mathrm{d}\xi \eqsim 2^{-\frac{3}{2}j}.$$

Thus

$$\sup_j 2^{\frac{3}{2}j}\, ||\psi_j^2(D)K_{\frac{3}{2}}||_{L^\infty} \lesssim 1,$$

which proves that $K_{\frac{3}{2}}(x) \in \mathcal{C}_*^{\frac{3}{2}}(\mathbb{R})$. As the full kernel has rapid decay and is smooth outside of the origin, and as $K_{\frac{3}{2}}$ and K_ω are both continuous, the asymptotics at the origin and the global integrability of K_T follow from the form and local integrability of $K_{-\frac{1}{2}} = \sqrt{2\pi/T|\cdot|}$. Finally, the decay rate is a direct consequence of Corollary I.2.4 and Paley–Wiener's theorem. ∎

We conclude this section by recording some mapping properties of the convolution operator $L_T = K_T*$. Let $\mathbb{S}$ be the one-dimensional unit sphere of circumference 2π, and note that the Hölder and Zygmund spaces are straightforward to define on the compact manifold $\mathbb{S}$ (these are the 2π-periodic functions in the larger spaces $C^s(\mathbb{R})$ and $\mathcal{C}^s(\mathbb{R})$).

Lemma I.2.7. *For each $T > 0$ and each $s \geq 0$, L_T is a continuous linear mapping $\mathcal{C}^s(\mathbb{R}) \to \mathcal{C}^{s+1/2}(\mathbb{R})$ and hence compact on $\mathcal{C}^s(\mathbb{S})$.*

Proof. Let $u \in \mathcal{C}^s(\mathbb{S})$. Using that $\psi_j^2(D)u = \mathcal{F}^{-1}(\psi_j^2(\xi)\hat{u}(\xi))$, a straightforward calculation using the boundedness and decay rate of $l_T \eqsim l_{-\frac{1}{2}}$ for $|\xi| \gg 1$ shows that $||\psi_j^2(D)L_T u||_{L^\infty} \leqslant 2^{-\frac{j}{2}+2}||\psi_j^2(D)u||_{L^\infty}$. We then have

$$\sup_j 2^{j(s+\frac{1}{2})}\,||\psi_j^2(D)L_T u||_{L^\infty} \lesssim \sup_j 2^{j\alpha}\,||\psi_j^2(D)u||_{L^\infty},$$

which proves the first assertion. Since $\mathbb{S}$ is compact it follows that the embedding $\mathcal{C}^{s+\frac{1}{2}}(\mathbb{S}) \hookrightarrow \mathcal{C}^s(\mathbb{S})$ is compact as well, and thus L is a compact operator on any Zygmund (or Hölder, or C^k) space defined over $\mathbb{S}$. ∎

I.3 One-dimensional bifurcation

An integral kernel in $L^1(\mathbb{R})$ may be periodised to an arbitrary period. Given $f \in L^\infty(\mathbb{R})$ we in particular define the 2π-periodic kernel K_p as the action of $L = K*$ in a single period:

$$\begin{aligned} Lf = \int_{\mathbb{R}} K(x-y)f(y)\,\mathrm{d}y &= \int_{-\pi}^{\pi} \left(\sum_{k\in\mathbb{Z}} K(x-y+2k\pi) \right) f(y)\,\mathrm{d}y \\ &= \int_{-\pi}^{\pi} K_p(x-y)f(y)\,\mathrm{d}y. \end{aligned}$$

To find nontrivial solutions of the equation (I.1.3), we fix $s > 1/2$ and define a map $F\colon \mathcal{C}^s_{\text{even}}(\mathbb{S}) \times \mathbb{R} \to \mathcal{C}^s_{\text{even}}(\mathbb{S})$ via

$$F(u,c) = u - cL_T(u) + L_T(u^2), \tag{I.3.1}$$

where $\mathcal{C}^s_{\text{even}}(\mathbb{S})$ is the subspace of even functions in $\mathcal{C}^s(\mathbb{S})$. Then the roots of F correspond to the even and 2π-periodic solutions of (I.1.3) with wavespeed c. Functions of Zygmund (Hölder) regularity $s > \frac{1}{2}$ have absolutely convergent Fourier series [14]. Hence, we have $F(0,c) = 0$ for all $c \in \mathbb{R}$ and the linearised operator

$$D_u F[0,c] = \mathrm{Id} - cL_T$$

has a nontrivial kernel in $\mathcal{C}^s(\mathbb{S})$ if and only if $c\,l_T(k) = 1$ for some $k \in \mathbb{N}_0$ (we intentionally include the case $k = 0$ as it will play a role in the two-dimensional bifurcation to come). In that case

$$\ker D_u F[0,c] = \operatorname{span}\{\cos(mx)\colon m \in \mathbb{N}_0 \text{ such that } l_T(m) = l_T(k)\}, \tag{I.3.2}$$

so the multiplicity of the kernel depends on the graph of the function $l_T(\xi)$. In particular, if $T > 1/3$ then $l_T(\xi)$ is monotone decreasing on $\mathbb{R}_+$ and hence the above kernel is simple. If $0 < T < 1/3$, however, the function l_T has exactly one local extremum in the interior of $\mathbb{R}_+$, whence opening the possibility of two different integers for which $l_T(m) = l_T(k)$.

Concentrating on the primary bifurcation branch, corresponding to $k = 1$ above, it follows that in this case the kernel will be simple if and only if $T \notin \{T_*(n)\}_{n\in\mathbb{N}_0}$, where

$$T_*(n) = \frac{n\tanh(1) - \tanh(n)}{n(n\tanh(n) - \tanh(1))},$$

while it will have multiplicity exactly two when $T = T_*(n)$ for some $n \in \mathbb{N}_0$. Note that the function T_* is strictly decreasing on $\mathbb{N}_0$ with $T_*(n) \to 0$ as $n \to \infty$. We here turn our attention to the branches of solutions $\{(u, c)\}$ bifurcating from the trivial line $u = 0$ at some wavespeed c_* for a fixed value of the surface tension $T > 0$ and where $\ker D_u F[0, c_*]$ is one-dimensional; two-dimensional bifurcation in the case $0 < T < \frac{1}{3}$ is dealt with in Section I.4. Note that while one-dimensional kernels appear both for sub- and supercritical wave speeds, separated by $c = 1$, two-dimensional kernels only appear for $c \in (0, 1]$.

I.3.1 The parameters

To investigate the bifurcations we will make use in the following sections of three positive quantities — the wavespeed c, the surface tension T, and a scaling in the period of the waves, κ. While the first two appear directly in the steady problem (I.1.3), the scaling $\xi \mapsto \kappa\xi$ is realised by introducing the corresponding dependence in the convolution operator L, so that

$$\widehat{L_{\kappa,T}}(\xi) = l_{\kappa,T}(\xi) := l_T(\kappa\xi). \tag{I.3.3}$$

This operator agrees with the original one for $\kappa = 1$. In addition, we see from (I.3.1) that if u is a 2π-periodic solution of $F(u, c) = 0$, and we consider $u(\kappa\,\cdot)$, then

$$\widehat{u}(\xi/\kappa) - cl_T(\xi)\widehat{u}(\xi/\kappa) + l_T(\xi)\widehat{u^2}(\xi/\kappa) = 0$$

is fulfilled on the Fourier side. The change of variables $\xi \mapsto \kappa\xi$ then justifies the definition in (I.3.3). This allows us to treat different wavelengths in the same equation by moving the wavelength parameter to $L_{\kappa,T}$.

Since surface tension is a property of the medium, while the speed and wavenumber are properties of particular waves, it is physically more relevant to use the two latter as bifurcation parameters, while holding the surface tension fixed. This is what we will do in the following.

I.3.2 Local bifurcation via Lyapunov–Schmidt

The following theorem establishes, for fixed wavelength and surface tension, the local bifurcation of small amplitude steady solutions the capillary Whitham equation. Although this is by now a standard Crandall–Rabinowitz type result [15], we prove the result using a direct Lyapunov–Schmidt reduction as to prepare for the two-dimensional bifurcation in Section I.4. This is similar to the strategy in [6]. As κ and T will be fixed — assuming that we already have a one-dimensional kernel as described in the beginning of this section — we shall here suppress the dependence upon these parameters.

Theorem I.3.1. *Let $k \in \mathbb{N}$ and set $c_0 = l_{\kappa,T}(k)^{-1}$. For any $T, \kappa > 0$ such that $\dim\ker D_u F(0, c_0) = 1$ there exists a smooth curve*

$$\{(u(t), c(t)) : 0 < |t| \ll 1\}$$

of small-amplitude solutions of the steady capillary Whitham equation (I.1.3) *with symbol given by* (I.3.3)*. These solutions satisfy*

$$\begin{aligned} u(t) &= t\cos(kx) + \mathcal{O}(t^2) \\ c(t) &= c_0 + \mathcal{O}(t). \end{aligned}$$

in $\mathcal{C}^s_{\text{even}}(\mathbb{S}) \times \mathbb{R}$, and constitute all nontrivial solutions in a neighbourhood of $(0, c_0)$ in that space.

Remark I.3.2. *There is an additional but qualitatively different bifurcation taking place at $c = 1$, where the straight curve of constant solutions $(u, c) = (c-1, c)$ crosses the trivial solution curve $(0, c)$. These solutions must be taken into consideration when constructing non-constant waves at $c = 1$ when the kernel is two-dimensional, see Theorem I.4.1.*

Remark I.3.3. *By considering the role of κ in the proof of Theorem I.3.1 one can see that by varying κ one obtains a one-dimensional family of solution curves, the starting points of which depend smoothly on κ. This may be seen also by applying the implicit function theorem directly to I.3.1. For each $k \in \mathbb{N}$ we thus obtain a two-dimensional sheet of solutions,*

$$\mathcal{S}^k = \{(u(t, \kappa), c(t, \kappa), \kappa) \colon 0 < |t| \ll 1, |\kappa - \kappa_0| \ll 1\} \tag{I.3.4}$$

parameterised by (t, κ) in a neighbourhood of a bifurcation point $(0, \kappa_0)$.

Proof. According to the assumptions and the discussion after (I.3.2), we have

$$\ker D_u F(0, c_0) = \ker(\mathrm{Id} - c_0 L) = \operatorname{span}\{\cos(k\cdot)\}.$$

We first write

$$\begin{aligned} u(t) &= t\cos(kx) + v(t), \\ c(t) &= c_0 + r(t), \end{aligned}$$

with $v(t) \in \mathcal{C}^s_{\text{even}}(\mathbb{S})$ such that $\int_{-\pi}^{\pi} \cos(kx) v \, \mathrm{d}x = 0$ and $r(t) \in \mathbb{R}$, and proceed to show the existence of v and r such that for $|t| \ll 1$ we have

$$F(t\cos(kx) + v(t), c_0 + r(t)) = 0. \tag{I.3.5}$$

As a subspace of $L^2(\mathbb{S})$, we equip $\mathcal{C}^s_{\text{even}}(\mathbb{S})$ with the L^2 inner product $\langle f, g\rangle = \frac{1}{\pi}\int_{-\pi}^{\pi} fg \, \mathrm{d}x$ and let $\Pi \colon \mathcal{C}^s_{\text{even}}(\mathbb{S}) \to \ker D_u F(0, c_0)$ be the projection onto $\operatorname{span}\{\cos(k\cdot)\}$ parallel to $\operatorname{range}(D_u F(0, c_0))$. We prove in Corollary I.3.5 below that $D_u F(0, c_0)$ is Fredholm with index 0, so that $\mathcal{C}^s_{\text{even}}(\mathbb{S})$ may be written as a direct sum between its kernel and range. Thus, (I.3.5) is equivalent to

$$\begin{aligned} \Pi F(t\cos(kx) + v, c_0 + r) &= 0, \\ (I - \Pi) F(t\cos(kx) + v, c_0 + r) &= 0, \end{aligned} \tag{I.3.6}$$

where we have suppressed the t-dependence in v and r. As

$$\begin{aligned}
&F(t\cos(kx)+v, c_0+r)\\
&= t\cos(kx)+v-(c_0+r)L(t\cos(kx)+v)+L(t\cos(kx)+v)^2\\
&= D_uF(0,c_0)(v+t\cos(kx))\\
&\quad - rL(t\cos(kx)+v)+L(t\cos(kx)+v)^2,
\end{aligned}$$

and $\cos(k\cdot)$ is in the kernel of $D_uF(0,c_0)$ the equation (I.3.5) may similarly be expressed as

$$D_uF(0,c_0)v = rL(t\cos(kx)+v)-L(t\cos(kx)+v)^2 =: g(t,r,v). \tag{I.3.7}$$

It then follows that (I.3.6) is equivalent to

$$\begin{aligned}
0 &= \Pi g(t,r,v)\\
D_uF(0,c_0)v &= (\mathrm{Id}-\Pi)g(t,r,v)
\end{aligned} \tag{I.3.8}$$

Note that since $D_uF(0,c_0)$ is invertible on $(I-\Pi)\mathcal{C}^s_{\mathrm{even}}(\mathbb{S})$, the second equation in (I.3.8) reads

$$v = [D_uF(0,c_0)]^{-1}(\mathrm{Id}-\Pi)g(t,r,v).$$

At $(t,r)=(0,0)$, we have both that $v=0$ is a solution and that the Frechèt derivative with respect to v is invertible on $(\mathrm{Id}-\Pi)\,\mathcal{C}^s_{\mathrm{even}}(\mathbb{S})$ (because $D_uF(0,c_0)$ is). Therefore, by the implicit function theorem on Banach spaces the second line of (I.3.8) has a unique solution $v(t,r)\in(\mathrm{Id}-\Pi)\,\mathcal{C}^s_{\mathrm{even}}(\mathbb{S})$ defined in a neighbourhood of $(t,r)=(0,0)$, and depending analytically on its arguments. By uniqueness, $v(0,r)=0$ for all $|r|\ll 1$. Moreover, differentiation with respect to t at $(t,r)=(0,0)$ in (I.3.7) shows that $\frac{\partial}{\partial t}v(0,r)=0$, which implies that v has no constant or linear terms in t. As it is smooth in t, it may be expanded in an (at least) quadratic series around $t=0$.

We now need to solve the equation

$$\Pi g(t,r,v(t,r)) = Q(r,t)\cos(kx) = 0$$

for r, with

$$Q(t,r) := \langle g(t,r,v(t,r)), \cos(k\cdot)\rangle.$$

Notice that that $Q(0,r)=0$ since $v(0,r)=0$ for all r, which together with the symmetry of L implies that we can write

$$Q(t,r) = t\left[r\,l(k)+R(t,r)\right],$$

where R is analytic with $R(0,0)=\partial_rR(0,0)=0$, again due to the properties of v (here, $l=l_{T,\kappa}$). An application of the implicit function theorem to the equation $r\,l(k)\pi+R(t,r)=0$ at $(t,r)=(0,0)$ then yields the existence of a locally unique smooth function $r\colon t\mapsto r(t)$ with $r(0)=0$ such that

$$Q(t,r(t))) = t(r(t)\,l(k)+\tilde{R}(t,r(t))) = 0$$

for all $|t|\ll 1$. This concludes the proof. ■

I.3.3 Global bifurcation (analytic)

We now extend the local bifurcation curves from Section I.3.2 to global ones by the means of the analytic bifurcation theory pioneered by Dancer [4, 5] and then developed further by Buffoni and Toland [3]. We define $N\colon \mathcal{C}^s(\mathbb{S}) \times \mathbb{R}_+ \to \mathcal{C}^{s+1/2}(\mathbb{S})$, $s \geq 0$, by

$$N(u, c) = L(cu - u^2).$$

Fixed points of N are solutions to the capillary-gravity Whitham equation (I.1.1) and conversely. Let

$$S = \{(u, c) \in \mathcal{C}^s(\mathbb{S}) \times \mathbb{R}_+ \colon F(u, c) = 0\}$$

be the set of solutions (fixed points of N). It then follows from Lemma I.2.7 that $S \subset \mathcal{C}^\infty \times \mathbb{R}_+$, so that all solutions are smooth. By combining this with a diagonal argument one obtains the following compactness result.

Lemma I.3.4. *Bounded and closed sets in S are compact in $\mathcal{C}^s(\mathbb{S}) \times \mathbb{R}_+$.*

Proof. Let $K \subset S \subset \mathcal{C}^s(\mathbb{S}) \times \mathbb{R}_+$ be closed and bounded, and pick a sequence $(u_j, c_j)_j \subset K$. Since $\{c \in \mathbb{R}_+ \colon (u, c) \in K\}$ is a closed and bounded subset of $\mathbb{R}$, it is compact. This means that $(c_j)_j$ has a convergent subsequence, name it $(c_k)_k$. The sequence $(u_k, c_k)_k \subset K$ then converges in the second component, where $u_k = N(u_k, c_k)$. Since $N(\cdot, c)$ is a compact operator on $\mathcal{C}^s(\mathbb{S})$ thanks to Lemma I.2.7, the sequence $(u_k)_k$ is pre-compact in $\mathcal{C}^s(\mathbb{S})$. Thus we can pick a further subsequence $(u_l)_l$ which converges in $\mathcal{C}^s(\mathbb{S})$ so that the sequence $(u_l, c_l)_l \subset K$ converges in $\mathcal{C}^s(\mathbb{S}) \times \mathbb{R}_+$. As K is closed the limit point belongs to K, and hence K is compact. ∎

Corollary I.3.5. *The Frechèt derivative $D_u F(u, c)$ is a Fredholm operator of index 0 at any point $(u, c) \in C^\alpha_{\text{even}}(\mathbb{S}) \times \mathbb{R}$.*

Proof. This follows immediately from Lemma I.3.4 as then

$$D_u F(u, c) = \mathrm{Id} - L(c - 2u)$$

is a compact perturbation of the identity. ∎

Theorem I.3.6. *Whenever*

$$\frac{3c_0 l(2k) - l(2k) - 2}{(c_0 - 1)(c_0 l(2k) - 1)} \tag{I.3.9}$$

is finite and non-vanishing the local bifurcation curve $t \mapsto (u(t), c(t))$, $|t| \ll 1$, from Lemma I.3.1 extends to a continuous and locally analytically re-parameterisable curve defined for all $t \in [0, \infty)$. One of the following alternatives holds:

(i) $\|(u(t), c(t))\|_{\mathcal{C}^s(\mathbb{S}) \times \mathbb{R}} \to \infty$ *as* $t \to \infty$.

(ii) $t \mapsto (u(t), c(t))$ *is P-periodic for some finite P, so that the curve forms a loop.*

Remark I.3.7. *The null set where the condition on* (I.3.9) *may fail is extremely small. In particular, for fixed $T < 1/3$ the numerator of* (I.3.9) *has two zeros in k, while for $T > 1/3$ it has one. It is possible that one could still do global bifurcation in this case by investigating fourth-order derivatives of the bifurcation curve, but we have not pursued this here.*

Proof. This theorem is a version of the global analytic bifurcation theorem in [3], and — apart from the bifurcation formulas — the proof goes as in the purely gravitation case in [7, 10]. The assumptions are fulfilled from Lemma I.3.4 and Corollary I.3.5 if one can just show that some derivative $c^{(k)}(0)$ is non-vanishing. We give the calculations for $\dot{c}(0)$ and $\ddot{c}(0)$ in the Appendix; the first is 0, and the second is given by (I.3.9). Note that a third alternative in the theorem in [3] does not happen here, as the set $\mathcal{C}^s(\mathbb{S}) \times \mathbb{R}$ lacks a boundary. ■

I.4 Two-dimensional local bifurcation

We now focus our attention on the case of a two-dimensional bifurcation kernel in $\mathcal{C}^s_{\text{even}}(\mathbb{S})$. To enable the necessary two degrees of freedom we shall make use of the wavelength κ in addition to the wavespeed c, while the surface tension T is assumed to be fixed. We shall therefore study the operator

$$F_\kappa(u, c) = u + L_\kappa(u^2 - cu)$$

and its linearisation

$$\mathcal{L} = D_u F_{\kappa_0}(0, c_0) = \mathrm{Id} - c_0 L_{\kappa_0}$$

assuming that $T, \kappa_0, c_0 > 0$ are constants such that

$$\ker(\mathcal{L}) = \operatorname{span}\{\cos(k_1 \cdot), \cos(k_2 \cdot)\}, \tag{I.4.1}$$

which happens when $\kappa_0, c_0 > 0$ and $k_1, k_2 \in \mathbb{N}_0$, $k_1 \neq k_2$, are such that

$$c_0 = l_{\kappa_0}(k_1)^{-1} = l_{\kappa_0}(k_2)^{-1},$$

as described at the start of Section I.3 (we suppress the dependence on T, as it will not be used apart from in this assumption). A two-dimensional kernel can arise only for $c_0 \in (0, 1]$. Let now $1 \leq k_1 \leq k_2$. With $\mathcal{S}^k$ being the sheet of $2\pi/k$-periodic solutions defined in (I.3.4) we shall show that in addition to the solutions in $\mathcal{S}^{k_1}$ and $\mathcal{S}^{k_2}$, we may obtain solutions in a set called $\mathcal{S}^{mixed}$ consisting of perturbations of functions in the span of $\cos(k_1 \cdot)$ and $\cos(k_2 \cdot)$. Assuming that $k_1 \leq k_2$, the resonant case when k_2 is a multiple of k_1 (sometimes referred to as Wilton ripples) is more difficult than the generic case, but we follow here the procedure in [6, 9] to construct a slit disk of solutions also in that case. Numerical calculations indicate that this set is optimal [22].

When one of the wave numbers is zero (meaning $c_0 = 1$), we instead call that one k_2, and we will automatically have the resonant case, as then $k_1 \mid k_2$. That case is included in the below theorem. Hence, at $c = 1$ there is a nontrivial bifurcation, but the arising waves always have a non-zero component in the constant direction.

Theorem I.4.1. *Let $T > 0$ be fixed and assume that* (I.4.1) *holds.*

(i) When k_1 does not divide k_2 there is a full, smooth, sheet

$$\mathcal{S}^{mixed} = \{(u(t_1,t_2), c(t_1,t_2), \kappa(t_1,t_2)) : 0 < |(t_1,t_2)| \ll 1\}$$

of solutions

$$\begin{aligned} u(t_1,t_2) &= t_1\cos(k_1 x) + t_2\cos(k_2 x) + \mathcal{O}(|(t_1,t_2)|^2),\\ c(t_1,t_2) &= c_0 + \mathcal{O}((t_1,t_2)),\\ \kappa(t_1,t_2) &= \kappa_0 + \mathcal{O}((t_1,t_2)), \end{aligned}$$

to the steady capillary-gravity Whitham equation (I.1.3)*. The set $\mathcal{S}^{k_1} \cup \mathcal{S}^{k_2} \cup \mathcal{S}^{mixed}$ contains all nontrivial solutions of this equation in a neighbourhood of $(0, c_0, \kappa_0)$.*

(ii) When k_1 divides k_2 there exists for any $\delta > 0$ a small but positive ε_δ and a slit, smooth, sheet of solutions

$$\mathcal{S}^{mixed}_\delta = \{(u(\varrho,\vartheta), c(\varrho,\vartheta), \kappa(\varrho,\vartheta)) : 0 < \varrho < \varepsilon_\delta,\ \delta < |\vartheta| < \pi - \delta\}$$

with

$$\begin{aligned} u(\varrho,\vartheta) &= \varrho\cos(\vartheta)\cos(k_1 x) + \varrho\sin(\vartheta)\cos(k_2 x) + \mathcal{O}(\varrho^2),\\ c(\varrho,\vartheta) &= c_0 + \mathcal{O}(\varrho),\\ \kappa(\varrho,\vartheta) &= \kappa_0 + \mathcal{O}(\varrho). \end{aligned}$$

In a neighbourhood of $(0, c_0, \kappa_0)$ the set $\mathcal{S} = \mathcal{S}^{k_2} \cup \mathcal{S}^{mixed}$ contains all nontrivial solutions of (I.1.3) *such that $\delta < |\vartheta| < \pi - \delta$.*

Proof. We start by writing

$$\begin{aligned} u(t_1,t_2) &= t_1\cos(k_1 x) + t_2\cos(k_2 x) + v,\\ c(t_1,t_2) &= c_0 + r,\\ \kappa(t_1,t_2) &= \kappa_0 + p, \end{aligned}$$

where, generically, we want to find v, r and p parameterised by (t_1,t_2) such that

$$F_{\kappa_0+p}(t_1\cos(k_1 x) + t_2\cos(k_2 x) + v, c_0 + r) = 0, \tag{I.4.2}$$

for sufficiently small values of (t_1,t_2). As in the proof of Theorem I.3.1 we let $\Pi\colon C^\alpha_{\text{even}}(\mathbb{S}) \to \ker(D_u F_{\kappa_0}(0,c_0))$ be the projection onto $\ker(D_u F_{\kappa_0}(0,c_0))$ parallel to $\operatorname{range}(D_u F_{\kappa_0}(0,c_0))$, where we have equipped $C^\alpha_{\text{even}}(\mathbb{S})$ with the L^2 inner product $\langle f, g\rangle = \frac{1}{\pi}\int_{-\pi}^{\pi} fg \ \mathrm{d}x$. According to Corollary I.3.5 equation (I.4.2) is then equivalent to

$$\begin{cases} \Pi F_{\kappa(t_1,t_2)}\left(u(t_1,t_2), c(t_1,t_2)\right) = 0\\ (\mathrm{Id} - \Pi) F_{\kappa(t_1,t_2)}\left(u(t_1,t_2), c(t_1,t_2)\right) = 0. \end{cases} \tag{I.4.3}$$

Note that under the above ansatz, where it is assumed that $\Pi v = 0$,

$$\begin{aligned} F_\kappa(u,c) &= t_1\cos(k_1x) + t_2\cos(k_2x) + v \\ &\quad + L_{\kappa_0+p}\left[(t_1\cos(k_1x) + t_2\cos(k_2x) + v)^2\right. \\ &\quad \left.-(c_0+r)(t_1\cos(k_1x) + t_2\cos(k_2x) + v)\right] \\ &= (v - c_0L_{\kappa_0+p}v) + t_1\left(\cos(k_1x) - c_0L_{\kappa_0+p}\cos(k_1x)\right) \\ &\quad + t_2\left(\cos(k_2x) - c_0L_{\kappa_0+p}\cos(k_2x)\right) \\ &\quad - rL_{\kappa_0+p}(t_1\cos(k_1x) + t_2\cos(k_2x) + v) \\ &\quad + L_{\kappa_0+p}(t_1\cos(k_1x) + t_2\cos(k_2x) + v)^2, \end{aligned}$$

and writing $L_{\kappa_0+p} = L_{\kappa_0} + (L_{\kappa_0+p} - L_{\kappa_0})$ we have

$$\begin{aligned} F_\kappa(u,c) &= D_uF_{\kappa_0}(0,c_0)v - c_0(L_{\kappa_0+p} - L_{\kappa_0})v \\ &\quad - t_1c_0(L_{\kappa_0+p} - L_{\kappa_0})\cos(k_1x) - t_2c_0(L_{\kappa_0+p} - L_{\kappa_0})\cos(k_2x) \\ &\quad - rL_{\kappa_0+p}(t_1\cos(k_1x) + t_2\cos(k_2x) + v) \\ &\quad + L_{\kappa_0+p}(t_1\cos(k_1x) + t_2\cos(k_2x) + v)^2 \\ &=: D_uF_{\kappa_0}(0,c_0)v - g(t_1,t_2,r,p,v). \end{aligned}$$

Therefore (I.4.2) is equivalent to

$$D_uF_{\kappa_0}(0,c_0)v = g(t_1,t_2,r,p,v), \tag{I.4.4}$$

and we can rewrite (I.4.3) as

$$\begin{cases} 0 = \Pi g(t_1,t_2,r,p,v) \\ D_uF_{\kappa_0}(0,c_0)v = (\mathrm{Id}-\Pi)g(t_1,t_2,r,p,v). \end{cases} \tag{I.4.5}$$

Note that since v is orthogonal to $\ker(D_uF_{\kappa_0}(0,c_0))$ the second equation in (I.4.5) reads $v = D_uF_{\kappa_0}(0,c_0)^{-1}(\mathrm{Id}-\Pi)g(t_1,t_2,r,p,v)$. It is clear that

$$D_uF_{\kappa_0}(0,c_0)v - (\mathrm{Id}-\Pi)g(t_1,t_2,r,p,v) = 0$$

has the solution $(t_1,t_2,r,p,v) = (0,0,0,0,0)$ and at that point the Frechèt derivative respect to v is $D_uF_{\kappa_0}(0,c_0)$, which is invertible on $(\mathrm{Id}-\Pi)C^\alpha_{\mathrm{even}}(\mathbb{S})$. The implicit function theorem then ensures the existence of a solution $v = v(t_1,t_2,r,p) \in (\mathrm{Id}-\Pi)C^\alpha_{\mathrm{even}}(\mathbb{S})$. By uniqueness we have that $v(0,0,r,p) = 0$ for all small enough values of r and p. Moreover, note that $\frac{\partial}{\partial t_1}v(0,0,0,0) = 0$ and $\frac{\partial}{\partial t_2}v(0,0,0,0) = 0$. This follows by differentiating (I.4.4) respect to t_1 or t_2, and evaluating at $(t_1,t_2,r,p) = (0,0,0,0)$ recalling that $D_uF_{\kappa_0}(0,c_0)$ is invertible on its range. As a consequence, v depends at least quadratically on t_1 and t_2.

We are now left with solving the finite-dimensional problem given by the first equation in (I.4.5). To this end, we decompose the projection Π as $\Pi = \Pi_1 + \Pi_2$, where Π_1 is the projection onto $\cos(k_1\cdot)$, and Π_2 is the projection onto $\cos(k_2\cdot)$. Then

$$\Pi g = \Pi_1 g + \Pi_2 g = Q_1\cos(k_1x) + Q_2\cos(k_2x),$$

with $Q_j = \langle g, \cos(k_j \cdot)\rangle$, and the first line of (I.4.5) is equivalent to showing that

$$Q_1 = Q_2 = 0. \tag{I.4.6}$$

The non-resonant case. Assume that $k_2/k_1 \notin \mathbb{N}_0$. Using the properties of v and Π_1, a direct calculation shows that

$$\begin{aligned} Q_1 = t_1 \big[& c_0\big(l((\kappa_0+p)k_1) - l(\kappa_0 k_1)\big) + r\, l((\kappa_0+p)k_1)\big] \\ & - l((\kappa_0+p)k_1)\left\langle \cos(k_1\cdot), (t_1\cos(k_1\cdot) + t_2\cos(k_2\cdot) + v(t_1,t_2,r,p))^2\right\rangle. \end{aligned} \tag{I.4.7}$$

As $v(0,t_2,r,p)$ is $2\pi/k_2$-periodic and $k_2 \neq k_1$, the inner product vanishes for $t_1 = 0$. Therefore we may write

$$Q_1(t_1,t_2,r,p) = t_1\, \Psi_1(t_1,t_2,r,p) \tag{I.4.8}$$

with

$$\Psi_1(t_1,t_2,r,p) = \int_0^1 \frac{\partial Q_1}{\partial t_1}(z t_1,t_2,r,p)\, \mathrm{d}z \tag{I.4.9}$$

so that

$$\Psi_1(0,0,r,p) = c_0\left[l((\kappa_0+p)k_1) - l(\kappa_0 k_1)\right] + r\, l((\kappa_0+p)k_1). \tag{I.4.10}$$

Similarly, we have

$$\begin{aligned} Q_2 = t_2 \big[& c_0\big(l((\kappa_0+p)k_2) - l(\kappa_0 k_2)\big) + r\, l((\kappa_0+p)k_2)\big] \\ & - l((\kappa_0+p)k_2)\left\langle \cos(k_2\cdot), (t_1\cos(k_1\cdot) + t_2\cos(k_2\cdot) + v(t_1,t_2,r,p))^2\right\rangle \end{aligned} \tag{I.4.11}$$

with the inner product vanishing at $t_2 = 0$ since we assumed $k_2/k_1 \notin \mathbb{N}_0$. Another application of the fundamental theorem of calculus yields

$$Q_2(t_1,t_2,r,p) = t_2\, \Psi_2(t_1,t_2,r,p) \tag{I.4.12}$$

with

$$\Psi_2(t_1,t_2,r,p) = \int_0^1 \frac{\partial Q_2}{\partial t_2}(t_1, z t_2,r,p)\, \mathrm{d}z \tag{I.4.13}$$

which gives

$$\Psi_2(0,0,r,p) = c_0\left[l((\kappa_0+p)k_2) - l(\kappa_0 k_2)\right] + r\, l((\kappa_0+p)k_2). \tag{I.4.14}$$

Hence, condition (I.4.6) is equivalent to

$$\begin{cases} t_1 \Psi_1(t_1,t_2,r,p) = 0 \\ t_2 \Psi_2(t_1,t_2,r,p) = 0. \end{cases}$$

We have four cases: $t_1 = t_2 = 0$ represents the trivial solutions. When $\Psi_1 = 0$ and $t_2 = 0$ we can apply the one-dimensional bifurcation theorem and the remark following it to obtain the solutions in $\mathcal{S}^{k_1}$. Similarly, when $t_1 = 0$ and $\Psi_2 = 0$ we instead retrieve

the solutions in $\mathcal{S}^{k_2}$. To obtain the mixed-period solutions we apply the implicit function theorem to solve $\Psi_1 = \Psi_2 = 0$. Calculating the jacobian of (Ψ_2, Ψ_2) we have

$$\begin{aligned}\det \begin{bmatrix} D_r\Psi_1(0,0,r,p) & D_p\Psi_1(0,0,r,p) \\ D_r\Psi_2(0,0,r,p) & D_p\Psi_2(0,0,r,p) \end{bmatrix}\Bigg|_{(r,p)=(0,0)} \\ = c_0\, l(\kappa_0 k_1)\left[l'(\kappa_0 k_2)\, k_2 - l'(\kappa_0 k_1)\, k_1\right] \end{aligned} \tag{I.4.15}$$

which is always different from 0 since l_T has only one stationary point and $l_T(\kappa_0 k_1) \neq 0$. Also note that there can be no cancellation in the parenthesis, since the two derivative terms always have opposite signs. The Implicit Function Theorem can then be applied, giving the solutions in $\mathcal{S}^{mixed}$. In every of the four cases the above shows that $r = r(t_1, t_2)$ and $p = p(t_1, t_2)$. The fact that $r(0,0) = p(0,0) = 0$ following from the implicit function theorem, shows that r and p have at least linear dependence on t_1 and t_2.

If instead $k_2/k_1 \in \mathbb{N}_0$, we do not know that the integral in the expression for Q_2 vanishes at $t_2 = 0$; however, we know that it vanishes at $t_1 = t_2 = 0$. It is then convenient to rewrite Q_2 with the help of polar coordinates $t_1 = \varrho\cos(\vartheta), t_2 = \varrho\sin(\vartheta)$ to obtain

$$\begin{aligned} Q_2(\varrho,\vartheta,r,p) = {} & \varrho\sin(\vartheta)c_0\big(l((\kappa_0+p)k_2) - l(\kappa_0 k_2)\big) \\ & + \varrho\sin(\vartheta) r\, l((\kappa_0+p)k_2) \\ & - l((\kappa_0+p)k_2)\frac{1}{\pi}\int_{-\pi}^{\pi}\cos(k_2 x)\big[\varrho\cos(\vartheta)\cos(k_1 x) \\ & + \varrho\sin(\vartheta)\cos(k_2 x) + v(\varrho\cos(\vartheta),\varrho\sin(\vartheta),r,p)\big]^2\,\mathrm{d}x, \end{aligned} \tag{I.4.16}$$

so that now $Q_2(0,\vartheta,r,p) = 0$. As before we apply the fundamental theorem of calculus to obtain

$$Q_2(\varrho,\vartheta,r,p) = \varrho\,\Psi_2(\varrho,\vartheta,r,p) \tag{I.4.17}$$

with

$$\Psi_2(\varrho,\vartheta,r,p) = \int_0^1 \frac{\partial Q_2}{\partial\varrho}(z\varrho,\vartheta,r,p)\,\mathrm{d}z \tag{I.4.18}$$

and

$$\begin{aligned}\Psi_2(0,\vartheta,r,p) = {} & \sin(\vartheta)\, c_0\left[l((\kappa_0+p)k_2) - l(\kappa_0 k_2)\right] \\ & + r\sin(\vartheta)\, l((\kappa_0+p)k_2). \end{aligned} \tag{I.4.19}$$

For Q_1, instead, all the previous calculations remain true and we can still define Ψ_1 as before, simply rewriting it in polar coordinates. We obtain that condition (I.4.6) is now equivalent to

$$\begin{cases} \varrho\cos(\vartheta)\Psi_1(\varrho,\vartheta,r,p) = 0 \\ \varrho\,\Psi_2(\varrho,\vartheta,r,p) = 0. \end{cases}$$

The case $\varrho = 0$ corresponds to trivial solutions, while the case $\cos(\vartheta) = 0, \Psi_2 = 0$ corresponds to solutions in $\mathcal{S}^{k_2}$. For the case $\Psi_1 = 0, \Psi_2 = 0$ we again apply the implicit function theorem to (Ψ_1, Ψ_2) at $\varrho = 0$. The determinant of the jacobian is given by

$$\begin{aligned}\det \begin{bmatrix} D_r\Psi_1(0,\vartheta,r,p) & D_p\Psi_1(0,\vartheta,r,p) \\ D_r\Psi_2(0,\vartheta,r,p) & D_p\Psi_2(0,\vartheta,r,p) \end{bmatrix}\Bigg|_{(r,p)=(0,0)} \\ = \sin(\vartheta)\, c_0\, l(\kappa_0 k_1)\left[l'(\kappa_0 k_2)\, k_2 - l'(\kappa_0 k_1)\, k_1\right], \end{aligned} \tag{I.4.20}$$

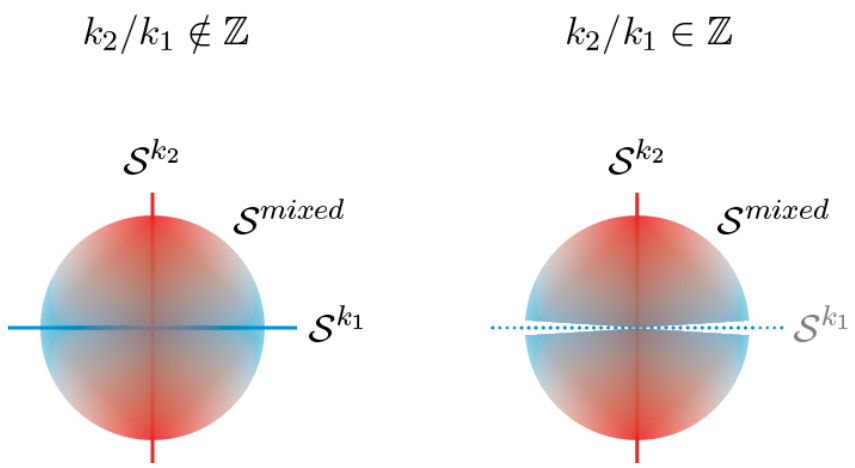

Figure I.1: A sketch of the solution disk for the Whitham equation at a point where the bifurcation kernel is tro-dimensional. Note, in particular, that it is possible to connect waves with k_1 mode to waves with k_2 mode via a curve of mixed-modes solutions.

so the matrix is invertible as long as $\sin(\vartheta) \neq 0$, i.e. we require $\delta < |\vartheta| < \pi - \delta$.

The quadratic dependence of v on ϱ follows as above by rewriting the second equation in (I.4.5) in polar coordinates and differentiating respect to ϱ. For r and p the linear dependence on ϱ comes from the application of the implicit function theorem, showing $r(0, \vartheta) = p(0, \vartheta) = 0$. ■

This theorem shows that near a two-dimensional bifurcation point in the case where $k_2/k_1 \notin \mathbb{N}_0$ there exist a full disk of solutions, while if $k_2/k_1 \in \mathbb{N}_0$ the disk is slit with one axis removed. This situation is summarised in Figure I.1. In particular this means that it is possible to find curves connecting solutions with different wavenumbers. Several numerical examples of this happening have been shown in [22, Section 4.3]. The phenomena of branches with different modes connecting through secondary bifurcation points has also been studied by Aston in [2] for the full Euler equations. While we were not able to relate our values of the parameters, the qualitative behaviour we find here for the Whitham equation is in line with those results for Euler, see in particular [2, Figure 4 and 5].

I.5 Appendix

This appendix contains higher order expansions of the quantities in Theroem I.3.1 and Theorem I.4.1. We start with the first and second order terms in the expansion for the speed $c(t)$ in the one-dimensional bifurcation case, which is required by the proof of the global extension in Theorem I.3.9, and then proceed to give the first order terms for the expansions of r and p in the two-dimensional bifurcation case.

I.5.1 One-dimensional bifurcation case

We here determine the derivatives $\dot{c}(0)$ and $\ddot{c}(0)$ of the bifurcation curve constructed in Theorem I.3.1. This can be done either directly using the Lyapunov–Schmidt reduction

carried out in the proof of Theorem I.3.1 or by the means of bifurcation formulas given for example in [15]. The latter requires an identification between the bifurcation function $\Phi(u,c) = \Pi F(u+\psi(u,c),c)$ used in [15] and the functions v and r used in the proof of Theorem I.3.1. This relation is given by $v(t) = \psi(t\cos(kx), c(t))$. We, however, start from the Lyapunov–Schmidt representation

$$\begin{aligned} 0 &= F(t\cos(kx) + v(t), c_0 + r(t)) \\ &= t\cos(kx) + v(t) \\ &\quad + L\left[(t\cos(kx)+v(t))^2 - (c_0+r(t))(t\cos(kx)+v(t))\right]. \end{aligned}$$

Differentiating once and using that $v(0) = \dot{v}(0) = r(0) = 0$, one easily sees that

$$\dot{c}(0) = \dot{r}(0) = \frac{1}{2}\frac{\int_{-\pi}^{\pi}(1+l(2k)\cos(2kx))\cos(kx)\,\mathrm{d}x}{l(k)\pi} = 0,$$

when $\ker(D_uF[0,c_0])$ is one-dimensional (in the case when $l(k) = l(2k)$ and we have a two-dimensional bifurcation, this quantity does not vanish). To determine $\ddot{c}(0)$ we instead differentiate twice with respect to t to obtain that

$$\ddot{F}|_{t=0} = (\mathrm{Id} - c_0L)\ddot{v}(0) + 2L\cos^2(kx) = 0,$$

as $r(t) = \dot{r}(t) = v(0) = \dot{v}(0) = 0$. In particular,

$$\ddot{v}(0) = -\left(D_uF[0,c_0]\right)^{-1} L\cos^2(kx). \tag{I.5.1}$$

In the same way, taking a third derivative respect to t and evaluating at $t=0$, one sees that

$$\dddot{F}|_{t=0} = (\mathrm{Id} - c_0L)\dddot{v}(0) - 3\dot{r}(0)L\cos(kx) + 6L\left(\cos(kx)\ddot{v}(0)\right) = 0,$$

so that

$$3l(k)\cos(kx)\ddot{r}(0) = (\mathrm{Id} - c_0L)\dddot{v}(0) + 6L\left(\cos(kx)\ddot{v}(0)\right). \tag{I.5.2}$$

By (I.5.1),

$$\begin{aligned} L\left(\cos(kx)\ddot{v}(0)\right) = &\left[\frac{l(k)}{c_0-1} + \frac{l(k)l(2k)}{2\left(c_0l(2k)-1\right)}\right]\cos(kx) \\ &+ \frac{l(k)l(3k)}{2\left(c_0l(2k)-1\right)}\cos(3kx), \end{aligned}$$

and as the first term in (I.5.2) is orthogonal to $\ker(D_uF[0,c_0])$, we may integrate against $\cos(kx)$ to get

$$\begin{aligned} &\langle 3l(k)\ddot{r}(0)\cos(kx), \cos(kx)\rangle \\ &\quad = \frac{6}{\pi}\int_{-\pi}^{\pi}\left[\frac{l(k)}{c_0-1} + \frac{l(k)l(2k)}{2\left(c_0l(2k)-1\right)}\right]\cos^2(kx)\,\mathrm{d}x \\ &\quad = 6l(k)\left(\frac{1}{c_0-1} + \frac{l(2k)}{2\left(c_0l(2k)-1\right)}\right). \end{aligned}$$

This means

$$\ddot{r}(0) = \frac{3c_0l(2k) - l(2k) - 2}{(c_0-1)(c_0l(2k)-1)}, \tag{I.5.3}$$

which is the expression (I.3.9) for $\ddot{c}(0)$ given in Theorem I.3.6.

I.5.2 Two-dimensional bifurcation case

Thanks to Theorem I.4.1 we know that

$$\begin{aligned} u(t_1,t_2) &= t_1\cos(k_1x) + t_2\cos(k_2x) + v(t_1,t_2),\\ c(t_1,t_2) &= c_0 + r(t_1,t_2),\\ \kappa(t_1,t_2) &= \kappa_0 + p(t_1,t_2); \end{aligned}$$

with v of order $\mathcal{O}(|(t_1,t_2)|^2)$ and r, p of order $\mathcal{O}(|(t_1,t_2)|)$. For the functions $r(t_1,t_2)$ and $p(t_1,t_2)$ we have the following:

Proposition I.5.1. *If $k_2/k_1 \notin \mathbb{N}_0$,*

$$\nabla r(0,0) = 0, \qquad \nabla p(0,0) = 0.$$

If instead $k_2/k_1 \in \mathbb{N}_0$, then in polar coordinates

$$r_\varrho(0,0) = 0, \qquad p_\varrho(0,0) = 0,$$

only if $k_2 \notin \{0, 2k_1\}$.

Proof. We start with the non-resonant case, $k_2/k_1 \notin \mathbb{N}_0$. By the definition of $r(t_1,t_2)$ and $p(t_1,t_2)$ we have the identity

$$\Psi_i(t_1,t_2,r(t_1,t_2),p(t_1,t_2)) = 0, \quad i = 1,2;$$

where the Ψ_i are the same as in Theorem I.4.1. Differentiating respect to t_j, $j = 1,2$, and evaluating at $(t_1,t_2) = (0,0)$, gives

$$\Psi_{i,t_j}(0,0,0,0) + \Psi_{i,r}(0,0,0,0)\, r_{t_j}(0,0) + \Psi_{i,p}(0,0,0,0)\, p_{t_j}(0,0) = 0.$$

Note that both of these systems, for $j = 1,2$, are solvable for the derivatives of r and p since the system matrix is invertible by Equation (I.4.15).

We are then left with finding the values of the terms $\Psi_{i,t_j}(0,0,0,0)$ which, by the definitions of Ψ_1 and Ψ_2, amounts to calculating the second order derivatives of Q_1 and Q_2. Differentiating Equation (I.4.7) twice respect to t_1 gives

$$\frac{\partial^2 Q_1}{\partial t_1^2}(0,0,0,0) = -\frac{2}{\pi}\, l(\kappa_0 k_1) \int_{-\pi}^{\pi} \cos^3(k_1x)\, \mathrm{d}x$$

and the integral vanishes. The same holds for the double derivative of Q_2 respect to t_2. The mixed derivative satisfies

$$\frac{\partial^2 Q_1}{\partial t_1 \partial t_2}(0,0,0,0) = -\frac{2}{\pi} l(\kappa_0 k_2) \int_{-\pi}^{\pi} \cos^2(k_1x)\cos(k_2x)\, \mathrm{d}x$$

where the integral vanishes since $k_2/k_1 \notin \mathbb{N}_0$. A similar calculation holds for the mixed derivative of Q_2. We therefore have $\Psi_{i,t_j} = 0$ for $i = 1,2$ and $j = 1,2$. This, together with the invertibility of the system matrices, gives $\nabla r(0,0) = 0$ and $\nabla p(0,0) = 0$.

If instead $k_1|k_2$, we need to solve the system

$$\Psi_{i,\varrho}(0,\vartheta,0,0) + \Psi_{i,r}(0,\vartheta,0,0)\, r_\varrho(0,\vartheta) + \Psi_{i,p}(0,\vartheta,0,0)\, p_\varrho(0,\vartheta) = 0. \tag{I.5.4}$$

Again, the system matrix is invertible by Equation (I.4.20). The function Ψ_1 is still defined as in Equation (I.4.9) but we rewrite it in polar coordinates. Taking one derivative respect to ϱ gives

$$\begin{aligned}\Psi_{1,\varrho}(\varrho,\vartheta,0,0) = \int_0^1 &\frac{\partial^2 Q_1}{\partial t_1^2}(z\varrho\cos(\vartheta), \varrho\sin(\vartheta), 0, 0)\, z\cos(\vartheta) \\ &+ \frac{\partial^2 Q_1}{\partial t_1 \partial t_2}(z\varrho\cos(\vartheta), \varrho\sin(\vartheta), 0, 0)\sin(\vartheta)\, \mathrm{d}z.\end{aligned}$$

For the sake of clarity we keep using the notation $\frac{\partial Q_1}{\partial t_1}$, marking that it is to be understood as the derivative respect to the first variable, and similarly for the mixed derivative. At $\varrho = 0$ the double derivative vanishes as before, but from the calculation done in the previous case we can already see that the mixed derivative will not vanish if $k_2 = 0$ or if $k_2 = 2\,k_1$. In those cases we have

$$\begin{aligned}\Psi_{1,\varrho}(0,\vartheta,0,0) &= -2\sin(\vartheta) l(\kappa_0 k_1) \quad \text{if} \quad k_2 = 0, \\ \Psi_{1,\varrho}(0,\vartheta,0,0) &= -\sin(\vartheta) l(\kappa_0 k_1) \quad \text{if} \quad k_2 = 2k_1,\end{aligned} \tag{I.5.5}$$

which are always non-zero since ϑ is bounded away from 0 and π as by the assumptions of Theorem I.4.1. This concludes the proof of the statement. For completeness, we give also the derivatives of Ψ_2, defined now as in Equation (I.4.18). Differentianting twice respect to ϱ we see that $\partial^2 Q_2/\partial\varrho^2$ may not vanish at $\varrho = 0$ if $k_2 = 0$ or $k_2 \neq 2\,k_1$. In those cases we calculate

$$\begin{aligned}\Psi_{2,\varrho}(0,\vartheta,0,0) &= -\cos^2(\vartheta) l(\kappa_0 k_2) \quad \text{if} \quad k_2 = 0, \\ \Psi_{2,\varrho}(0,\vartheta,0,0) &= -\frac{1}{2}\cos^2(\vartheta) l(\kappa_0 k_2) \quad \text{if} \quad k_2 = 2k_1,\end{aligned} \tag{I.5.6}$$

which are non-zero for $\vartheta \neq \pi/2$.

■

Remark I.5.2. *The special case $k_2 = 2k_1$ has been found also in the Euler equations (with gravity and vorticity) by the authors of [1]. The special case $k_2 = 0$ is instead due to the transcritical double bifurcation allowed by the capillary Whitham equation.*

Remark I.5.3. *An explicit example where $r_\varrho(0,\vartheta) \neq 0$ can be seen in [22, Figure 6], where the branch of nontrivial solutions has a non-vertical tangent at the bifurcation point in the speed-height plane.*

References

[1] A. Aasen and K. Varholm. "Traveling Gravity Water Waves with Critical Layers". In: *Journal of Mathematical Fluid Mechanics* 20.1 (2018), pp. 161–187.

[2] P.J. Aston. "Local and global aspects of the (1,n) more interaction for capillary-gravity waves". In: *Physica D* 52 (1991), pp. 415–428.

[3] B. Buffoni and J. Toland. *Analytic Theory of Global Bifurcation - An Introduction*. Princeton Series in Applied Mathematics. Princeton University Press, 2003.

[4] E.N. Dancer. "Bifurcation theory for analytic operators". In: *Proc. Lond. Math. Soc* XXVI (1973), pp. 359–384.

[5] E.N. Dancer. "Global structure of the solutions set of non-linear real-analytic eigenvalue problems". In: *Proc. Lond. Math. Soc* XXVI (1973), pp. 747–765.

[6] M. Ehrnström, J. Escher, and Erik Wahlén. "Steady water waves with multiple critical layers". In: *SIAM J. Math. Anal.* 43 (2011), pp. 1436–1456.

[7] M. Ehrnström and H. Kalisch. "Global Bifurcation for the Whitham Equation". In: *Mathematical Modelling of Natural Phenomena* 8 (5 2013), pp. 13–30.

[8] M. Ehrnström and H. Kalisch. "Traveling Waves for the Whitham Equation". In: *Differential and Integral Equations* 22.11-12 (2009), pp. 1193–1210.

[9] M. Ehrnström and E. Wahlén. "Trimodal Steady Water Waves". In: *Archive for Rational Mechanics and Analysis* 216.2 (2015), pp. 449–471.

[10] M. Ehrnström and E. Wahlèn. "On Whitham's conjecture of a highest cusped wave for a nonlocal dispersive equation". In: *arXiv* (2016). arXiv:1602.05384.

[11] Loukas Grafakos. *Modern Fourier analysis*. Third. Vol. 250. Graduate Texts in Mathematics. Springer, New York, 2014.

[12] V. M. Hur and M. A. Johnson. "Modulational instability in the Whitham equation with surface tension and vorticity". In: *Nonlinear Anal.* 129 (2015), pp. 104–118.

[13] R.S. Johnson. *A Modern Introduction to the Mathematical Theory of Water Waves*. Cambridge Texts in Applied Mathematics. Cambridge University Press, Cambridge, 1997.

[14] Y. Katznelson. *An introduction to harmonic analysis*. third. Cambridge Mathematical Library. Cambridge Univerisity Press, 2004.

[15] Hansjörg Kielhöfer. *Bifurcation theory*. Vol. 156. Applied Mathematical Sciences. New York: Springer-Verlag, 2004.

[16] V. Kozlov and E. Lokharu. "N-Modal Steady Water Waves with Vorticity". In: *Journal of Mathematical Fluid Mechanics* (2017), pp. 1–15.

[17] D. Lannes and J.-C. Saut. "Remarks on the full dispersion Kadomtsev-Petviashvli equation". In: *Kinet. Relat. Models* 6.4 (2013), pp. 989–1009.

[18] F. Linares, D. Pilod, and J.-C. Saut. "Dispersive perturbations of Burgers and hyperbolic equations I: Local theory". In: *SIAM J. Math. Anal.* 46.2 (2014), pp. 1505–1537.

[19] C.I. Martin and B.-V. Matioc. “Existence of Wilton Ripples for Water Waves with Constant Vorticity and Capillary Effects”. In: *SIAM Journal on Applied Mathematics* 73.4 (2013), pp. 1582–1595.

[20] D. Moldabayev, H. Kalisch, and D. Dutykh. “The Whitham equation as a model for surface water waves”. In: *Phys. D* 309 (2015), pp. 99–107.

[21] J. Reeder and M. Shinbrot. “On Wilton ripples, II: Rigorous results”. In: 77 (Dec. 1981), pp. 321–347.

[22] F. Remonato and H. Kalisch. “Numerical Bifurcation for the Capillary Whitham Equation”. In: *Physica D* 343 (2017), pp. 51–62.

[23] R. L. Schilling, R. Song, and Z. Vondraĉek. *Bernstain Functions*. second. Vol. 37. de Gruyter Studies in Mathematics. Walter de Gruyter & Co., Berlin, 2012.

[24] M. E. Taylor. *Partial Differential Equations III. Nonlinear Equations*. Second. Applied Mathematical Sciences. Springer, 2011.

[25] O. Trichtchenko, B. Deconinck, and J. Wilkening. “The instability of Wilton ripples”. In: *Wave Motion* 66 (2016), pp. 147–155.

[26] G. B. Whitham. “Variational methods and applications to water waves”. In: *Proc. of the Royal Society of London Series A* 299.1456 (1967), pp. 6–25.

[27] G.B. Whitham. *Linear and Nonlinear Waves*. Pure and Applied Mathematics. John Wiley & Sons Inc., New York, 1974.

However beautiful the theory,
one should occasionally look at
results.

Winston Churchill

Paper II

Numerical bifurcation for the capillary Whitham equation

Filippo Remonato and Henrik Kalisch

Published in Physica D, volume 343 (2017), pages 51–62

Numerical Bifurcation for the Capillary Whitham Equation

Filippo Remonato[1,2] and Henrik Kalisch[3]

[1] Department of Mathematical Sciences, NTNU, Trondheim, Norway
[2] Department of Mathematics, University of Pavia, Pavia, Italy
[3] Department of Mathematics, University of Bergen, Bergen, Norway

Abstract

The so-called Whitham equation arises in the modeling of free surface water waves, and combines a generic nonlinear quadratic term with the exact linear dispersion relation for gravity waves on the free surface of a fluid with finite depth.

In this work, the effect of incorporating capillarity into the Whitham equation is in focus. The capillary Whitham equation is a nonlocal equation similar to the usual Whitham equation, but containing an additional term with a coefficient depending on the Bond number which measures the relative strength of capillary and gravity effects on the wave motion.

A spectral collocation scheme for computing approximations to periodic traveling waves for the capillary Whitham equation is put forward. Numerical approximations of periodic traveling waves are computed using a bifurcation approach, and a number of bifurcation curves are found. Our analysis uncovers a rich structure of bifurcation patterns, including subharmonic bifurcations, as well as connecting and crossing branches. Indeed, for some values of the Bond number, the bifurcation diagram features distinct branches of solutions which intersect at a secondary bifurcation point. The same branches may also cross without connecting, and some bifurcation curves feature self-crossings without self-connections.

II.1 Introduction

The Korteweg-de Vries (KdV) equation

$$\eta_t + c_0\,\eta_x + \frac{3}{2}\frac{c_0}{h_0}\,\eta\,\eta_x + \frac{1}{6}c_0 h_0^2\,\eta_{xxx} = 0 \tag{II.1.1}$$

is a simplified model equation for waves at the surface of a fluid contained in a rectangular channel. The equation includes the competing effects of nonlinear steepening and

frequency dispersion [19]. Balancing these two effects is the basic mechanism behind the existence of both solitary-wave solutions and periodic travelling waves. Equation (II.1.1) is given in dimensional form, $c_0 = \sqrt{gh_0}$ is the limiting long-wave speed, h_0 denotes the undisturbed water depth, and g is the gravitational constant of acceleration. The function $\eta(x,t)$ describes the deflection of the fluid surface from the rest position at a point x at time t. The equation is a valid approximation describing the evolution of surface water waves in the case when the waves are long compared to the undisturbed depth h_0 of the fluid, the average amplitude of the waves is small when compared to h_0, transverse effects are assumed to be weak, and the waves are predominantly propagating in a single direction [5, 8, 20, 27].

The linear phase speed of a wave described by the KdV equation is given by

$$c(\xi) = c_0 - \frac{1}{6} c_0 h_0^2 \xi^2, \tag{II.1.2}$$

where $\xi = \frac{2\pi}{\lambda}$ is the wave number, and λ is the wavelength. This is a second-order approximation to the wave speed

$$c(\xi) = \frac{\omega}{\xi} = \sqrt{\frac{g \tanh \xi h_0}{\xi}}, \tag{II.1.3}$$

of the linearized water-wave problem. The latter expression for $c(\xi)$ appears when the full water-wave problem is linearized around the vanishing solution, and solutions of the form $\exp(ix\xi - i\omega t)$ are sought [27].

Comparing the expressions (II.1.2) and (II.1.3), it appears that the linearized KdV equation does not give a faithful representation of the full dispersion relation even for intermediate values of the wave number ξ. Recognizing this problem of the KdV equation as a model equation for water waves, Whitham introduced what is now called the Whitham equation [28]. The idea was to use the exact form of the wave speed (II.1.3) instead of a second-order approximation like (II.1.2). The equation proposed by Whitham has the form

$$\eta_t + \frac{3}{2} \frac{c_0}{h_0} \eta \, \eta_x + K_{h_0} * \eta_x = 0, \tag{II.1.4}$$

where the convolution is in the x-variable. The equation is written in dimensional variables, with $\eta(x,t)$ representing the deflection of the surface from rest, just as in the KdV equation. The convolution kernel is defined via the Fourier transform $\mathcal{F}$ by

$$\mathcal{F} K_{h_0} = c(\xi) = \sqrt{\frac{g \tanh h_0 \xi}{\xi}}. \tag{II.1.5}$$

It should be mentioned that the Whitham equation has excited some interest because it was conjectured to feature wave breaking and peaking. Wave breaking in this context is defined as the development of an infinite gradient in the solution. In a physical context, this kind of breaking may not happen naturally for a free equation such as (II.1.4), but may require some forcing either by a sloping bottom, or an imposed discharge [4]. While the KdV equation does not allow the formation of infinite gradients, it features convective wave breaking which is related to spilling at the wavecrest [7]. Wave peaking describes

the situation where a steady wave profile features a singular point, such as a peak or a cusp, such as in the well known highest wave which was conjectured to be peaked by Stokes, and proved to exist in [1, 25].

Both the existence of peaked and breaking waves were investigated to some degree already by Whitham [28, 27], and studied at length for a number of related equations by Naumkin and Shishmarev in the monograph [23]. Recently, proofs of both phenomena have become available. In particular, it was shown in [14] that the Whitham equation features waves which develop an infinite gradient, and the existence of a highest, peaked wave was proved in [11].

In the present article, the Whitham equation is studied in the case when surface tension is important. The motivation for this pursuit lies partially in the analysis in [22] where it was shown that the Whitham equation is a valid model for surface waves of smaller wavelengths than the KdV equation. As a result, it is possible to use the Whitham equation for surface waves which are short enough for capillary effects to play a role. On the other hand, there are situations where capillarity is strong, such as in the presence of a surface film or an interfacial hydrate layer [2, 13, 17]. In this case, capillarity can be important even for longer waves.

In the general case where both capillary and gravity effects are present, the relation between the wavenumber ξ and the radial frequency ω in the linearized surface water wave problem is given by

$$\omega^2 = g\xi \tanh(\xi h_0) \left(1 + \tfrac{\tau}{\rho g}\xi^2\right), \tag{II.1.6}$$

where ρ is the density of the fluid, and τ is the surface tension of the free surface.

If restricted to waves propagating into a single direction, the phase velocity can be written as

$$c(\xi) = \sqrt{\tfrac{g \tanh h_0\xi}{\xi}\big(1 + \tfrac{\tau}{\rho g}\xi^2\big)}.$$

Thus in the case of capillary-gravity waves, this definition of $c(\xi)$ is used in the definition of the integral kernel in (II.1.5). If the undisturbed depth h_0 is taken as a unit of length, and h_0/c_0 is taken as unit of time, then the Whitham equation with surface tension is

$$u_t + \frac{3}{2}uu_x + K_T * u_x = 0, \tag{II.1.7}$$

where the integral kernel K_T is given by its Fourier transform, viz.

$$\mathcal{F}K_T(x) = \sqrt{\tfrac{(1+T\xi^2)\tanh(\xi)}{\xi}}, \tag{II.1.8}$$

where $T = \frac{\tau}{\rho g h_0^2}$ is the inverse of the Bond number which measures the relative strength of gravity and capillary effects on the wave motion. This equation has recently appeared in [16] where the stability of progressive waves of small-amplitude was in focus.

Note that the equation (II.1.7) is completely different in structure from the capillary KdV equation

$$u_t + c_0\, u_x + \frac{3}{2}uu_x + \frac{1}{6}\, u_{xxx} - \frac{T}{2}u_{xxx} = 0. \tag{II.1.9}$$

This latter equation reduces to the case of the KdV equation with the sign of the dispersive term being positive or negative depending on the value of T. Since these two cases are equivalent via a change of sign, they do not differ in a qualitative way [3]. The one case of greater interest is when T is close to $1/3$ as a fifth-order term is then needed in order to get the correct order of approximation. The resulting equation is known as the Kawahara equation, and it features competing third and fifth order derivatives. On the other hand, equation (II.1.7) features two competing nonlocal terms for any value of T, and as will be seen presently, this configuration has repercussions on the possible solutions of the equation.

In the present work, steady solutions of (II.1.7) are under consideration and we will look for solutions in the space of continuous $2\pi/k$-periodic functions, which will be denoted by $C_{2\pi/k}$. For convenience, we use a further rescaling to put (II.1.7) in the tidy form

$$u_t + 2u\,u_x + K_T * u_x = 0, \tag{II.1.10}$$

and then use the assumption $\eta(x,t) = u(x-\mu t)$ to search for travelling wave solutions with propagation speed μ. The equation can then be written in integrated form as

$$W(\mu, u) = -\mu\,u + u^2 + K_T * u = 0. \tag{II.1.11}$$

As will be shown in the body of this article, with the definition of K_T in (II.1.8), equation (II.1.11) features a large variety of solutions. In particular, there are branches which contain secondary bifurcation points leading to connections with other branches. There are also crossings of distinct branches without connections, and there are self-crossing (but not intersecting) bifurcation branches. Such patterns have been seen before in some cases, such as in the case of tri-modal surface water waves ([12]), but the nature of the connections appears to be different in the present case. The existence of crossing and self-crossing branches leads to non-uniqueness of solutions of the steady problem (II.1.11) which is an interesting problem in itself.

The plan of the paper is as follows. In Section II.2, analytic bifurcation formulae are provided in order to guide the numerical experiments. In Section II.3, the numerical scheme is explained in detail, and in Section II.4, numerical experiments are shown.

II.2 Analytic expansions

We now want to provide an analytical expansion of the wave profile and speed near the bifurcation point. We look for an expansion in the form

$$u_\epsilon = u_1\,\epsilon + u_2\,\epsilon^2 + u_3\,\epsilon^3 + u_4\,\epsilon^4 + \dots \tag{II.2.1}$$

$$\mu_\epsilon = \mu_0 + \mu_1\,\epsilon + \mu_2\,\epsilon^2 + \mu_3\,\epsilon^3 + \dots. \tag{II.2.2}$$

In this pursuit, it is important to understand the behavior of the dispersion relation in terms of different values of T.

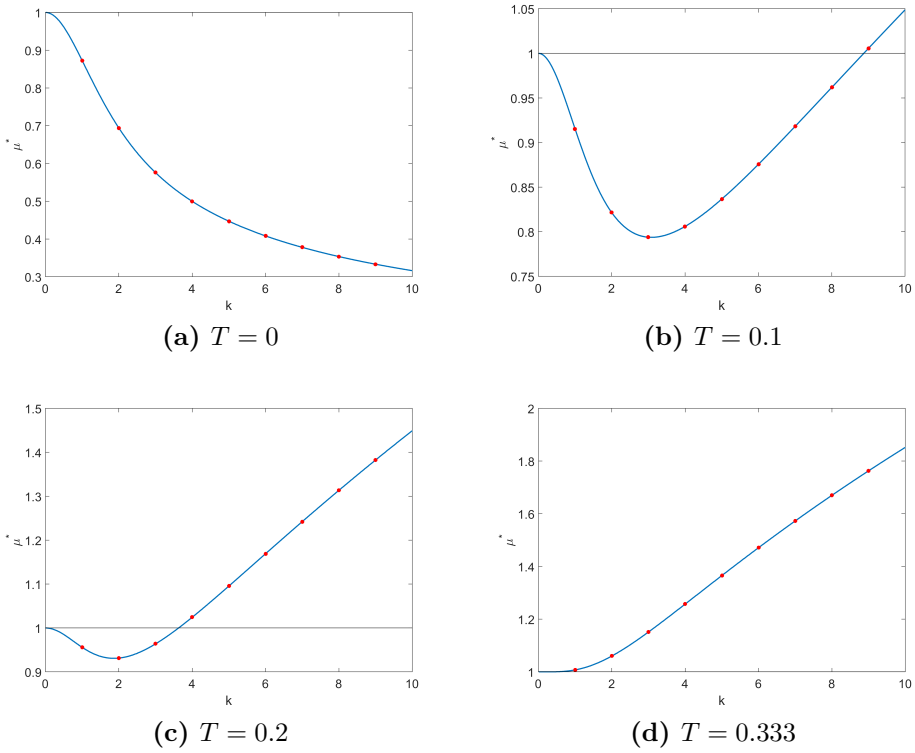

(a) $T = 0$ **(b)** $T = 0.1$

(c) $T = 0.2$ **(d)** $T = 0.333$

Figure II.2: The bifurcation speed μ^* as a function of the wave number k for various values of T. The case $T = 0$ corresponds to the gravitational case of Equation (II.1.11). Panels (b) and (c) illustrate two cases where the dispersion curve is non-monotone. Panel (d) shows the case where $T = 1/3$. For $T \geq 1/3$, the curve is monotone.

II.2.1 Bifurcation speed

Analyzing the linearized version of (II.1.11), it is intuitively clear that given $k \in \mathbb{N}$, the speed at which non-trivial $2\pi/k$-periodic solutions bifurcate from the trivial solution curve is given by

$$\mu^* = m(k) = \sqrt{\frac{(1 + Tk^2)\tanh(k)}{k}} \tag{II.2.3}$$

and the kernel of $D_u W$ at the bifurcation point is the span of $\{\cos(kx)\}$. A firm proof of this fact can be established in the same way as it was shown for the purely gravitational case in [10].

It can be shown that for $T = 0$, Equation (II.2.3) is monotonically decreasing in k, while it has a global minimum for any value of $T > 0$. In particular, $\min m(k) \in (0, 1)$ for $0 < T < \frac{1}{3}$, while for $T \geqslant \frac{1}{3}$ the minimum is 1 and $m(k)$ is monotonically increasing in k. Some examples are shown in Figure II.2.

This means that given two wavenumbers k_1, k_2, we can always find a T such that $m(k_1) = m(k_2)$, and hence the two branches bifurcate from the same point. Such T is given by

$$T(k_1, k_2) = \frac{k_1 \tanh(k_2) - k_2 \tanh(k_1)}{k_1 k_2 \left(k_1 \tanh(k_1) - k_2 \tanh(k_2)\right)} \tag{II.2.4}$$

Note that this implies that for $T = T(k_1, k_2)$, the kernel of $D_u W$ is two-dimensional at the bifurcation point, and in particular the kernel is the span of $\{\cos(k_1 x), \cos(k_2 x)\}$. This fact, along with the existence of local *sheets* of solutions, is outside of the scope of the present paper, but will be rigorously proved in future work.

II.2.2 Expansion coefficients and multi-modal waves

In the case of a one-dimensional kernel, i.e. when $T \neq T(k_1, k_2)$, the constants in formulas (II.2.1) and (II.2.2) are given below:

$$\begin{aligned}
u_1 &= \cos(kx), \\
u_2 &= \frac{1}{2\left(m(k)-1\right)} + \frac{1}{2\left(m(k)-m(2k)\right)}\cos(2kx), \\
u_3 &= \frac{1}{2\left(m(k)-m(3k)\right)\left(m(k)-m(2k)\right)}\cos(3kx), \\
u_4 &= A_0 + A_{2k}\cos(2kx) + A_{4k}\cos(4kx).
\end{aligned}$$

The last function is defined in terms of the constants

$$\begin{aligned}
A_0 &= -\frac{1}{4\left(m(k)-1\right)^3} - \frac{1}{8\left(m(k)-1\right)^2\left(m(k)-m(2k)\right)} \\
&\quad + \frac{1}{8\left(m(k)-1\right)\left(m(k)-m(2k)\right)^2}, \\
A_{2k} &= -\frac{1}{4\left(m(k)-m(2k)\right)^3} + \frac{1}{4\left(m(k)-m(2k)\right)^2\left(m(k)-m(3k)\right)}, \\
A_{4k} &= \frac{1}{8\left(m(k)-m(2k)\right)^2\left(m(k)-m(4k)\right)}, \\
&\quad + \frac{1}{2\left(m(k)-m(2k)\right)\left(m(k)-m(3k)\right)\left(m(k)-m(4k)\right)}.
\end{aligned}$$

For the expansion of the wave speed μ, we have

$$\begin{aligned}
\mu_0 &= m(k), \\
\mu_1 &= 0, \\
\mu_2 &= \frac{1}{m(k)-1} + \frac{1}{2(m(k)-m(2k))}, \\
\mu_3 &= 0.
\end{aligned}$$

Note that these expansions coincide, up to the second order in ϵ, with the bifurcation formulas given in [9].

Due to Formula (II.2.4) there exist some values of T for which the above expansion is not valid, e.g. when $T = T(k, 2k)$. In those cases a more in-depth analysis is required.

However, since all the terms in the denominator are of the form $(m(k)-m(ak)), a \in \mathbb{N}_0$, the expansions (II.2.1) and (II.2.2) remain valid also when $T = T(k_1, k_2)$ provided $k_2 \neq ak_1$. In the other cases, we can still select T in order for (II.2.1) and (II.2.2) to hold while making the coefficients in a component u_n arbitrarily large. This explains the existence of multi-modal waves, which are associated with the property that the bifurcation kernel can be two-dimensional. For instance, in [12], tri-modal waves were found in the case of the full-water wave problem with a background shear current. Several examples are presented in Section II.4.

II.2.3 Tangent and direction of nontrivial curves at the bifurcation point

Due to Equation (II.2.3) it is natural to use the wave speed as a bifurcation parameter, and we are interested in the shape of curves of nontrivial solutions close to the bifurcation point. This information is given by the expansion (II.2.2) for the wave speed except in the cases of a two-dimensional kernel.

In the purely gravitational case we know that any nontrivial branch has a vertical tangent at the bifurcation point. This is due to the fact that $\mu_1 = 0$, and as we have have just shown it is preserved also in the capillary case.

Moreover, for gravity waves it was shown in [9, Theorem 4.6] that the main branch (k=1) satisfies $\ddot{\mu}(0) = \mu_2 < 0$, which means that in a neighborhood of the bifurcation point the main branch will go to the left, in the direction of decreasing velocities. Due to the effect of T on $m(k)$, we can see from the above bifurcation formulas that there are values of T for which μ_2 changes sign, and therefore the main branch can bifurcate going to the right, in the direction of increasing velocities. The value of $\text{sign}(\mu_2)$ is plotted in Figure II.3 for the first four wavenumbers. Note that the branches for $k = 3, 4$, among others, bifurcate going to the right also in the purely gravitational case.

II.3 The numerical scheme

We employ a variation of the method presented in [9]. We want to apply a Fourier-collocation method, which is convenient given the definition of K. Also note that, thanks to symmetry, we can perform all computations on the half-wavelength $L = \lambda/2 = \pi/k$. Given k, let N be the total number of collocation points and define the subspace of $L^2(0, \pi)$

$$\mathcal{S}_h = \text{span}\{\cos(nx) : 0 \leqslant n \leqslant N-1\}$$

and the collocation points $x_i = \frac{(2i-1)\,\pi}{2Nk}$ for $i = 1, \ldots, N$. We then discretize Equation (II.1.11) and search for a solution $u_h \in \mathcal{S}_h$, $u_h(x_i) = u_i$ such that

$$-\mu\, u_h + u_h^2 + K\, u_h = 0 \tag{II.3.1}$$

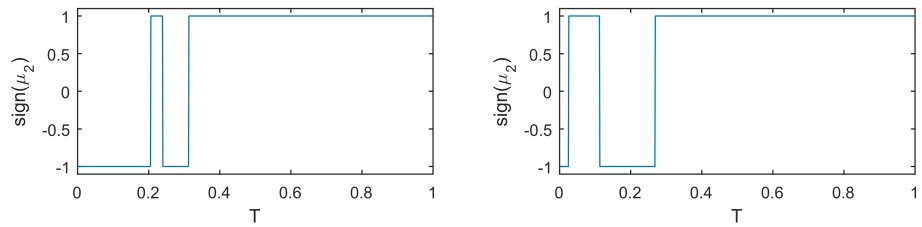

(a) $k = 1$ **(b)** $k = 2$

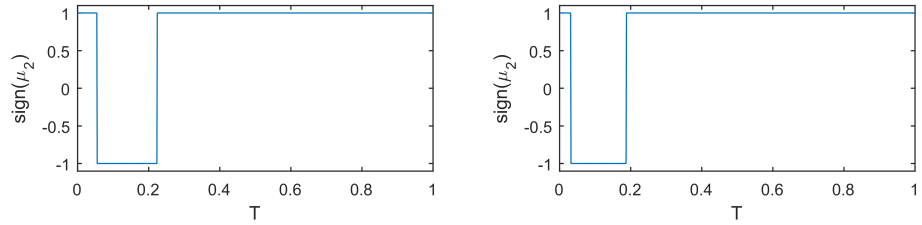

(c) $k = 3$ **(d)** $k = 4$

Figure II.3: Values of $\operatorname{sign}(\mu_2)$ for $T \in (0, 1)$ and $k = 1, \dots, 4$. Positive values mean the branch goes to the right of μ^*, negative values that it goes to the left.

To understand the term $K_h \, u_h$, we need to see how K acts on functions in $\mathcal{S}_h$, therefore we expand u_h in its discrete Fourier (cosine) series:

$$u_h(x) = \sum_{n=0}^{N-1} w_n \, a_n \cos(nx), \quad a_n = w_n \sum_{i=1}^{N} u_i \cos(kx_i), \tag{II.3.2}$$

where as usual

$$w_n = \begin{cases} 1/\sqrt{N} & n = 0 \\ 2/\sqrt{N} & n \geqslant 1. \end{cases}$$

We then see that K acts on u_h as follows:

$$K * u_h = \int K(y) \, u_h(x - y) \, \mathrm{d}y = \int K(y) \sum_{n=0}^{N-1} w_n \, a_n \, \cos(nx - ny) \, \mathrm{d}y$$

$$= \int K(y) \sum_{n=0}^{N-1} w_n \, a_n \, \frac{e^{i(nx-ny)} + e^{-i(nx-ny)}}{2} \, \mathrm{d}y.$$

We now split the integral in the two parts, change variables $y \mapsto -y$ in the second integral, and exploit the fact that K is even, and get that the above becomes

$$K * u_h = \sum_{n=0}^{N-1} w_n \, a_n \, \frac{e^{inx} - e^{-inx}}{2} \int K(y) e^{-iny} \, \mathrm{d}y$$

$$= \sum_{n=0}^{N-1} w_n \, a_n \, \cos(nx) \sqrt{\frac{(1 + Tn^2) \tanh(n)}{n}}.$$

Expanding the definition of a_n and rearranging the sums we finally have

$$= \sum_{i=1}^{N} \sum_{n=0}^{N-1} w_n^2 \sqrt{\tfrac{(1+Tn^2)\tanh(n)}{n}} \cos(nx_i)\cos(nx)\, u_i.$$

So if we define the matrix $\boldsymbol{K}$ as

$$\boldsymbol{K}(i,j) = \sum_{n=0}^{N-1} w_n^2 \sqrt{\tfrac{(1+Tn^2)\tanh(n)}{n}} \cos(nx_i)\cos(nx_j),$$

we have that the above is transformed into the matrix-vector multiplication $K * u_h = \boldsymbol{K}\boldsymbol{u}_h$, where $\boldsymbol{u}_h$ is the vector $[u_1, \ldots, u_N]$ whose entries are the discrete solution evaluated at the collocation points. We can therefore collocate Equation (II.3.1) in the collocation points x_i, and obtain a system of N nonlinear equations

$$W_h(\mu, \boldsymbol{u}_h) = -\mu\, \boldsymbol{u}_h + \boldsymbol{u}_h^2 + \boldsymbol{K}\, \boldsymbol{u}_h = 0. \tag{II.3.3}$$

II.3.1 Choice of parametrization

Problem (II.3.3) requires solving a nonlinear system of equations, written in general from as $F(y) = 0$. This can be done with standard Newton iterations $y^{n+1} = y^n - \left(J_F(y^n)\right)^{-1} F(y^n)$, where J_F is the Jacobian of F. Choosing different F's allows to parametrize the problem in different ways, depending on what is most convenient at any given time. We present here two possible strategies to parametrize and follow the bifurcation branch: One is based on parameter-continuation, while the other is based on the pseudo-arclength method.

Parameter-continuation approach

The idea of a parameter-continuation approach consists in choosing a quantity p to be the parameter, it can be for example the speed of the wave, and then in setting F so that a solution to $F(y) = 0$ will satisfy (II.3.3) as well as a constraint linked to the parameter we have chosen. Once a solution is found, the parameter is updated by a small step $p \rightsquigarrow p + h$ and a new solution is computed. Looking at (II.3.3), the most natural choice seems to be

$$F_\mu(u) = W_h(\mu, u_h), \tag{II.3.4}$$

which corresponds to using the speed as a parametrization of the branch. We can picture the branch as a curve plotted in the (μ, ζ) plane, where ζ can be any other quantity used as vertical axis, e.g. the wave height. Given a fixed speed $\bar{\mu}$ and a corresponding solution u of (II.3.4), we modify the speed with a small step $\bar{\mu} + h$ and use the previous solution u as an initial guess for Newton. The algorithm will then "move" vertically from the point $(\bar{\mu} + h, u)$ and converge to a new solution on the branch with speed equal to $\bar{\mu} + h$. While this is very robust numerically, it clearly breaks down when the curve has a turning point or a vertical tangent, as then the implicit function theorem no longer applies.

Since we already know that nontrivial branches have a vertical tangent at the bifurcation point, and that turning points may happen, we want to include other types of parametrizations. Since μ can no longer be used as a parameter, it needs to be treated as an unknown, and consequently we must include an additional equation in the system. One idea would be to use the waveheight as a parameter, and we can identify the numerical wave height as $|u_N - u_1|$. We will then choose F to be

$$F_{\text{WH}}(u, \mu) = \begin{pmatrix} W_h(\mu, u_h) \\ u_N - u_1 - \text{WH} \end{pmatrix} \tag{II.3.5}$$

where $\text{WH} \in \mathbb{R}_+$.

While this is convenient in case of turning points or vertical tangents in the branch, it is based on the assumption that $|u_N - u_1|$ really describes the wave height, i.e. that u_N and u_1 are the crest and the trough of the wave. As we have seen, however, there are cases where the wave can be multimodal, and therefore crests may not be positioned at u_N. See for example Figure II.9d. When this happens, this parametrization will not give any control on the height of the wave, and may make it difficult to accurately follow the branch.

A third option that can be used is to parametrize the curve with the square of the L^2-norm of the solution. This results in a choice of F as

$$F_{\text{L2}}(u, \mu) = \begin{pmatrix} W_h(\mu, u_h) \\ \frac{1}{N}(u_1^2 + u_2^2 + \dots u_N^2) - \text{L2} \end{pmatrix} \tag{II.3.6}$$

where as before $\text{L2} \in \mathbb{R}_+$.

Our strategy in the parameter-continuation setting is to perform the first few iterations along the branch using the discrete L^2-norm parametrization, then switch to (II.3.4). At every step we control the conditioning of the Jacobian of the parametrization in use, and when it exceeds a certain tolerance we switch to a different parametrization.

Pseudo-arclength continuation

Another continuation method that can be used is the pseudo-arclength, which is a *predictor-corrector* scheme based on the idea that a natural parametrization for a curve is the arclength. Let $y = [\mu, u_1, u_2, \dots, u_N]$. Given a solution y_n on the branch, we compute the next solution y_{n+1} in three steps: First we compute the tangent vector $z_n \in \mathbb{R}^{n+1}$ at y_n solving

$$\begin{cases} D_{\mu,u_h} W_h(y_n) \cdot z_n = 0 \\ z_n \cdot z_{n-1} = \alpha \end{cases} \tag{II.3.7}$$

where $\alpha > 0$. The first of (II.3.7) is the tangency condition, while the second is used to choose the tangent vector with the correct orientation.

Then, given z_n (properly normalised) we compute y^p_{n+1}, *predictor* point to y_{n+1}, simply by

$$y^p_{n+1} = y_n + h\, z_n. \tag{II.3.8}$$

Finally, the new point y_{n+1} is found by projecting y^p_{n+1} onto the branch in a direction perpendicular to z_n. That is, we obtain y_{n+1} by solving

$$\begin{cases} W_h(y_{n+1}) = 0 \\ (y_{n+1} - y^p_{n+1}) \cdot z_n = 0 \end{cases} \tag{II.3.9}$$

which is the *corrector* step of the method.

This method is surprisingly robust, and enables us to easily follow the branch even in presence of turning points. It is clear, however, that it requires an initial guess for the first tangent vector z_0. The last N components of z_0 can be chosen, according to what was said in Section II.2, as $\cos(kx_i), i = 1, \ldots, N$. For the first component the optimal choice would be to use the information coming from (II.2.2); however as we have noted that expansion is not always valid. In order to circumvent this problem and obtain information on the "direction" for the speed, we decided to first use the parametrization (II.3.6), which returns some value $\tilde{\mu}_1$ as a solution, and then simply set the first component in z_0 as $\text{sign}(\tilde{\mu}_1 - \mu^*)$.

II.4 Numerical Results

We present in this section the numerical results we obtained applying the scheme presented earlier. All results have been obtained employing the pseudo-arclength parametrization described in Section II.3.1. For notational simplicity we will refer to the branch obtained for $k = 1$ as the *main* branch even in the presence of multi-modal waves.

The computed profiles have been tested in a discrete time integrator in order to ascertain their validity as numerical solutions of the Whitham problem. To this end, a fully discrete time dependent collocation scheme was developed which is similar to the scheme used in [9]. While a detailed discussion of the time integration scheme and corresponding results is beyond the scope of this work, we note that well posedness of a class of nonlocal equations was proved in [21], and convergence of spectral collocation projections of similar nonlocal equations was proved in [18, 24], so that this discussion is therefore omitted here.

II.4.1 General branches

Figure II.4 presents the plots of the branches for $k = 1, \ldots, 9$, for the same values of the capillarity parameter T as considered in Figure II.2.

Note that in the purely gravitational case $T = 0$, Figure II.4a, we took advantage of the known theoretical result stating that $u \leqslant \mu/2$. To the best of our knowledge no similar result is available for the capillary case, hence in Figures II.4b, II.4c, and II.4d we are showing the branches up to the wave height value of 0.2, in order to keep the plots readable. It is important to note, however, that the code can continue the branches also after those heights, and in particular we are able to continue the branches well over heights of 1. In several cases we tested the highest computed profiles in the time integrator and let the profile evolve for several periods; all tested waves resulted to be orbitally stable. However, these waves may still feature modulational instability, such as discussed in [15,

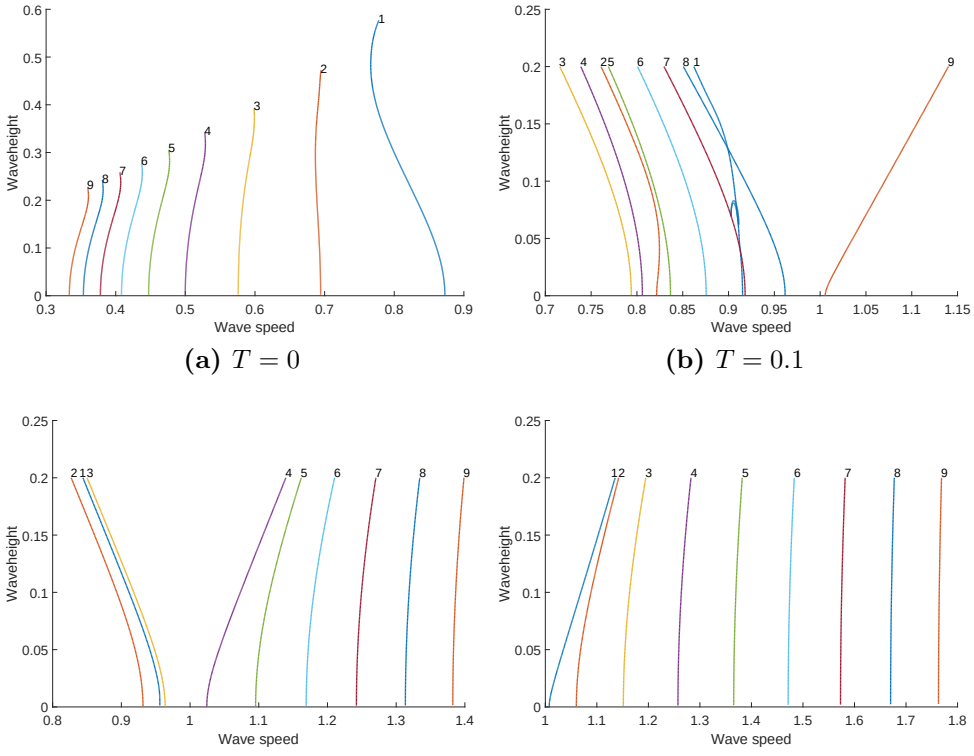

(a) $T = 0$ **(b)** $T = 0.1$

(c) $T = 0.2$ **(d)** $T = 0.333$

Figure II.4: Branches of solutions for $k = 1, \ldots, 9$ for different values of the capillarity parameter T. The value of k is indicated above the corresponding branch. In panel (b), it can be seen that the branch $k = 1$ crosses both the branch $k = 7$ and the branch $k = 8$.

26] for the purely gravitational Whitham equation and a more general class of equations in [6]. We also briefly note here that waves high up on the branches may have very steep profiles, which in turn makes the time evolution error very sensitive to the stepsize used. We present one such example in Figure II.5.

To the naked eye the plot of the profile can appear so steep that it seems to almost develop cusps of depression. From the theory it is clear that any solution of the Whitham problem has to be smooth, in particular C^∞, so cusps cannot really develop, but this may be an indication of a possible blow-up in the derivative.

Going back to Figure II.4 we see that, as expected, the bifurcation speed of the branches increases with T and for $T > \frac{1}{3}$, $\mu^*(k) > 1 \, \forall k$. We can also see that the branches bifurcate in the direction of increasing or decreasing velocities in accordance with Section II.2.3 (see also Figure II.3). Moreover, we note that turning points are present also in the capillary case: See for example the branch for $k = 2$ in Figure II.4b.

Section II.4.3 contains a more detailed discussion of the complex interaction happening between the main branch and the branch for $k = 7$ that can be seen in Figure II.4b.

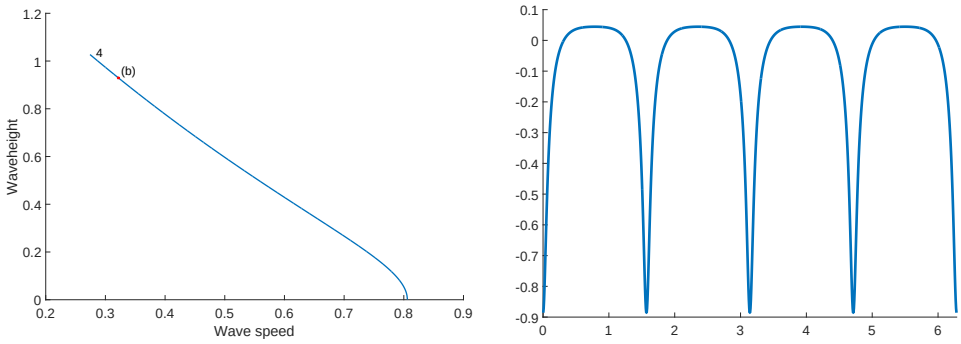

(a) $T = 0.1$ **(b)**

Figure II.5: Bifurcation branch for $T = 0.1$ and wave number $k = 4$. The bifurcation point is $\mu^* \approx 0.806$. Panel (b) displays a very steep wave of waveheight close to 1.

II.4.2 Two-dimensional Bifurcation

This section is devoted to the cases where T is chosen as in (II.2.4). For these values we know from Section II.2 that the bifurcation kernel is two-dimensional and the analytical expansions with the coefficients given in II.2.2 may no longer be valid. Also, as will be proved in future work, the two-dimensional bifurcation kernel leads to the existence of two-dimensional *sheets* of small amplitude solutions. Our code, however, is currently capable of following only *branches* of solutions. In the case of a two-dimensional kernel, this corresponds to following the intersection curve between the sheet of solutions and the plane $T = \text{const}$.

Figure II.6 shows the plot for the branches for $k_1 = 1$ and $k_2 = 7$ when $T = T(1, 7) \approx 0.09918$. Note that the profiles of the waves at the points labelled (b), (c), and (d) are shown in the corresponding subfigures. In this case the bifurcation kernel is spanned by $\{\cos(x), \cos(7x)\}$ and the branches bifurcate from the same point as expected. As we can see the main branch contains waves with mixed wavenumbers: At the beginning (Figure II.6b) waves have simple cosine-like profiles, but further up the branch (Figure II.6c) the influence from the $\cos(7x)$ component becomes more pronounced and they develop 7 crests. This change happens somewhat rapidly in the lower part of the branch, while in the higher part the profiles seem to stabilize to a mix of $\cos(x)$ and $\cos(7x)$, and little change in shape is observed between waves even over great distances in the branch. The waves in the k_2 branch, on the other hand, maintain a pure $\cos(7x)$-profile throughout the branch.

Changing T with the help of (II.2.4) we can produce two-dimensional kernels containing any k_1 and k_2: Figure II.7 shows a case similar to the above for the wavenumbers $k_1 = 1$ and $k_2 = 2$. Note that since now $k_2 = 2\,k_1$, the expansion formulae with the coefficients written in Section II.2.2 are no longer valid, and in particular we see that the k_1-branch does not have a vertical tangent at the bifurcation point. As in the previous case, the main branch contains mixed waves: In the lower part the principal mode is $\cos(x)$, while as one follows the branch the contribution from the $\cos(2x)$ mode becomes noticeable and the profile develops two crests. The profile of waves in the k_2 branch,

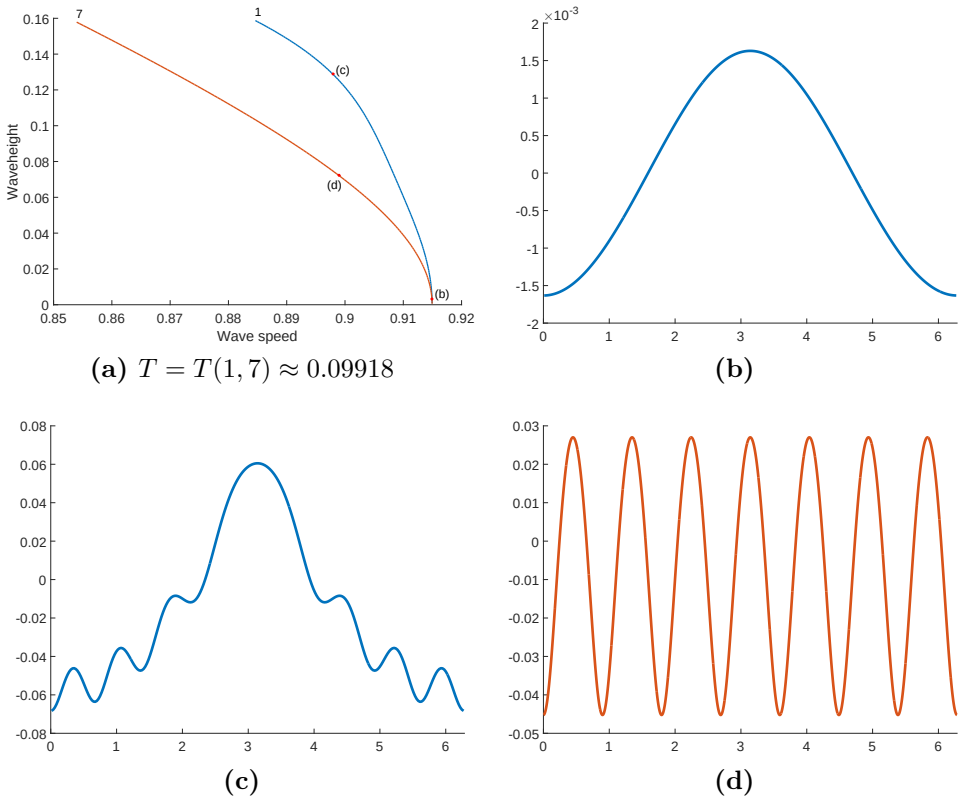

(a) $T = T(1,7) \approx 0.09918$ **(b)**

(c) **(d)**

Figure II.6: Two bifurcation branches originating from the same bifurcation point $\mu^* \approx 0.915$. Here T is given by $T(1,7)$ according to formula (II.2.4). Panel (a) shows the two bifurcation branches. Panels (b) and (c) show wave profiles on the upper (blue) bifurcation curve, and panel (c) shows a wave profile on the lower (red) bifurcation curve.

instead, is not affected by the lower k_1-mode and remains of the form $\cos(2x)$. This fact is clear from a functional-analytical point of view since $C_{2\pi/2}$, the space of continuous, $2\pi/2$ periodic functions, is a subset of $C_{2\pi}$.

More generally, if $k_2 = a\,k_1$ for some $a \in \mathbb{N}$, then $C_{2\pi/k_2} \subsetneq C_{2\pi/k_1}$ and the k_1-branch will contain solutions with components mixing the wavenumbers k_1 and k_2. If instead k_2 is not an integer multiple of k_1, $C_{2\pi/k_2} \nsubseteq C_{2\pi/k_1}$ and therefore the k_1 branch will not contain any component with period $2\pi/k_2$: See for example Figure II.8. The numerical tests show that it is still possible for the k_1-branch to include period-halving components, which will lead to the formation of two new crests in place of the original ones. Looking at the coefficients in Section II.2.2 it is clear that the height on the branch where this will happen is proportional to $m(k_1) - m(2k_1)$, but anyway there will not be components with pure k_2 wavenumbers.

II.4.3 Connecting branches

In this section we explore in more detail the cases where the k_1 branch actually connects to the k_2 one. A first example could already be seen in Figure II.4b, where the main branch connects to the $k = 7$ branch. We will look at this case in detail, and briefly present other

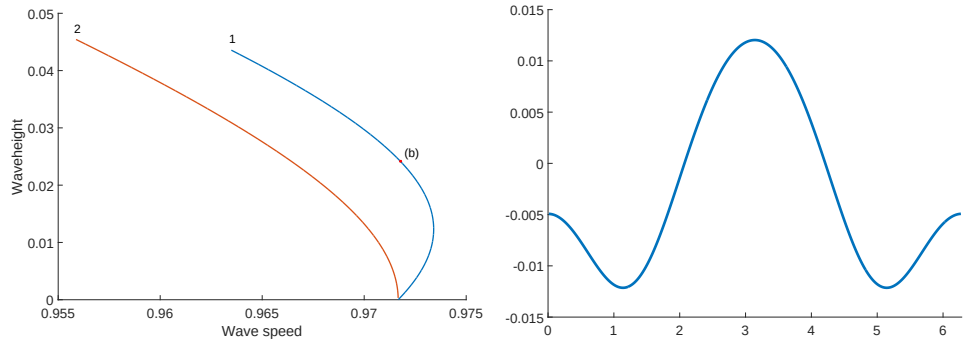

(a) $T = T(1,2) \approx 0.23968$ **(b)**

Figure II.7: A Pair of bifurcation branches originating from the bifurcation point $\mu^* \approx 0.972$. T is given by $T(1,2)$ according to formula (II.2.4). Panel (a) shows the two bifurcation branches. Panel (b) shows a wave profile on the upper (blue) bifurcation curve.

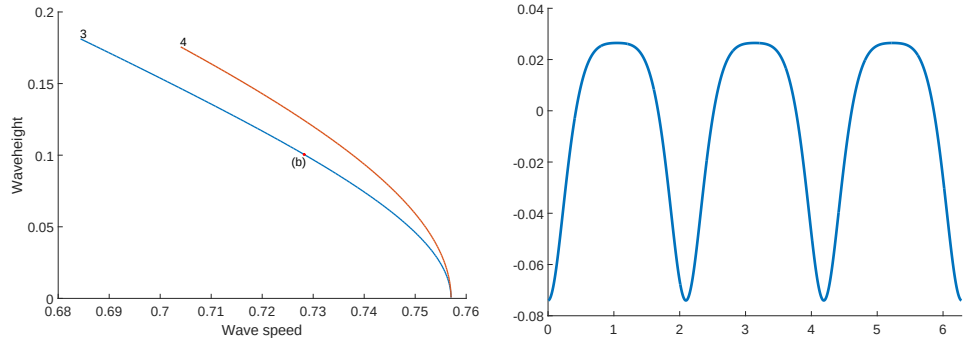

(a) $T = T(3,4) \approx 0.08086$ **(b)**

Figure II.8: A Pair of bifurcation branches originating from the bifurcation point $\mu^* \approx 0.757$. T is given by $T(3,4)$ according to formula (II.2.4). Panel (a) shows the two bifurcation branches. Panel (b) shows a wave profile on the lower (blue) bifurcation curve.

cases later.

When $k_1 = 1$, $k_2 = 7$, and $T = T(1,7)$, we have seen in the previous section that the two branches bifurcate from the same point. We can therefore view the bifurcation point as a point of connection between these two branches. Looking at Figure II.6 we see that the main branch lies on the right and above the $2\pi/7$-branch; however we know from Formula (II.2.3) and Figure II.2 that with an increase in T, $\mu^*(k_2)$ will increase faster than $\mu^*(k_1)$. We therefore expect the representations of the two branches in the wavespeed-waveheight plane to *cross* each other at a certain point. The question now is: Can we make the two branches *connect*, i.e. can we make small variations in T such that there still exists a point (which was originally at $(0, \mu^*)$) where the two branches share the same wave? The answer in general is yes, provided a multiplicity condition on the wavenumbers is fulfilled.

Figure II.9 shows the plots for $k_1 = 1$ and $k_2 = 7$, with $T = 0.1$. Recall from before that $T(1,7) \approx 0.09918$ so now we have $T \approx T(1,7) + 0.00082$. Closeup pictures of the connection point are presented in Figure II.10.

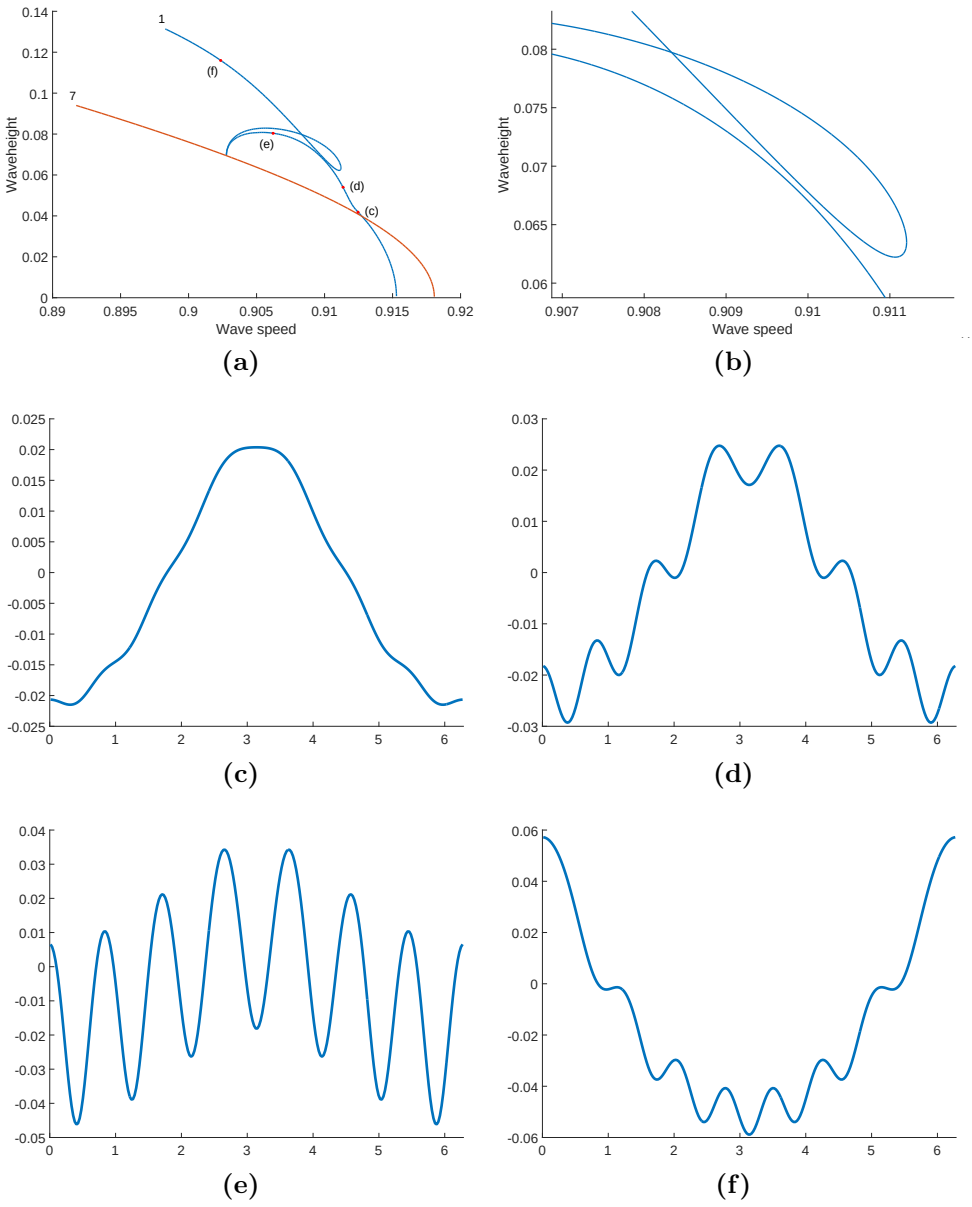

Figure II.9: A Pair of bifurcation branches originating from different but comparable bifurcation points in the case $T = 0.1$. Panel (a) shows the two bifurcation branches, and panel (b) shows a close-up of the self-crossing branch. Panels (c) through (f) show various solution profiles on the self-crossing branch.

As expected, the main branch now starts to the left and below the k_2 branch, and near the point labelled (c), they cross each other without connecting since they do not share the same solution at that point. Very similarly to what we have seen in Section II.4.2, the profile of the wave starts as $\cos(x)$ right after the bifurcation point, then loses monotonicity (Figure II.9c) and rapidly develops seven crests (Figure II.9d). The further we go up the branch the more evident is the presence of a "carrier" signal like $\cos(x)$ and a high frequency modulation given by the $\cos(7x)$ component: See Figure II.9e. The

main branch then curves and connects to the $2\pi/7$ one: Figure II.10 shows two close-ups of the connection point. While approaching the $2\pi/7$ branch, the main branch crosses itself twice but does not self-intersect. After that it also crosses the $2\pi/7$ branch, then turns back and actually connects to it; the connection point being the left one in Figure II.10b. Near that point we see that the profiles are essentially identical (Figures II.10c and II.10d). After the connection the main branch separates again and moves up, forming a loop (Figure II.9a and closeup in Figure II.9b) before continuing in the direction of increasing heights. Again, there is no self-intersection in the loop, but only a crossing. After the connection point with the k_2 branch, the profiles in the main branch are flipped vertically and the contribution from the $\cos(7x)$ component diminishes until it reaches a situation like the one presented in Figure II.9f. The profiles remain essentially unchanged in shape further up in the branch.

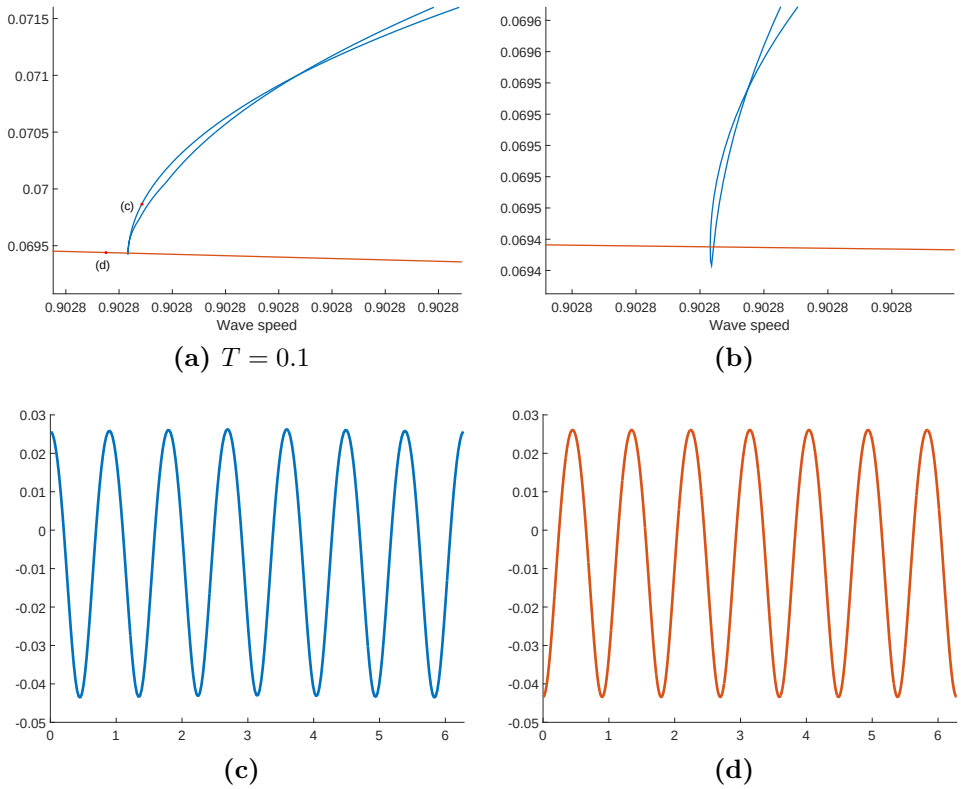

(a) $T = 0.1$ **(b)** **(c)** **(d)**

Figure II.10: Panels (a) and (b) show close-ups of the intersection zone of the two bifurcation branches shown in Figure II.9. In panel (b), the secondary bifurcation point where the two branches connect is the left one. Panel (c) shows a solution profile on the blue branch, and panel (d) shows a solution profile on the red branch.

It is possible to replicate the above picture using any k_1 provided k_2 is chosen as

$$k_2 = (4 + a)\, k_1, \quad a \in \mathbb{N}_0. \tag{II.4.1}$$

In particular, our numerical experiments show that if a is odd, and hence k_2 is an odd multiple of k_1, then the lower-mode branch connects with the higher one, but after the

connection it continues and is unbounded as we can see in the previous Figure II.9a. If instead a is even, then the k_1 branch terminates at the connection point and no further solutions are found: See Figure II.11.

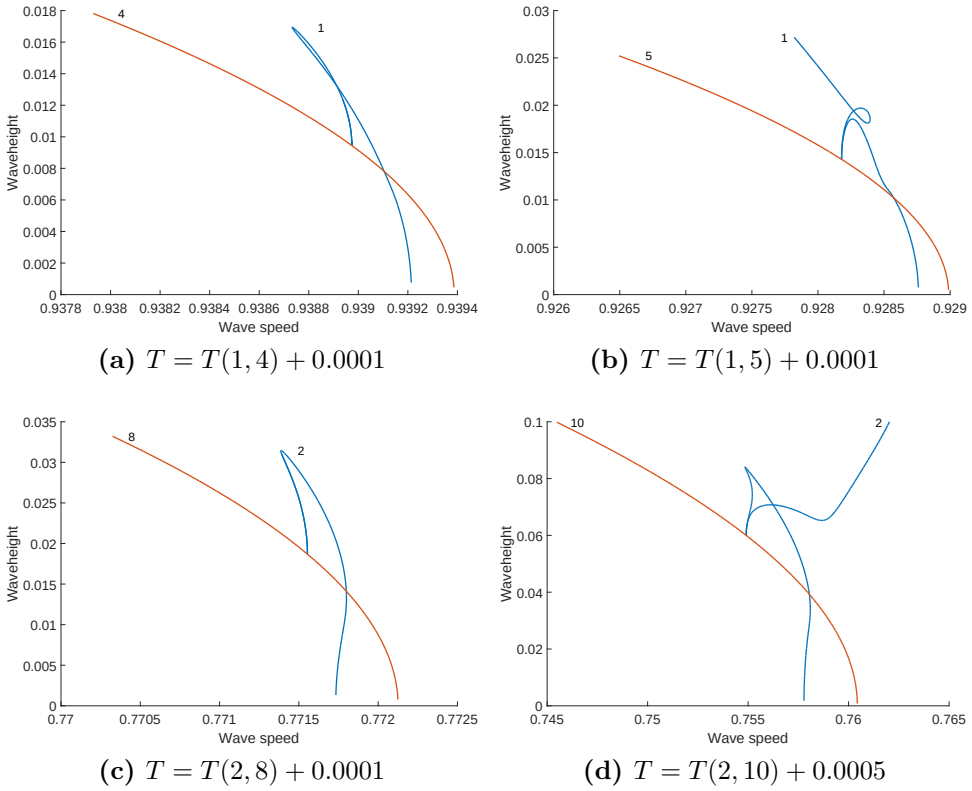

(a) $T = T(1,4) + 0.0001$ **(b)** $T = T(1,5) + 0.0001$

(c) $T = T(2,8) + 0.0001$ **(d)** $T = T(2,10) + 0.0005$

Figure II.11: Various intersecting and self-crossing branches. Panels (b) and (d) feature secondary bifurcations.

II.5 Acknowledgments

This research was supported in part by the Research Council of Norway through grants 213474/F20 and 231668. The authors would like to thank Mats Ehrnström for help in the preparation of this manuscript. The authors would also like to thank Mathew Johnson and Kyle Claassen for interesting discussions on the pseudo-arclength parametrization.

References

[1] C.J. Amick, L.E. Fraenkel, and J.F. Toland. "On the Stokes conjecture for the wave of extreme form". In: *Acta Mathematica* 148 (1982), pp. 193–214.

[2] T.B. Benjamin. "A new kind of solitary wave". In: *J. Fluid Mech.* 245 (1992), pp. 401–411.

[3] T.B. Benjamin. "The solitary wave with surface tension". In: *Quart. Appl. Math.* 40 (1982), pp. 231–234.

[4] M. Bjørkavåg and H. Kalisch. "Wave breaking in Boussinesq models for undular bores". In: *Phys. Lett. A* 375 (2011), pp. 1570–1578.

[5] J.L. Bona, T. Colin, and D. Lannes. "Long wave approximations for water waves". In: *Arch. Ration. Mech. Anal.* 178 (2005), pp. 373–410.

[6] J.C. Bronski, V.M. Hur, and M.A. Johnson. "Modulational instability in equations of KdV type". In: *New Approaches to Nonlinear Waves*. Springer, 2016. Chap. 4, pp. 83–133.

[7] M.K. Brun and H. Kalisch. "Convective wave breaking in the KdV equation". In: *arXiv:1603.09104* (2016).

[8] W. Craig. "An existence theory for water waves and the Boussinesq and Korteweg de Vries scaling limits". In: *Comm. Partial Differential Equations* 10 (1985), pp. 787–1003.

[9] M. Ehrnström and H. Kalisch. "Global Bifurcation for the Whitham Equation". In: *Mathematical Modelling of Natural Phenomena* 8 (5 2013), pp. 13–30.

[10] M. Ehrnström and H. Kalisch. "Traveling Waves for the Whitham Equation". In: *Differential and Integral Equations* 22.11-12 (2009), pp. 1193–1210.

[11] M. Ehrnström and E. Wahlén. "On Whitham's conjecture of a highest cusped wave for a nonlocal dispersive equation". In: *arXiv:1602.05384* (2016).

[12] M. Ehrnström and E. Wahlén. "Trimodal steady water waves". In: *Arch. Ration. Mech. Anal.* 216 (2015), pp. 449–471.

[13] J. Hove and P.M. Haugan. "Dynamics of a CO2-seawater interface in the deep ocean". In: *J. Marine. Res.* 63 (2005), pp. 563–577.

[14] V.M. Hur. "Breaking in the Whitham equation for shallow water waves". In: *arXiv* (2015). arXiv:1506.04075v3.

[15] V.M. Hur and M.A. Johnson. "Modulational instability in the Whitham equation of water waves". In: *Studies in Applied Mathematics* 134 (2015), pp. 120–143.

[16] V.M. Hur and M.A. Johnson. "Modulational instability in the Whitham equation with surface tension and vorticity". In: *Nonlinear Analysis* 129 (2015), pp. 104–118.

[17] H. Kalisch. "Derivation and comparison of model equations for interfacial capillary-gravity waves in deep water". In: *Math. Comput. Simulation* 74 (2007), pp. 168–178.

[18] H. Kalisch. “Error analysis of a spectral projection of the regularized Benjamin-Ono equation”. In: *BIT Numerical Mathematics* 45 (2005), pp. 69–89.

[19] D.J. Korteweg and G. de Vries. “On the change of form of long waves advancing in a rectangular canal, and on a new type of long stationary waves”. In: *Phil. Mag.* 5 (1895), pp. 422–443.

[20] D. Lannes. *The Water Waves Problem*. Vol. 188. Mathematical Surveys and Monographs. Amer. Math. Soc., Providence, 2013.

[21] F. Linares, D. Pilod, and J.-C. Saut. “Dispersive perturbations of Burgers and hyperbolic equations I: local theory”. In: *SIAM J. Math. Anal.* 46 (2014), pp. 1505–1537.

[22] D. Moldabayev, H. Kalisch, and D. Dutykh. “The Whitham Equation as a model for surface water waves”. In: *Phys. D* 309 (2015), pp. 99–107.

[23] P.I. Naumkin and I.A. Shishmarev. *Nonlinear nonlocal equations in the theory of waves*. Vol. 133. Translations of Mathematical Monographs. American Mathematical Society, Providence, 1994.

[24] B. Pelloni and V.A. Dougalis. “Error estimates for a fully discrete spectral scheme for a class of nonlinear, nonlocal dispersive wave equations”. In: *Appl. Numer. Math.* 37 (2001), pp. 95–107.

[25] P.I. Plotnikov. “A proof of the Stokes conjecture in the theory of surface waves”. In: *Dinamika Splosh. Sredy* 57 (1982). English translation Stud. Appl. Math., 2002, vol. 108, 217–244, pp. 41–76.

[26] N. Sanford, K. Kodama, J.D. Carter, and H. H Kalisch. “Stability of traveling wave solutions to the Whitham equation”. In: *Phys. Lett. A* 378 (2014), pp. 2100–2107.

[27] G.B. Whitham. *Linear and nonlinear waves*. Pure and Applied Mathematics. John Wiley and Sons Inc., New York, 1974.

[28] G.B. Whitham. “Variational methods and applications to water waves”. In: *Proc. R. Soc. Lond. A* 299 (1967), pp. 6–25.

He who seeks for methods without having a definite problem in mind seeks in the most part in vain.

David Hilbert

Paper III

Isogeometric methods for free boundary problems

Monica Montardini, Filippo Remonato and Giancarlo Sangalli

Submitted to IMA Journal of Numerical Analysis, March 2018

Isogeometric methods for free boundary problems

Monica Montardini[1], Filippo Remonato[1,2], and Giancarlo Sangalli[1,3]

[1] Department of Mathematics, University of Pavia, Pavia, Italy
[2] Department of Mathematical Sciences, NTNU, Trondheim, Norway
[3] IMATI-CNR "E. Magenes", Pavia, Italy

Abstract

We present in detail three different quasi-Newton isogeometric algorithms for the treatment of free boundary problems. Two algorithms are based on standard Galerkin formulations, while the third is a fully-collocated scheme. With respect to standard approaches, isogeometric analysis enables the accurate description of curved geometries, and is thus particularly suitable for free boundary numerical simulation. We apply the algorithms and compare their performances to several benchmark tests, considering both Dirichlet and periodic boundary conditions. In this context, iogeometric collocation turns out to be robust and computationally more efficient than Galerkin. Our results constitute a starting point of an in-depth analysis of the Euler equations for incompressible fluids.

III.1 Introduction

This work focuses on the isogeometric analysis (IGA) of free boundary problems. IGA, first presented in [9], is a recent extension of the standard finite element method where the unknown solution of the partial differential equation is approximated by the same functions that are adopted in computer-aided design for the parametrization of the problem domain. These functions are typically splines and extensions, such as non-uniform rational B-splines (NURBS). We refer to the monograph [2] for a detailed description of this approach.

In this work we present three general free boundary algorithms. The first algorithm is an extension to IGA of the finite elements approach of [11, 12]. Since the finite element basis produces meshes with straight edges, the authors needed a workaround to approximate the curvature of the boundary; in the new IGA framework this can be avoided thanks to the natural description of curved geometries through spline functions. IGA of

free boundary problems was already considered in [10, 22]; our second algorithm uses and extends these approaches to problems with periodic conditions. Our third and most efficient scheme uses instead an isogeometric variational collocation approach based on the superconvergent points presented in [7, 13]. The choice of applying an IGA collocation method is a novelty in this setting and, moreover, allows for a fast computation of the solution. While speed is marginally important in the benchmarks considered in this work, it becomes a major concern when one needs to address more complicated problems.

All the algorithms are based on shape calculus techniques, see for example [4, 17]. This results in the three algorithms being of quasi-Newton type, achieving superlinear convergence.

Our interest in free boundary problems is motivated by a separate analysis, in progress at the time of writing, of the periodic solutions of the Euler equations describing the flow of an incompressible fluid over a rigid bottom. The analytical literature on this problem is quite extensive, with results regarding irrotational flows [8], the limiting Stokes waves [18], or waves on a rotational current containing one or multiple critical layers [5, 21]. The numerical experiments so far have used finite differences methods [3], boundary-integral formulations [16], or finite elements [14]. Several other examples and numerical experiments, also based on boundary formulations, can additionally be found in [19].

This paper is organised as follows: In Section III.2 we describe the details of free boundary problem, and present two weak formulations that will constitute our starting point for the algorithms. In Section III.3 we first introduce the necessary shape calculus tools, and then proceed to linearise the aforementioned weak forms. This will produce the correct formulations on which to base our quasi-Newton steps. Section III.4 describes the discrete spaces used in the numerical schemes along with the structure of the algorithms. Finally, Section III.5 presents the numerical benchmarks and the results we obtained. We summarise the results and draw our conclusions in Section III.6.

III.2 Free Boundary Problem

Let Ω_0 be a domain used as reference configuration with $\partial\Omega_0 = \Gamma_{\mathcal{D}} \cup \Gamma_{\mathcal{P}} \cup \Gamma_0$; $\Gamma_{\mathcal{D}}$ being the (fixed) bottom boundary with Dirichlet data, $\Gamma_{\mathcal{P}}$ the (fixed) vertical boundary with periodic conditions, and Γ_0 the (free) upper part of the boundary. Moreover, let D be a rectangle with basis Γ_D, containing Ω_0 and all its possible deformations. For M a domain and Γ a curve, we denote with $C^{k,\lambda}(M, \mathbb{R}^2)$ the space of $(k, \lambda)-$Hölder continuous functions defined on M with values in $\mathbb{R}^2$ and by $C_0^{k,\lambda}(\Gamma, \mathbb{R}^2)$ the subspace of $C^{k,\lambda}(\Lambda; \mathbb{R}^2)$ with compact support, in particular vanishing at the two extremes of the curve. Then, the set of admissible vector fields acting on the reference domain is defined as $\Theta = \{\mathcal{V} \in C^{0,1}(D, \mathbb{R}^2) \cap C_0^{1,1}(\Gamma_0, \mathbb{R}^2) \,|\, \mathcal{V} = 0 \text{ on } \Gamma_{\mathcal{D}} \text{ and } \mathcal{V}(\cdot, y) \text{ periodic}\}$. We encode the deformation of the upper part of the boundary, Γ_0, as the action of a vector field $\mathcal{V} \in \Theta$ such that the deformed domain is smooth enough, does not have self intersections and does not touch the bottom Γ_D. For this reason we denote the deformed free boundary with $\Gamma_{\mathcal{V}} = \{x \in \mathbb{R}^2 \,|\, x = x_0 + \mathcal{V}(x_0),\, x_0 \in \Gamma_0\}$. Analogously, $\Omega_{\mathcal{V}}$ will denote the physical domain with boundary $\partial\Omega_{\mathcal{V}} = \Gamma_{\mathcal{D}} \cup \Gamma_{\mathcal{P}} \cup \Gamma_{\mathcal{V}}$; see Figure III.12 for a representation of this setting. We remark that Γ_0 is in general not flat.

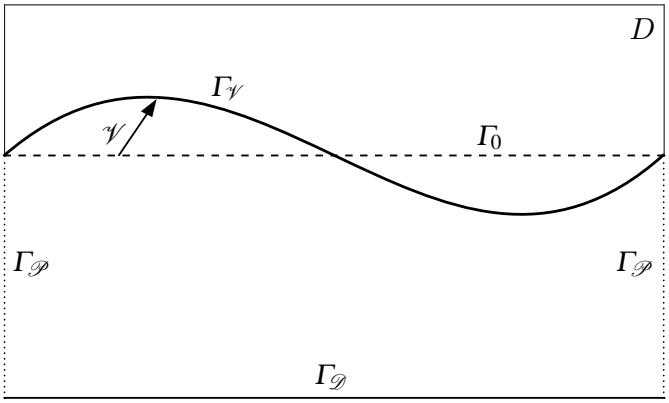

Figure III.12: The setting of our problem. The vector field $\mathcal{V}$ deforms the reference free boundary Γ_0 (dashed line) into the free boundary $\Gamma_{\mathcal{V}}$ (thick solid line). The vertical dotted lines represent the periodic boundary $\Gamma_{\mathcal{P}}$, while the thin solid line represents the fixed flat bottom boundary $\Gamma_{\mathcal{D}}$. The physical domain and its deformations are contained in a larger rectangle D.

The Bernoulli-type free boundary problem (FBP) we are interested in can then be posed as searching for a pair $(u, \mathcal{V})$, both periodic in the x-direction, such that

$$-\Delta u = f \quad \text{in } \Omega_{\mathcal{V}} \tag{III.2.1a}$$
$$u = h \quad \text{on } \Gamma_{\mathcal{V}} \cup \Gamma_{\mathcal{D}} \tag{III.2.1b}$$
$$\partial_n u = g \quad \text{on } \Gamma_{\mathcal{V}} \tag{III.2.1c}$$

where $\partial_n u = \nabla u \cdot n$ is the outward normal derivative of u. The functions f, h, and g are defined in D and are compatible with the periodicity requirement. We will consider h and g continuous, with g strictly positive and bounded away from zero[1].

Remark III.2.1. *The analytical treatment of the problem with periodic boundary conditions does not differ much from the case with pure Dirichlet conditions, which we also consider in our numerical benchmarks.*

III.2.1 Weak Formulation

To obtain a formulation of (III.2.1) suitable for a numerical scheme we first follow the steps presented in [11]. This approach leads to two distinct, coupled weak forms. Given

[1]The strict positivity is not strictly necessary: If $g < 0$ one could, for instance, keep track of the sign of g in the numerical method directly. However, g has to have a definite sign everywhere on $\Gamma_{\mathcal{V}}$.

the space $H^1_{per}(\Omega_\mathcal{V}) = \{u \in H^1(\Omega_\mathcal{V}) \,|\, u(\cdot, y) \text{ periodic}\}$, for a known function r periodic in the x-direction we define the space

$$H^1_{r,\Gamma_\mathcal{D}}(\Omega_\mathcal{V}) = \{\varphi \in H^1_{per}(\Omega_\mathcal{V}) \,|\, \varphi = r \text{ on } \Gamma_\mathcal{D}\}.$$

The first weak form is then obtained using (III.2.1a), (III.2.1c), and the part of (III.2.1b) pertaining to $\Gamma_\mathcal{D}$. We select test functions $\varphi \in H^1_{0,\Gamma_\mathcal{D}}(\Omega_\mathcal{V})$ and apply Green's formula once to obtain

$$\int_{\Omega_\mathcal{V}} \nabla u \cdot \nabla \varphi \, \mathrm{d}\Omega - \int_{\Gamma_\mathcal{V}} g\, \varphi \, \mathrm{d}\Gamma = \int_{\Omega_V} f\, \varphi \, \mathrm{d}\Omega. \tag{III.2.2}$$

Using the part of (III.2.1b) on $\Gamma_\mathcal{V}$ we employ test functions $v \in H^1_{per}(\Gamma_\mathcal{V})$ and write the second weak form simply as

$$\int_{\Gamma_\mathcal{V}} uv \, \mathrm{d}\Gamma = \int_{\Gamma_\mathcal{V}} hv \, \mathrm{d}\Gamma. \tag{III.2.3}$$

We select the trial function space by requiring $u \in H^1_{h,\Gamma_\mathcal{D}}(\Omega_\mathcal{V})$, thereby strongly imposing the Dirichlet boundary conditions on $\Gamma_\mathcal{D}$. This leads to the definition of two linear forms:

$$\mathcal{M}_1(u, \mathcal{V}; \varphi) = \int_{\Omega_\mathcal{V}} \nabla u \cdot \nabla \varphi \, \mathrm{d}\Omega - \int_{\Gamma_\mathcal{V}} g\, \varphi \, \mathrm{d}\Gamma - \int_{\Omega_\mathcal{V}} f\, \varphi \, \mathrm{d}\Omega, \tag{III.2.4}$$

$$\mathcal{M}_2(u, \mathcal{V}; v) = \int_{\Gamma_\mathcal{V}} uv \, \mathrm{d}\Gamma - \int_{\Gamma_\mathcal{V}} hv \, \mathrm{d}\Gamma. \tag{III.2.5}$$

Thus, with this approach the problem is defined as: Search for $(u, \mathcal{V}) \in H^1_{h,\Gamma_\mathcal{D}}(\Omega_\mathcal{V}) \times \Theta$ such that

$$\mathcal{M}_1(u, \mathcal{V}; \varphi) = 0,$$
$$\mathcal{M}_2(u, \mathcal{V}; v) = 0,$$

for all test functions $(\varphi, v) \in H^1_{0,\Gamma_\mathcal{D}}(\Omega_\mathcal{V}) \times H^1_{per}(\Gamma_\mathcal{V})$.

III.2.2 Very-Weak Formulation

We now follow the approach of [22]. The main difference from the previous formulation is that we write a single very-weak formulation containing information from all boundary conditions.

Considering the subspace $H^2_{0,\Gamma_\mathcal{D}}(\Omega_\mathcal{V}) = \{\varphi \in H^1_{0,\Gamma_\mathcal{D}}(\Omega_\mathcal{V}) \,|\, \varphi \in H^2(\Omega_\mathcal{V})\}$, we multiply (III.2.1a) by a test function $\varphi \in H^2_{0,\Gamma_\mathcal{D}}(\Omega_\mathcal{V})$; integrating by parts twice leads to

$$-\int_{\Omega_\mathcal{V}} (u - h)\, \Delta\varphi \, \mathrm{d}\Omega + \int_{\Omega_\mathcal{V}} \nabla h \cdot \nabla \varphi \, \mathrm{d}\Omega = \int_{\Omega_\mathcal{V}} f\, \varphi \, \mathrm{d}\Omega + \int_{\Gamma_\mathcal{V}} \varphi\, g \, \mathrm{d}\Gamma, \tag{III.2.6}$$

which we demand to be satisfied for all $\varphi \in H^2_{0,\Gamma_\mathcal{D}}(\Omega_\mathcal{V})$. In view of the above formulation we can then select the trial function space simply as $H^1_{per}(\Omega_\mathcal{V})$. The Dirichlet boundary conditions are therefore all imposed weakly.

From Equation (III.2.6) we define the linear form

$$\mathcal{N}(u,\mathcal{V};\varphi) = -\int_{\Omega_\mathcal{V}} (u-h)\,\Delta\varphi \,\mathrm{d}\Omega + \int_{\Omega_\mathcal{V}} \nabla h\cdot\nabla\varphi \,\mathrm{d}\Omega \\ -\int_{\Omega_\mathcal{V}} f\,\varphi \,\mathrm{d}\Omega - \int_{\Gamma_\mathcal{V}} \varphi\, g \,\mathrm{d}\Gamma. \tag{III.2.7}$$

Thus, with this approach the problem is defined as: Search for $(u,\mathcal{V}) \in H^1_{per}(\Omega_\mathcal{V}) \times \Theta$ such that

$$\mathcal{N}(u,\mathcal{V};\varphi) = 0$$

for all test functions $\varphi \in H^2_{0,\Gamma_\mathcal{D}}(\Omega_\mathcal{V})$.

Note that this very-weak formulation cannot be used directly to implement a numerical scheme, as the trial and test spaces are unbalanced.

III.3 Linearising the FBP

We now proceed in deriving a quasi-Newton algorithm to solve the free boundary problem. The dependence on the domain's geometry is handled through shape calculus techniques to express the derivatives with respect to the vector field $\mathcal{V}$.

III.3.1 Shape Derivatives

Here we briefly state the shape calculus results we will need for the linearisation. An in-depth analysis of the assumptions and regularity requirements can be found in the original work by Delfour, Zolésio, and Sokolowski [4, 17]. An overview of shape calculus presented with a more modern approach can also be found in [10].

Let $\mathcal{O}$ be a family of admissible (smooth enough) domains; a functional $\mathcal{J}$ is called a *shape functional* if $\mathcal{J} : \mathcal{O} \to \mathbb{R}$. Note therefore that for a fixed function u and test functions φ and v, the maps defined by the linear forms introduced earlier are shape functionals provided we identify each element $\mathcal{V} \in \Theta$ with the domain $\Omega_\mathcal{V}$ in which Ω_0 is deformed by the action of $\mathcal{V}$.

In the particular case of a domain functional $\mathcal{J}(\mathcal{V}) = \int_{\Omega_\mathcal{V}} \psi \,\mathrm{d}\Omega$ and a boundary functional $\mathcal{F}(\mathcal{V}) = \int_{\Gamma_\mathcal{V}} \phi \,\mathrm{d}\Gamma$, with ψ and ϕ smooth functions in $\mathbb{R}^2$ independent of $\mathcal{V}$, the shape derivatives of $\mathcal{J}$ and $\mathcal{F}$ are described by the following *Hadamard formulas*:

$$\langle\, \partial_\mathcal{V}\mathcal{J}(\mathcal{V}),\, \delta\mathcal{V} \,\rangle = \int_{\Gamma_\mathcal{V}} \psi\, \delta\mathcal{V}\cdot n \,\mathrm{d}\Gamma \tag{III.3.1a}$$

$$\langle\, \partial_\mathcal{V}\mathcal{F}(\mathcal{V}),\, \delta\mathcal{V} \,\rangle = \int_{\Gamma_\mathcal{V}} (\partial_n\phi + \mathrm{H}\phi)\, \delta\mathcal{V}\cdot n \,\mathrm{d}\Gamma \tag{III.3.1b}$$

where $\delta\mathcal{V} \in \Theta$ is a perturbation of the vector field, H is the *signed (additive) curvature* of $\Gamma_\mathcal{V}$ and n is the normal vector pointing outward. In particular, considering a parametrization of the free boundary $\Gamma_\mathcal{V}$ defined as $\gamma(t) = (t, y(t))$, then

$$\mathrm{H} = -\frac{y''}{[1+(y')^2]^{3/2}}.$$

III.3.2 Linearisation of the weak formulation

Let us first consider the linear forms (III.2.4) and (III.2.5). We want to linearise $\mathcal{M}_1$ and $\mathcal{M}_2$ with respect to u and $\mathcal{V}$ at an arbitrary approximated solution $(u^*, \mathcal{V}^*) \in H^1_{h,\Gamma_\mathcal{D}}(\Omega_{\mathcal{V}^*}) \times \Theta$.

Since the dependence of $\mathcal{M}_1$ and $\mathcal{M}_2$ on u is affine, their Gâteaux derivatives with respect to u in the direction $\delta u \in H^1_{0,\Gamma_\mathcal{D}}(\Omega_{\mathcal{V}^*})$ are simply given by:

$$\langle\, \partial_u \mathcal{M}_1[u^*, \mathcal{V}^*; \varphi], \delta u \,\rangle = \int_{\Omega_{\mathcal{V}^*}} \nabla \delta u \cdot \nabla \varphi \, \mathrm{d}\Omega \tag{III.3.2a}$$

$$\langle\, \partial_u \mathcal{M}_2[u^*, \mathcal{V}^*; v], \delta u \,\rangle = \int_{\Gamma_{\mathcal{V}^*}} \delta u \, v \, \mathrm{d}\Gamma. \tag{III.3.2b}$$

The linearisation with respect to the vector field $\mathcal{V}$ in the direction $\delta\mathcal{V} \in \Theta$ is performed using the Hadamard formulas; we obtain:

$$\begin{aligned}\langle\, \partial_\mathcal{V} \mathcal{M}_1[u^*, \mathcal{V}^*; \varphi], \delta\mathcal{V} \,\rangle = &\int_{\Gamma_{\mathcal{V}^*}} \nabla u^* \cdot \nabla \varphi \; \delta\mathcal{V} \cdot n \, \mathrm{d}\Gamma \\ &- \int_{\Gamma_{\mathcal{V}^*}} [\mathcal{K}_\mathrm{H} \varphi \; + g \, \partial_n \varphi] \; \delta\mathcal{V} \cdot n \, \mathrm{d}\Gamma \end{aligned} \tag{III.3.3a}$$

$$\begin{aligned}\langle\, \partial_\mathcal{V} \mathcal{M}_2[u^*, \mathcal{V}^*; v], \delta\mathcal{V} \,\rangle = &\int_{\Gamma_{\mathcal{V}^*}} (\partial_n u^* - \partial_n h + \mathrm{H}(u^* - h)) \, v \; \delta\mathcal{V} \cdot n \, \mathrm{d}\Gamma \\ &+ \int_{\Gamma_{\mathcal{V}^*}} (u^* - h) \, \partial_n v \, \delta\mathcal{V} \cdot n \, \mathrm{d}\Gamma \end{aligned} \tag{III.3.3b}$$

where $\mathcal{K}_\mathrm{H} = \partial_n g + \mathrm{H} g + f$, and H is the curvature of $\Gamma_{\mathcal{V}^*}$.

A Newton step at the point $(u^*, \mathcal{V}^*)$ has then the following structure: Search for $\delta u \in H^1_{0,\Gamma_\mathcal{D}}(\Omega_{\mathcal{V}^*})$ and $\delta\mathcal{V} \in \Theta$ such that

$$\langle\, \partial_u \mathcal{M}_1[u^*, \mathcal{V}^*; \varphi], \delta u \,\rangle + \langle\, \partial_\mathcal{V} \mathcal{M}_1[u^*, \mathcal{V}^*; \varphi], \delta\mathcal{V} \,\rangle = -\mathcal{M}_1(u^*, \mathcal{V}^*; \varphi) \tag{III.3.4a}$$

$$\langle\, \partial_u \mathcal{M}_2[u^*, \mathcal{V}^*; v], \delta u \,\rangle + \langle\, \partial_\mathcal{V} \mathcal{M}_2[u^*, \mathcal{V}^*; v], \delta\mathcal{V} \,\rangle = -\mathcal{M}_2(u^*, \mathcal{V}^*; v) \tag{III.3.4b}$$

for all $(\varphi, v) \in H^1_{0,\Gamma_\mathcal{D}}(\Omega_{\mathcal{V}^*}) \times H^1_{per}(\Gamma_{\mathcal{V}^*})$.

Therefore, summing up all the contributions, we search for $\tilde{u} = u^* + \delta u \in H^1_{h,\Gamma_\mathcal{D}}(\Omega_{\mathcal{V}^*})$ and $\delta\mathcal{V} \in \Theta$ such that

$$\begin{aligned}\int_{\Omega_{\mathcal{V}^*}} \nabla \tilde{u} \cdot \nabla \varphi \, \mathrm{d}\Omega + \int_{\Gamma_{\mathcal{V}^*}} (\partial_n u^* - g) \, \partial_n \varphi \; \delta\mathcal{V} \cdot n \, \mathrm{d}\Gamma + \int_{\Gamma_{\mathcal{V}^*}} \nabla_\Gamma u^* \cdot \nabla \varphi \; \delta\mathcal{V} \cdot n \, \mathrm{d}\Gamma \\ - \int_{\Gamma_{\mathcal{V}^*}} \mathcal{K}_\mathrm{H} \varphi \; \delta\mathcal{V} \cdot n \, \mathrm{d}\Gamma = \int_{\Omega_{\mathcal{V}^*}} f \, \varphi \, \mathrm{d}\Omega + \int_{\Gamma_{\mathcal{V}^*}} g \, \varphi \, \mathrm{d}\Gamma \end{aligned} \tag{III.3.5a}$$

$$\begin{aligned}\int_{\Gamma_{\mathcal{V}^*}} \tilde{u} \, v \, \mathrm{d}\Gamma + \int_{\Gamma_{\mathcal{V}^*}} [(\partial_n u^* - \partial_n h + \mathrm{H}(u^* - h)) \, v + (u^* - h) \, \partial_n v] \; \delta\mathcal{V} \cdot n \, \mathrm{d}\Gamma \\ = \int_{\Gamma_{\mathcal{V}^*}} h \, v \, \mathrm{d}\Gamma \end{aligned} \tag{III.3.5b}$$

for all $\varphi \in H^1_{0,\Gamma_\mathcal{D}}(\Omega_{\mathcal{V}^*})$ and $v \in H^1_{per}(\Gamma_{\mathcal{V}^*})$.

In the above steps we used the *tangential gradient splitting*, with the tangential gradient of a real function being defined as $\nabla_\Gamma(\cdot) = \nabla(\cdot) - \partial_n(\cdot)n$.

So far we carried out the computations in full generality, and (III.3.5) is an exact Newton scheme. We now proceed to comment on, and apply, some simplifications.

Simplification 1. *Without loss of generality one can consider $\partial_n h = 0$ on $\Gamma_{\mathcal{V}^*}$. Furthermore, we consider the case of constant data $h = h_0$, so then $\nabla_\Gamma h = 0$ and $\nabla h = 0$ on $\Gamma_{\mathcal{V}^*}$.*

Simplification 2. *The above formulas can be simplified further by considering, on $\Gamma_{\mathcal{V}^*}$, $u^* = h_0$ and $\partial_n u^* = g$. These conditions are consistent with the* exact solution *of the FBP, and lead to a quasi-Newton method as in [11, 22].*

Applying the above simplifications produces the following quasi-Newton scheme: Search for $\tilde{u} \in H^1_{h,\Gamma_\mathcal{D}}(\Omega_{\mathcal{V}^*})$ and $\delta\mathcal{V} \in \Theta$ such that

$$\int_{\Omega_{\mathcal{V}^*}} \nabla\tilde{u} \cdot \nabla\varphi \,\mathrm{d}\Omega - \int_{\Gamma_{\mathcal{V}^*}} \mathcal{K}_\mathrm{H}\, \varphi\, \delta\mathcal{V} \cdot n \,\mathrm{d}\Gamma = \int_{\Omega_{\mathcal{V}^*}} f\varphi \,\mathrm{d}\Omega + \int_{\Gamma_{\mathcal{V}^*}} g\,\varphi \,\mathrm{d}\Gamma \tag{III.3.6a}$$

$$\int_{\Gamma_{\mathcal{V}^*}} \tilde{u}\, v \,\mathrm{d}\Gamma + \int_{\Gamma_{\mathcal{V}^*}} g\, v\, \delta\mathcal{V} \cdot n \,\mathrm{d}\Gamma = \int_{\Gamma_{\mathcal{V}^*}} h_0\, v \,\mathrm{d}\Gamma \tag{III.3.6b}$$

for all $(\varphi, v) \in H^1_{0,\Gamma_\mathcal{D}}(\Omega_{\mathcal{V}^*}) \times H^1_{per}(\Gamma_{\mathcal{V}^*})$.

Remark III.3.1. *The Simplification 2 above is the reason why the scheme* (III.3.6) *is not and exact Newton scheme, but only quasi-Newton method: The derivatives are not calculated in the current approximation, but rather they are an approximation of the derivatives at the exact solution. This has the consequence that* (III.3.6) *does not achieve quadratic convergence, but only superlinear.*

III.3.3 Linearisation of the very-weak formulation

We now want to derive a linearisation for (III.2.7) at an arbitrary approximated solution $(u^*, \mathcal{V}^*)$, where as before $u^* \in H^1_{per}(\Omega_{\mathcal{V}^*})$ and $\mathcal{V}^* \in \Theta$. The Gâteaux derivative of $\mathcal{N}$ at $(u^*, \mathcal{V}^*)$ with respect to u in the direction δu is given by

$$\langle\, \partial_u \mathcal{N}[u^*, \mathcal{V}^*; \varphi], \delta u \,\rangle = -\int_{\Omega_{\mathcal{V}^*}} \delta u\, \Delta\varphi \,\mathrm{d}\Omega. \tag{III.3.7}$$

The linearisation with respect to the vector field is again performed using the Hadamard formulas (III.3.1):

$$\begin{aligned}\langle\, \partial_\mathcal{V} \mathcal{N}[u^*, \mathcal{V}^*; \varphi], \delta\mathcal{V} \,\rangle = &\int_{\Gamma_{\mathcal{V}^*}} \nabla h \cdot \nabla\varphi\, \delta\mathcal{V} \cdot n \,\mathrm{d}\Gamma - \int_{\Gamma_{\mathcal{V}^*}} (u^* - h)\Delta\varphi\, \delta\mathcal{V} \cdot n \,\mathrm{d}\Gamma \\ &- \int_{\Gamma_{\mathcal{V}^*}} [\mathcal{K}_\mathrm{H}\, \varphi + g\, \partial_n\varphi]\, \delta\mathcal{V} \cdot n \,\mathrm{d}\Gamma.\end{aligned} \tag{III.3.8}$$

A Newton step at the point $(u^*, \mathcal{V}^*)$ has then the following form: Search for $\delta u \in H^1_{0,\Gamma_\mathcal{D}}(\Omega_{\mathcal{V}^*})$ and $\delta\mathcal{V} \in \Theta$ such that

$$\langle\, \partial_u \mathcal{N}[u^*, \mathcal{V}^*; \varphi], \delta u \,\rangle + \langle\, \partial_\mathcal{V} \mathcal{N}[u^*, \mathcal{V}^*; \varphi], \delta\mathcal{V} \,\rangle = -\mathcal{N}(u^*, \mathcal{V}^*; \varphi)\,, \tag{III.3.9}$$

for all $\varphi \in H^2_{0,\Gamma_\mathcal{D}}(\Omega_\mathcal{V})$.

Summing the various terms we then search for $\tilde{u} = u^* + \delta u \in H^1_{h,\Gamma_\mathcal{D}}(\Omega_{\mathcal{V}^*})$ and $\delta\mathcal{V} \in \Theta$ such that

$$\begin{aligned}&\int_{\Omega_{\mathcal{V}^*}} (h - \tilde{u})\, \Delta\varphi \,\mathrm{d}\Omega - \int_{\Gamma_{\mathcal{V}^*}} [\mathcal{K}_\mathrm{H}\varphi + g\, \partial_n\varphi + (u^* - h)\Delta\varphi]\ \delta\mathcal{V}\cdot n \,\mathrm{d}\Gamma \\ &+ \int_{\Gamma_{\mathcal{V}^*}} \nabla h \cdot \nabla\varphi\, \delta\mathcal{V}\cdot n \,\mathrm{d}\Gamma = \int_{\Gamma_{\mathcal{V}^*}} g\varphi \,\mathrm{d}\Gamma + \int_{\Omega_{\mathcal{V}^*}} f\varphi \,\mathrm{d}\Omega - \int_{\Omega_{\mathcal{V}^*}} \nabla h\cdot\nabla\varphi \,\mathrm{d}\Omega,\end{aligned} \tag{III.3.10}$$

for all $\varphi \in H^2_{0,\Gamma_\mathcal{D}}(\Omega_\mathcal{V})$.

We proceed to apply Simplifications 1 and 2, thereby obtaining the followings quasi-Newton scheme: Search for $\tilde{u} \in H^1_{h,\Gamma_\mathcal{D}}(\Omega_{\mathcal{V}^*})$ and $\delta\mathcal{V} \in \Theta$ such that

$$\begin{aligned}\int_{\Omega_{\mathcal{V}^*}} (h - \tilde{u})\, \Delta\varphi \,\mathrm{d}\Omega \ &- \int_{\Gamma_{\mathcal{V}^*}} [\mathcal{K}_\mathrm{H}\varphi + g\, \partial_n\varphi]\ \delta\mathcal{V}\cdot n \,\mathrm{d}\Gamma \\ &= \int_{\Gamma_{\mathcal{V}^*}} g\varphi \,\mathrm{d}\Gamma + \int_{\Omega_{\mathcal{V}^*}} f\varphi \,\mathrm{d}\Omega - \int_{\Omega_{\mathcal{V}^*}} \nabla h\cdot\nabla\varphi \,\mathrm{d}\Omega\,,\end{aligned} \tag{III.3.11}$$

for all $\varphi \in H^2_{0,\Gamma_\mathcal{D}}(\Omega_\mathcal{V})$.

As we pointed out above, we cannot yet employ this formulation to produce a numerical scheme; we need to extract the strong form implied by (III.3.11) and then write a new weak formulation. Using standard variational arguments one can see that such strong form is:

$$-\Delta\tilde{u} = f \qquad \text{in } \Omega_{\mathcal{V}^*} \tag{III.3.12a}$$

$$\partial\tilde{u}_n - \mathcal{K}_\mathrm{H}\, \delta\mathcal{V}\cdot n = g \qquad \text{on } \Gamma_{\mathcal{V}^*} \tag{III.3.12b}$$

$$\tilde{u} = h \qquad \text{on } \Gamma_\mathcal{D} \tag{III.3.12c}$$

$$g\, \delta\mathcal{V}\cdot n = h_0 - \tilde{u} \quad \text{on } \Gamma_{\mathcal{V}^*}. \tag{III.3.12d}$$

Thanks to the initial requirement on g not vanishing, one can solve (III.3.12d) for $\delta\mathcal{V}\cdot n$, obtaining the boundary update formula

$$\delta\mathcal{V}\cdot n = \frac{h_0 - \tilde{u}}{g}. \tag{III.3.13}$$

Substituting in (III.3.12b) and using (III.3.12a)–(III.3.12c) allows to write the new weak formulation: Search for $\tilde{u} \in H^1_{h,\Gamma_\mathcal{D}}(\Omega_{\mathcal{V}^*})$ such that

$$\int_{\Omega_{\mathcal{V}^*}} \nabla\tilde{u}\cdot\nabla\varphi \,\mathrm{d}\Omega - \int_{\Gamma_{\mathcal{V}^*}} \left(\mathcal{K}_\mathrm{H}\, \frac{h_0 - \tilde{u}}{g} + g\right)\varphi \,\mathrm{d}\Gamma = \int_{\Omega_{\mathcal{V}^*}} f\varphi \ \,\mathrm{d}\Omega, \tag{III.3.14}$$

for all $\varphi \in H^1_{0,\Gamma_\mathcal{D}}(\Omega_{\mathcal{V}^*})$.

Remark III.3.2. *Solving Equation* (III.3.6b) *for* $\delta\mathcal{V}\cdot n$ *one obtains exactly Equation* (III.3.13)*. Plugging then into Equation* (III.3.6b) *gives Equation* (III.3.14)*. This shows that the two methods, the coupled system* (III.3.6) *and the formulation* (III.3.14) *with boundary update as in* (III.3.13)*, are variationally equivalent, so we can expect the behaviours of these two approaches to be very similar. On the other hand, even though they are equivalent in an infinite-dimensional setting, the difference in the way the vector field is handled (as a coupled projection in the former case, or a splitting method in the latter case) may be reflected in the performances at the discretised level. This will indeed be the case, as our numerical tests illustrate.*

The strong form (III.3.12) will also be used in the implementation of a collocation scheme, outlined in the next section. In passing, we comment that in the case of non-constant Dirichlet data on the free boundary, from Equation (III.3.10) one could split the gradient of h in the third integral in its tangential and normal component, and apply the tangential Green's identity [4, p. 367]. See also [22] for details.

III.4 Numerical Schemes

In our numerical tests we used two Galerkin methods, one arising from (III.3.6) and one from (III.3.14). The main difference between them is that from the former one obtains a coupled method, while the latter yields a decoupled splitting method. We implemented, moreover, a collocation method to solve the strong form (III.3.12).

III.4.1 B-splines based Isogeometric analysis

This section presents the essentials of B-splines. For more details we refer the interested reader to any of the specialised books on the subject, for instance [6].

A *knot vector* is a set of non-decreasing points $\Xi = \{\xi_1 \leq \ldots \leq \xi_{n+p+1}\}$ with $\xi_i \in \mathbb{R}$ and n the number of basis functions of degree p to be built.

A knot vector is said to be *open* if its first and last knots have multiplicity $p+1$, and in this case it is customary to take $\xi_1 = 0$ and $\xi_{n+p+1} = 1$. The maximum multiplicity of each internal knot can never exceed p. A knot vector is said to be *uniform* if the knots are equispaced; in this case it is common to take $\xi_1 = -p\tau$ and $\xi_{n+p+1} = p\tau$, with τ the distance between two consecutive knots.

Univariate B-splines functions can be defined using the Cox-de Boor recursion formulas [1] as follows:

for $p = 0$:

$$\hat{\psi}_{i,0}(\xi) = \begin{cases} 1 & \xi_i \leq \xi < \xi_{i+1} \\ 0 & \text{otherwise} \end{cases}$$

for $p \geq 1$:

$$\hat{\psi}_{i,p}(\xi) = \begin{cases} \dfrac{\xi - \xi_i}{\xi_{i+p} - \xi_i}\hat{\psi}_{i,p-1}(\xi) + \dfrac{\xi_{i+p+1} - \xi}{\xi_{i+p+1} - \xi_{i+1}}\hat{\psi}_{i+1,p-1}(\xi) & \xi_i \leq \xi < \xi_{i+p+1} \\ 0 & \text{otherwise} \end{cases}$$

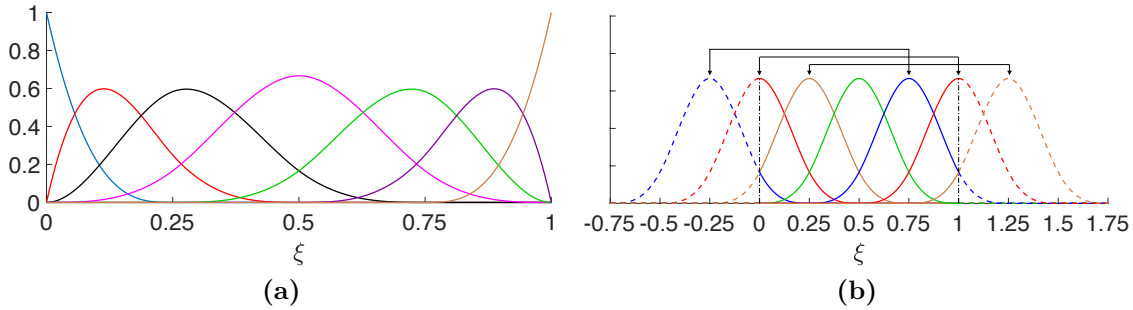

Figure III.13: Example of open and periodic B-spline basis. **(a)** Cubic basis on an open knot vector. **(b)** A periodic cubic basis on a uniform knot vector.

where we adopt the convention $0/0 = 0$. A B-spline basis function is therefore a piecewise polynomial in every knot span and at the knots it achieves regularity C^{p-l} where l is the multiplicity of the knot. We will always use internal knots of multiplicity one, in order to have maximal regularity.

We denote with $\hat{S}^p = \text{span}\{\hat{\psi}_{i,p} \mid i = 1, \dots, n\}$ the space spanned by n B-splines of degree p. We will often omit to explicitly indicate the polynomial degree. On a uniform knot vector one can in addition construct a *periodic* basis by appropriately identifying together functions laying at the beginning and at the end of the parametric domain:

$$\hat{S}^p_{per} = \text{span}\{\hat{\psi}^{per}_k\} \quad \text{with} \quad \begin{cases} \hat{\psi}^{per}_k := \hat{\psi}_k + \hat{\psi}_{n-p+k}, & k = 1, \dots, p; \\ \hat{\psi}^{per}_k = \hat{\psi}_k, & \text{otherwise} \end{cases} \tag{III.4.1}$$

Note that $\dim(\hat{S}^p_{per}) = n - p$. Figure III.13b shows an example of maximum-regularity periodic B-splines basis with degree $p = 3$.

We can derive bivariate B-splines spaces, which we indicate in boldface, simply considering the tensor product of univariate ones. Moreover, in our numerical tests we will use the same degree in each parametric direction.

Now, let $\mathbf{F} : \hat{\Omega} \to \Omega$ be a B-spline parametrisation of the physical domain Ω, and let $\hat{\mathbf{S}}^p$ be a space spanned by N bivariate B-splines $\hat{\phi}_k$ defined on the parametric domain $\hat{\Omega}$. Then, the corresponding space on Ω is defined as $\mathbf{S}^p = \text{span}\{\phi_k \mid \phi_k = \hat{\phi}_k \circ \mathbf{F}^{-1},\ k = 1, \dots, N\}$. We moreover need to introduce a bivariate spline space spanned by functions periodic in x, that we denote $\mathbf{S}^p_{per}$. This space is defined as the push-forward through the geometrical map $\mathbf{F}$ of the cross product between the periodic space $\hat{S}^p_{per}$, and the space $\hat{S}^p$ built from an open knot vector.

III.4.2 Isogeometric Galerkin methods

In both Galerkin-based schemes we choose as a trial space for $\tilde{u}$

$$\mathbf{V}^p_h := \mathbf{S}^p_{per} \cap H^1_{h,\Gamma_\mathcal{D}}(\Omega_{\mathcal{V}^*}), \tag{III.4.2}$$

while as test space

$$\mathbf{V}^p_0 := \mathbf{S}^p_{per} \cap H^1_{0,\Gamma_\mathcal{D}}(\Omega_{\mathcal{V}^*}). \tag{III.4.3}$$

The structure of the two algorithms is illustrated below.

Algorithm 1 - Coupled Galerkin scheme

1: Choose the starting $\mathcal{V}_0$,
2: Given $\mathcal{V}_k$, compute $(\tilde{u}_k, \delta\mathcal{V} \cdot n_k)$ solution of (III.3.6) in the domain $\Omega_{\mathcal{V}_k}$,
3: Update the free boundary with $\mathcal{V}_{k+1} = \mathcal{V}_k + (\delta\mathcal{V} \cdot n_k)m_k$,
4: Repeat steps 2–3 until $\|\delta\mathcal{V} \cdot n_k\| \leq \text{tol}$.

Algorithm 2 - Decoupled (splitting) Galerkin scheme

1: Choose the starting $\mathcal{V}_0$,
2: Given $\mathcal{V}_k$, compute $\tilde{u}_k$ solution of (III.3.14) in the domain $\Omega_{\mathcal{V}_k}$,
3: Compute $\delta\mathcal{V} \cdot n_k$ from (III.3.13),
4: Update the free boundary with $\mathcal{V}_{k+1} = \mathcal{V}_k + (\delta\mathcal{V} \cdot n_k)m_k$,
5: Repeat steps 2–4 until $\|\delta\mathcal{V} \cdot n_k\| \leq \text{tol}$.

The vector field $m_k : \Gamma_{\mathcal{V}_k} \to \mathbb{R}$ represents the direction in which the update of the free boundary is performed, and has to satisfy $m_k \cdot n_k = 1$. In our tests we choose to perform a vertical update, therefore selecting $m_k = [0,\, 1/(n_k)_y]$. This choice allows to consider as unknown $\delta\mathcal{V} \cdot n$ instead of $\delta\mathcal{V}$, which permits to discretise (III.3.6b) and (III.3.13) directly, using S^p_{per} as both the test and trial space. A choice of $m_k = n_k$ in the algorithms would instead amount to performing the update in the direction normal to the boundary.

Remark III.4.1. *It is important to realise that when performing the update with Equation* (III.3.13) *one has to divide two spline functions. The resulting function is therefore, in general, not a spline, and a projection onto the appropriate spline space is then required. In our tests we treated this by means of an L^2 projection into the space defined by the boundary test functions. After each boundary update, the internal mesh is then fitted using a Coons interpolation technique.*

III.4.3 Isogeometric collocation method

The isogeometric collocation method presented here is built from (III.3.12): We solve (III.3.12d) for $\delta\mathcal{V} \cdot n$ and replace its value in (III.3.12b), obtaining the following:

$$-\Delta\tilde{u} = f \qquad \text{in } \Omega, \tag{III.4.4a}$$

$$\nabla\tilde{u} \cdot n - (\partial_n g + \mathrm{H}\, g + f)\, \frac{h_0 - \tilde{u}}{g} = g \qquad \text{on } \Gamma_{\mathcal{V}}, \tag{III.4.4b}$$

$$\tilde{u} = h \qquad \text{on } \Gamma_{\mathcal{D}}, \tag{III.4.4c}$$

$$\delta\mathcal{V} \cdot n = \frac{h_0 - \tilde{u}}{g} \qquad \text{on } \Gamma_{\mathcal{V}}. \tag{III.4.4d}$$

The structure of this algorithm is summarised below.

Algorithm 3 - Collocation scheme

1: Choose the starting $\mathcal{V}_0$,
2: Given $\mathcal{V}_k$, compute $\tilde{u}_k$, collocated solution of (III.4.4a)–(III.4.4c),
3: Compute $\delta\mathcal{V} \cdot n_k$ from (III.4.4d),
4: Update the free boundary with $\mathcal{V}^{(k+1)} = \mathcal{V}^{(k)} + (\delta\mathcal{V} \cdot n_k)m_k$,
5: Repeat steps 2–4 until $\|\delta\mathcal{V} \cdot n_k\| \leq$ tol.

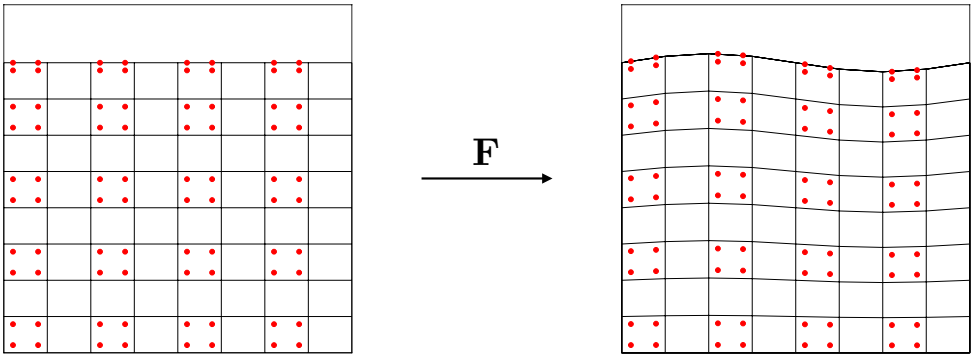

Figure III.14: CSP collocation points in the parametric and in the physical domain. The points are the cross product of the periodic CSP points in the x-direction and the Dirichlet CSP points in the y-direction.

The solution of (III.4.4a)–(III.4.4c) and the boundary update (III.4.4d) are performed using a collocation approach. Given the finite dimensional spaces $\mathbf{V}_h^p$ and S_{per}^p in which we search for a solution $(\tilde{u}, \delta\mathcal{V} \cdot n)$, the idea is to accurately choose a number of points $\tau_1, \ldots, \tau_n \in \Omega$, called *collocation points*, where n is the number of degrees of freedom of the problem, and enforce the equations to hold strongly at those points.

The appropriate selection of collocation points is crucial for the rate of convergence. Most of the classical choices of collocation points, for example, return suboptimal convergence rate even in a Poisson problem, contrary to the Galerkin approach which is optimal [15]. However, the recent work [13] suggests the use of a particular subset of Galerkin-superconvergent points, called clustered superconvergent points (CSP), as collocation points. This choice, that is the one that we adopt here, succeeds in achieving optimality for at least odd degrees B-splines discretisations. In particular, the collocation points we use for the periodic problem (III.4.4) are obtained by taking the cross product between univariate periodic CSP and univariate Dirichlet CSP (see [13] for more details). In our tests we however included also problems with only Dirichlet boundary conditions. In that case the collocation points are selected as the push-forward of the cross-product of the univariate Dirichlet CSP points in the two parametric directions. Figure III.14 shows an example of CSP points in both the parametric and physical domain. Note that we do not take any collocation points on the boundary $\{y = 0\}$, because we enforce the Dirichlet boundary conditions in the finite dimensional space that we consider, cf. (III.4.2).

Similarly, the free boundary update is performed by collocating equation (III.4.4d) in the univariate periodic CSP, producing a fully-collocated scheme for problem (III.4.4).

III.5 Numerical Results

This section collects our numerical results. All algorithms have been implemented in Matlab using the GeoPDEs suite. GeoPDEs is an Octave/Matlab software package for isogeometric analysis of partial differential equations [20]. We applied the above Algorithms 1, 2, and 3 to different types of problems with either Dirichlet or periodic boundary conditions on the vertical sides. It is clear that the error quantities in the problem are driven by the position of the free boundary: If the computed boundary matches the exact boundary solution, then the error on the internal function u is simply the standard finite elements (IGA) or collocation approximation error. For this reason, when evaluating the performance of the algorithms we have chosen the error quantities of interest to be the *Dirichlet error*, $\|\tilde{u}(\Gamma_{\mathcal{V}}) - h_0\|_{L^2}$, the error the computed function u commits in satisfying the Dirichlet condition on the free boundary, and the *surface position error*, $\|\Gamma_{\mathcal{V}} - \Gamma_{ex}\|_{L^2}$, the error in the position of the computed free surface.

III.5.1 Test 1: Parabolic boundary, Dirichlet b.c.

This problem is constructed from the exact solution

$$u_{ex}(x,y) = \frac{y}{1+\alpha(x)} + \alpha(x)\,\frac{y}{1+\alpha(x)}\left(1 - \frac{y}{1+\alpha(x)}\right) \tag{III.5.1}$$

with

$$\alpha(x) = \frac{1}{4}\,x\,(1-x).$$

The solution u_{ex} attains constant value $u_{ex}|_{\Gamma_{\mathcal{V}}} = 1$ on the *parabolic curve* given by $\Gamma_{ex} = \{(x,y) \mid y = 1+\alpha(x),\, 0 \leqslant x \leqslant 1\}$, which is therefore the exact free-boundary solution of the problem.

The data for problem (III.2.1) are then found as follows:

$$\begin{aligned} f &= -\Delta u_{ex}, \\ g &= \nabla u_{ex} \cdot \left(\tfrac{1}{2}\,x - \tfrac{1}{4}, 1\right) / \sqrt{1 + \left(\tfrac{1}{2}\,x - \tfrac{1}{4}\right)^2}. \end{aligned}$$

We cast this problem with complete Dirichlet boundary conditions. This amounts to imposing $h_0 = 1$ on the free boundary and $h = y$ on $\Gamma_{\mathcal{D}} \cup \Gamma_{\mathcal{P}}$. We start our algorithms with $\Gamma_0 = \{y = 1,\, 0 \leqslant x \leqslant 1\}$ as an initial guess for the boundary.

Figure III.15 shows the first three iterations of the boundary update, together with the exact boundary solution, performed with a mesh with only 1 element and quadratic basis functions. Those iterations have in particular been performed with Algorithm 2, but Algorithm 1 and Algorithm 3 yielded identical results. Figure III.16 shows the convergence history of Algorithm 2 for both the Dirichlet error and the surface position error for various mesh sizes, using a quadratic basis.

Figure III.17 instead shows a comparison of the three different approaches using cubic basis functions. The error plots show that Algorithm 1 improves the convergence speed once the solution is close enough. The same behaviour is present also in the collocated scheme, Algorithm 3, albeit to a less degree, while it is not that apparent in Algorithm 2.

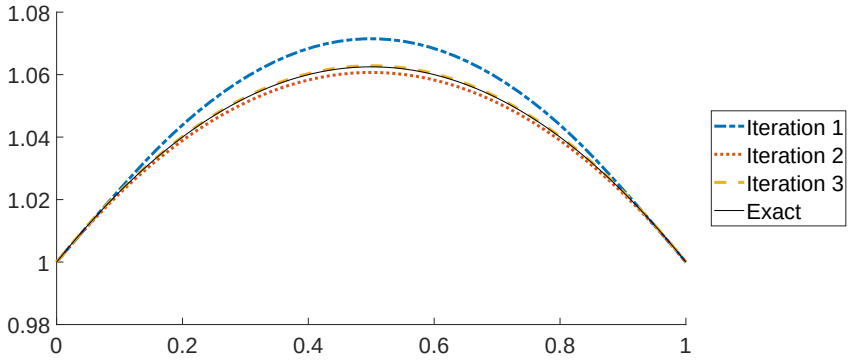

Figure III.15: The first three iterations of Algorithm 2 for the Test 1 case, using a one element mesh and quadratic basis starting from a flat boundary with $y = 1$.

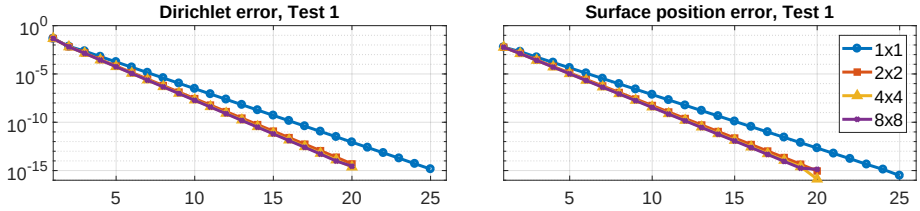

Figure III.16: Error quantities for Algorithm 2, with a quadratic basis, on various mesh sizes. **(Left)** The Dirichlet error $\|\tilde{u}(\Gamma_{\mathcal{V}}) - h\|_{L^2}$ as a function of the iterations. **(Right)** The surface position error $\|\Gamma_{\mathcal{V}} - \Gamma_{ex}\|_{L^2}$. Machine precision is achieved for any mesh size.

However, all three algorithms' performances are quite similar on this test problem. When it comes to runtime, Algorithm 3 is much faster per iteration than the two Galerkin approaches, which is expected of a collocation scheme.

Note that this is the same setting as the "Testcase I: Parabolic Free-Boundary" presented in [22, Section 5.2]. However, in contrast to the results presented there we do not see a plateau in the error quantities, and machine precision is reached for any mesh size because the exact free boundary curve Γ_{ex} and the exact solution u_{ex} restricted to Γ_{ex} belong to the discrete space of the numerical approximation.

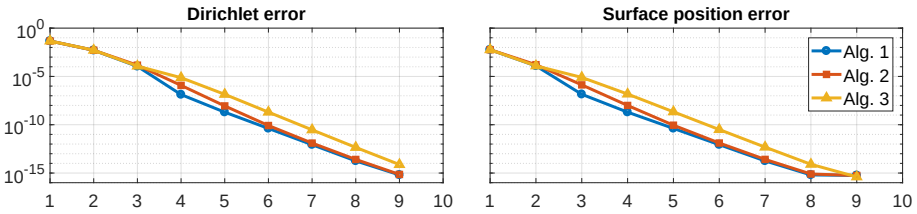

(a) Mesh 8x8

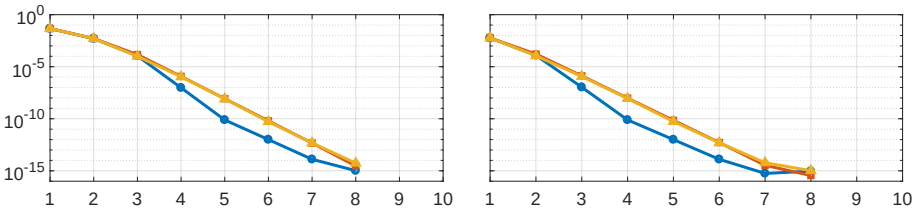

(b) Mesh 16x16

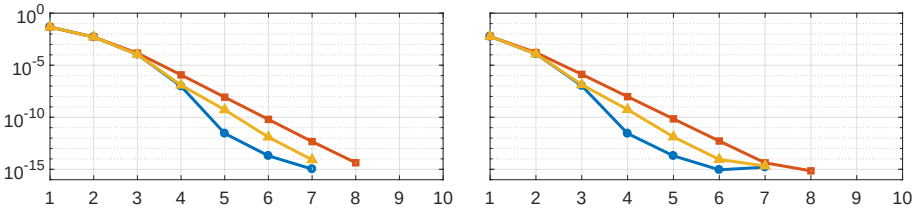

(c) Mesh 32x32

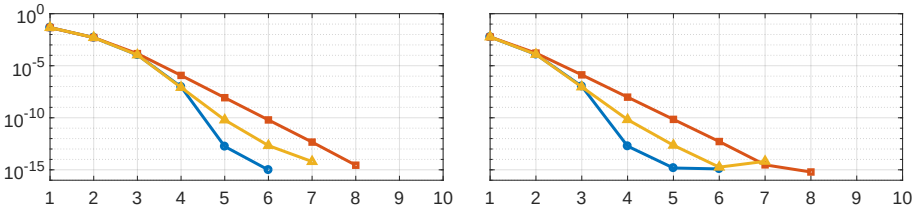

(d) Mesh 64x64

Figure III.17: A comparison of the three algorithms on Test 1 for different mesh sizes with cubic basis functions.

III.5.2 Test 2: Sinusoidal boundary, Dirichlet b.c.

We now give an example where a plateau in the error is to be expected, and is actually found. The problem data is derived as for Test 1 with an exact solution given by Equation (III.5.1) but with

$$\alpha_{ex}(x) = \frac{1}{16}\sin(2\pi x),$$

so that the exact boundary $\Gamma_{ex} = \{(x, y) \mid y = 1 + \alpha(x),\ 0 \leqslant x \leqslant 1\}$ is now a sinusoidal curve. The boundary conditions are maintained of Dirichlet type, with $h_0 = 1$ on the free boundary, and $h = y$ on $\Gamma_{\mathcal{D}} \cup \Gamma_{\mathcal{P}}$. Figure III.18 shows the first three boundary updates performed by Algorithm 3. The mesh is made of 8 elements, and the basis is cubic. The initial boundary is again taken as the flat curve $\Gamma_0 = \{y = 1,\ 0 \leqslant x \leqslant 1\}$

Figure III.19 shows the error quantities vs iterations for the three algorithms.

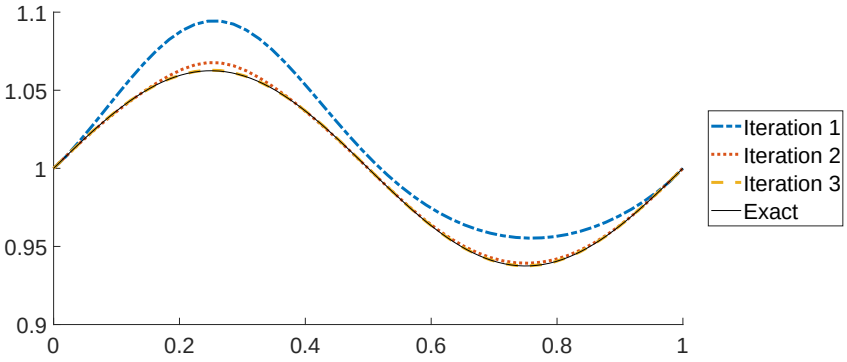

Figure III.18: The first three iterations of Algorithm 3 for the Test 2 case, with sinusoidal boundary and Dirichlet conditions, with an 8 elements mesh and cubic basis. Starting from a flat boundary with $y = 1$.

As the mesh is refined we note that the collocation algorithm, Algorithm 3, has a slightly higher error than the other two approaches. The surface position error, moreover, is abated with finer meshes in all approaches but remains always present. This is due to the fact that a cubic B-spline cannot exactly represent a sinusoidal curve, and therefore the exact free boundary solution to this problems lies outside of the trial function space. Lastly, Figure III.19 shows how closely related Algorithms 1 and 2 are, achieving almost identical performance on this benchmark test.

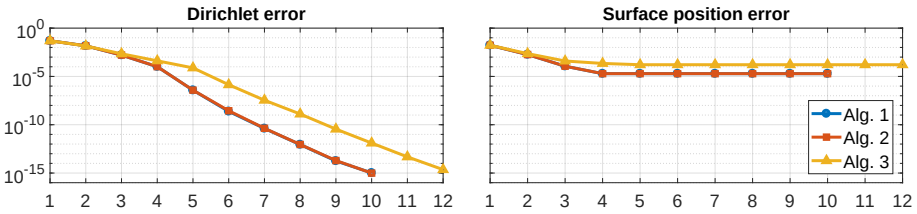

(a) Mesh 8x8

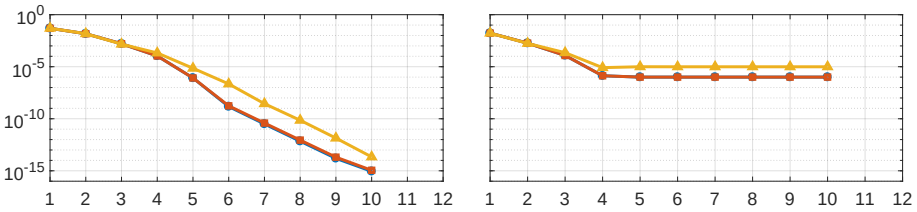

(b) Mesh 16x16

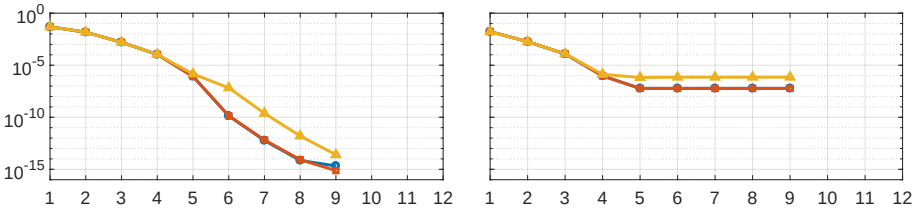

(c) Mesh 32x32

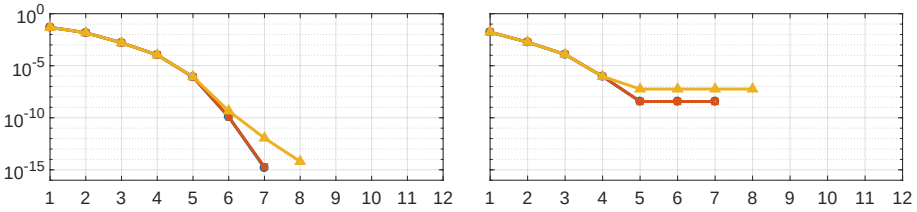

(d) Mesh 64x64

Figure III.19: A comparison of the three algorithms on Test 2 for different mesh sizes with cubic basis functions.

III.5.3 Test 3: Sinusoidal boundary, periodic b.c.

In our third benchmark we employ the same problem data as in Test 2, but now periodic boundary conditions are placed on the lateral sides instead of Dirichlet ones. In this test case we used the highest-possible regularity for the periodic conditions, meaning that the boundary functions are "glued" together with C^{p-1} continuity.

The introduction of the periodic conditions affects the behaviour of the three quasi-Newton schemes, but not dramatically. As shown in Figure III.20, the algorithms require a couple extra iterations to reach the tolerance respect to the Dirichlet boundary condition case. The convergence of the surface position error is also a bit rougher than in the previous cases. However, the relative performances are not at all affected, and all three algorithms are still comparable. As before Algorithms 1 and 2 display essentially equal

results. In this test we kept the same choice for the initial guess for the free boundary: The flat curve $\Gamma_0 = \{y = 1,\ 0 \leqslant x \leqslant 1\}$.

Since the position of the exact free boundary does not lie in the trial functions space formed by the cubic B-splines basis, as in Test 2 a plateau is always reached, even though the level of the plateau is lowered with finer meshes.

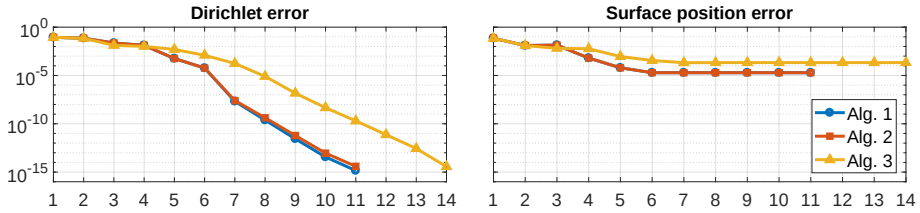

(a) Mesh 8x8

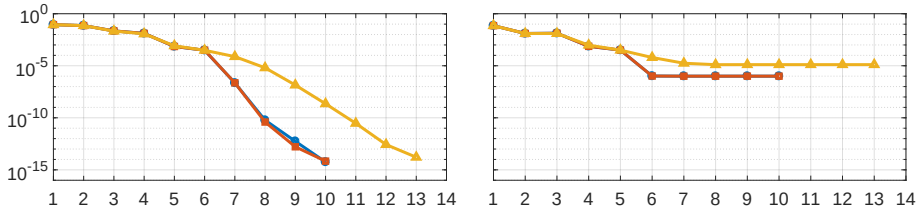

(b) Mesh 16x16

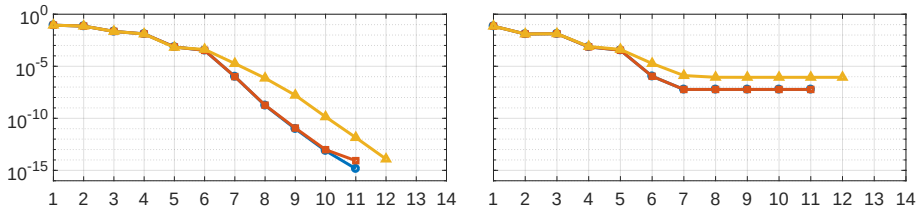

(c) Mesh 32x32

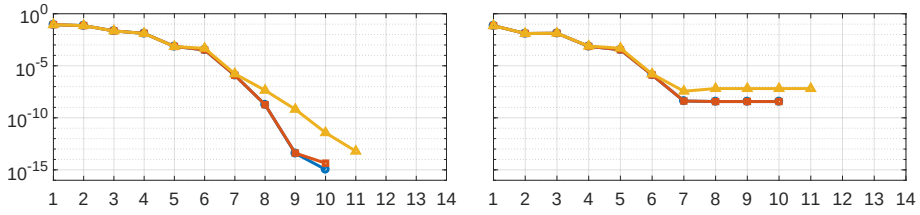

(d) Mesh 64x64

Figure III.20: A comparison of the three algorithms on Test 3 for different mesh sizes with cubic basis functions.

III.6 Conclusions

In this work we presented three different isogeometric-based algorithms for free boundary problems: Two follow a Galerkin approach and are an extension or modification of previously existing works, while one is a novel fully collocated scheme. The dependence

on the unknown geometry of the domain is handled through shape calculus, which results in a quasi-Newton method to be underlying the update strategy of the free boundary position. While our interests in such algorithms is motivated by future applications, in the present paper we focused on giving a clear description of the implementation and numerical aspects.

We applied and compared the three algorithms to benchmark tests, with either Dirichlet or periodic boundary conditions on the lateral vertical sides of the domain. The results show that, while having slight variations, the performances of all three algorithms are qualitatively comparable, and each of them converged to the correct solution of the problem.

The treatment of free boundary problems is computationally intense, especially in more complex problems. For this reason the efficiency and speed of the algorithm is an important feature that needs to be taken into account. In this respect, even if the collocated algorithm appeared to have slightly worse accuracy and sometimes required one or two extra iterations to reach the convergence tolerance, it proved to significantly outmatch the two Galerkin-based schemes on runtime, requiring in general less than half the time to complete the benchmarks.

Our future aim is now to apply the algorithms developed here to the resolution of the bifurcation branches of the Euler equations. That problem presents several challenges due to the greater complexity of the equations and the intrinsic non-uniqueness of solutions at the bifurcation points, therefore both efficiency and precision are expected to play an important role.

III.7 Acknowledgements

MM and GS were partially supported by the European Research Council through the FP7 Ideas Consolidator Grant *HIGEOM* n.616563. FR was supported by grants no. 231668 and 250070 from the Norwegian Research Council. This support is gratefully acknowledged. MM and GS are members of the INdAM Research group GNCS.

References

[1] C. de Boor. *A practical guide to splines*. New York: Springer-Verlag, 2001.

[2] J.A. Cottrell, T.J.R. Hughes, and Y. Bazilevs. *Isogeometric Analysis, Toward Integration of CAD and FEA*. Wiley, 2009.

[3] Robert A Dalrymple. "A numerical model for periodic finite amplitude waves on a rotational fluid". In: *Journal of Computational Physics* 24.1 (1977), pp. 29–42.

[4] M.C. Delfour and J.P. Zolésio. *Shapes and Geometries: Metrics, analysis, differential calculus, and optimization*. Society for Industrial and Applied Mathematics (SIAM), Philadelphia, PA, 2011.

[5] M. Ehrnström, J. Escher, and E. Wahlén. "Steady Water Waves with Multiple Critical Layers". In: *SIAM J. Math. Anal.* 43.3 (2011), pp. 1436–1456.

[6] G. Farin. *Curves and Surfaces for CAGD*. Academic Press, 1990.

[7] Hector Gomez and Laura De Lorenzis. "The variational collocation method". In: *Computer Methods in Applied Mechanics and Engineering* 309 (2016), pp. 152–181.

[8] Mark D Groves. "Steady water waves". In: *Journal of Nonlinear Mathematical Physics* 11.4 (2004), pp. 435–460.

[9] Thomas JR Hughes, John A Cottrell, and Yuri Bazilevs. "Isogeometric analysis: CAD, finite elements, NURBS, exact geometry and mesh refinement". In: *Computer methods in applied mechanics and engineering* 194.39-41 (2005), pp. 4135–4195.

[10] E. H. Van Brummelen K. g. Van der Zee and R. de Borst. "Goal-oriented error estimation and adaptivity for free-boundary problems: the shape-linearization approach". In: *SIAM J. Sci. Comput* 32.2 (2010), pp. 1093–1118.

[11] K. T. Kärkkäinen and T. Tiihonen. "Free surfaces: Shape sensitivity analysis and numerical methods". In: *International Journal for Numerical Methods in Engineering* 44 (1999), pp. 1079–1098.

[12] K. T. Kärkkäinen and T. Tiihonen. "Shape calculus and free boundary problems". In: *European Congress on Computational Methods in Applied Sciences and Engineering ECCOMAS*. 2004.

[13] M. Montardini, G. Sangalli, and L. Tamellini. "Optimal-order isogeometric collocation at Galerkin superconvergent points". In: *Comput. Methods Appl. Mech. Engrg.* 316 (2017), pp. 741–757.

[14] C. H. Rycroft and J. Wilkening. "Computation of three-dimensional standing water waves". In: *Journal of Computational Physics* 255 (2013), pp. 612–638.

[15] D. Schillinger, J. A. Evans, A. Reali, M. A. Scott, and J.R. Hughes. "Isogeometric Collocation: Cost Comparison with Galerkin Methods and Extension to Adaptive Hierarchical NURBS Discretizations". In: *Comput. Methods Appl. Mech. Engrg.* 267 (2013), pp. 170–232.

[16] J. A. Simmen and P. G. Saffman. "Steady Deep-Water Waves on a Linear Shear Current". In: *Studies in Applied Mathematics* 73.1 (1985), pp. 35–57.

[17] J. Sokolowski and J.P. Zolésio. *Introduction to shape optimization: shape sensitivity analysis*. Springer, Berlin: Springer series in computational mathematics, 1992.

[18] J. F. Toland. "Stokes waves". In: *Topological Methods in Nonlinear Analysis* 7.1 (1996), pp. 1–48.

[19] J.-M. Vanden-Broeck. *Gravity-Capillary Free-Surface Flows*. Cambridge University Press, 2010.

[20] R. Vázquez. "A new design for the implementation of isogeometric analysis in Octave and Matlab: GeoPDEs 3.0". In: *Computers & Mathematics with Applications* 72.3 (2016), pp. 523–554.

[21] E. Wahlén. "Steady water waves with a critical layer". In: *Journal of Differential Equations* 246.6 (2009), pp. 2468–2483.

[22] K.G. van der Zee, G.J. van Zwieten, C.V. Verhoosel, and E.H. van Brummelen. "Shape-Newton Method for Isogeometric Discretization of Free-Boundary Problems". In: *MARINE 2011, IV International Conference on Computational Methods in Marine Engineering : selected papers : part III*. Springer, 2013, pp. 85–102.

The thing that doesn't fit is the thing that's the most interesting: the part that doesn't go according to what you expected.

Richard P. Feynman

A

Historical Notes

Historical Notes

A.1 On some history of Water Waves: From a solitary wave to the Whitham Equation

In this section I will give a brief overview of the main steps that lead to the Whitham equation. Being very aware of my own gaps when it comes to History in general, I am not claiming that what follows is a precise list of all the important facts that surrounded the development of the field in general, or even the Whitham equation in particular. However, I think it is a fascinating story that not many other equations have, and as such it deserves a space in this thesis; if anything, at least to encourage any future masters student reading it to continue on the path of Science.

A.1.1 A chance encounter with a peculiar wave

The first encounter of John Scott Russell with what will later be knows as the *solitary wave* has been recorded many times in several works on the subject of water waves, so I will not dwell too much on the details. The interested reader is invited to take vision of Russell's original report, *On Waves*, [7].

John Scott Russell was a Scottish engineer, specialised in naval architecture and ship building. In August 1834 he was strolling on his horse along the Union Canal, a canal in Scotland connecting Falkirk to Edinburgh, following a boat that was being pulled forward by a pair of horses. An obstacle suddenly stopped the boat in its course, and the heap of water accumulated on the front of the hull started rolling forward, as a wave. Russell immediately noticed and was puzzled by the phenomenon, which he described as *"a large solitary elevation, a rounded, smooth and well-defined heap of water, which continued its course along the channel apparently without change of form or diminution of speed."*. He kept following the wave, which after some time began losing its height until eventually disappearing in the channel, about three kilometres ahead of the starting point.

From the description we find three notable features to what Russell called *the great wave of translation*: It preserved its shape, its speed, and was a single, solitary bump. Russell then built his own wave tank to experiment with the creation of such waves, and

described these experiments, together with his first encounter with the solitary wave, in his today well known report [7] in 1845. However, his work has initially not been met very positively; his descriptions were in contrast to the available mathematical theory, which predicted waves to be periodic and to either vanish, i.e. diminish in height, or steepen at the top and break. Two of the most well known opponents to Russell were Sir George Biddell Airy and Sir George Gabriel Stokes.

A.1.2 Airy and Stokes on Russell's wave

Sir G.B. Airy was a British mathematician and astronomer which at that time was considered perhaps the best authority on the subject of waves[1] [6]. In his treatise *Tides and Waves* [1] in 1845, while still recognising the importance of the experimental works of Russell, in particular saying *"They* [Russell's experiments] *constitute, upon the whole, the most important body of experimental information in regard to the motion of Waves which we possess."* and praising Russell's ingenious measurements techniques, Airy first rejects the importance of the discovery, stating that the phenomenon of a solitary wave was already predicted by his (Airy's) linear theory[2], and then says that such a wave would have to disperse in its basic components, consequently losing height[3].

Sir George Gabriel Stokes was an Irish physicist and mathematician who produced important results in several fields in Science. Among his outstanding contributions are the famous Navier-Stokes equation, which is regarded as *the* equation describing fluid flows, listed in the Millennium Prize Problems[4], and the equally famous Stokes' theorem in vector calculus. In his report to the British Association in 1846 [9], Stokes is more hesitant than Airy in judging the results on the solitary wave. He points out that *"the laws of the motion of a solitary wave, deduced by Mr. Green from the theory of long waves, agree with the observations of Mr. Russell"* but warns that this was done considering infinitely-long waves, and that when one tries to take the finite-length of Russell's wave into consideration, the problem becomes exceedingly difficult, and its solution has been attempted through the use of discontinuous functions, which are physically not justified. Stokes further notes a work by Earnshaw and comments that *"it turns out that the motion is possible, as far as the wave itself is concerned [...] the formula for the velocity of propagation of the positive wave, at which Mr. Earnshaw has arrived, agrees very well with the experiments of Mr. Russell; the formula for the negative wave also agrees, but not so closely"* but further remarks that *"However, in order that the motion in question should actually take place, it is necessary that there should be an instantaneous generation or destruction of a finite velocity, and likewise an abrupt change of pressure, [...] both of which are evidently impossible."*. In the final part of the paragraph dedicated to the

[1] Among his many achievements is also the decision of Greenwich as the zeroth-meridian.

[2] *"We are not disposed to recognize this wave as deserving the epithets "great" or "primary", and we conceive that, ever since it was known that the theory of shallow waves of great length was contained in the equation* $\frac{d^2X}{dt^2} = gk\frac{d^2X}{dx^2}$*, [...] the theory of the solitary wave has been perfectly well known."*

[3] *"The wave, therefore, would tend to split into several waves, each of which would move with its own velocity; and this appears to have happened in some instances (rejected in Mr. Russell's table of results)."*

[4] The Millennium Prize Problems are seven problems selected by the Clay Mathematics Institute as some of the major challenges in Science; the solution of each of which is rewarded with $1 million.

solitary wave, Stokes cautiously concludes with *"It is the opinion of Mr. Russell that the solitary wave is a phænomenon sui generis, in nowise deriving its character from the circumstances of the generation of the wave. His experiments seem to render this conclusion probable. Should it be correct, the analytical character of the solitary wave remains to be discovered."*, letting transpire that he expects further analyses to eventually confirm Russell's results. However, shortly after, in 1847, Stokes publishes the report *On the Theory of Oscillatory Waves* [8] where he considers nonlinear waves approximation. There he shows that the velocity of the wave is independent of the height (as observed by Russell) only up to a second order approximation, but not to a third order[5]. In particular, he concludes that the only wave with the property of being propagated at constant speed and without changing shape must be infinitely-periodic and of the form

$$y = a\cos(mx) - Ka^2\cos(2mx),$$

so that *"a solitary wave cannot be propagated in this manner."*.

At this point then, Russell's claims were dismissed by Airy on the basis of linear theory, and by Stokes on the basis of nonlinear theory. Few would have guessed that it is exactly the balanced interplay of linear and nonlinear effects that allows for the existence of a solitary travelling wave.

A.1.3 Boussinesq and Rayleigh on Russell's wave

It was only a few years later, at the beginnings of 1870, that important mathematical results were generated in favour of Russell, in particular by Boussinesq and Rayleigh.

Joseph Valentin Boussinesq, a French mathematician, made important contributions to the theory of hydrodynamics, elasticity and heat. His interest in the solitary wave was first shown in the works [2, 4], where he develops much of his theory for the movement of fluids in a rectangular channel. In particular, in [4] is the first explicit appearance of the famous Boussinesq equation, on which his analysis is based. In those works Boussinesq confirms some of the earlier formulas which Russell derived experimentally, with particular regard to the speed of the wave, but it is only in the much more extensive work [3], expanding on the previous two papers, that he calculates the profile of the wave, deriving the sech^2 shape and the corresponding speed in accordance to the results of Russell.

Lord John William Strutt Rayleigh was an English physicist and former student of Stokes. Together with William Ramsey he discovered the element *Argon*, which made him win the Nobel prize in Physics in 1904, and is moreover known for several phenomena that now bring his name, like Rayleigh waves, Rayleigh scattering, and Rayleigh flows. In his paper *On Waves* [6], in 1876, he first starts by recalling and acknowledging the objections of Airy and Stokes, but then on the basis of his analysis firmly supports Russell, confirming, as Boussinesq before him, the sech^2 shape and the formula for the velocity: *"The velocity of propagation is given by* [Formula] *(H), which is Scott Russell's formula exactly. In words, the velocity of the wave is that due to half the greatest depth of the water."*. Furthermore, Rayleigh concludes the section dedicated to the solitary wave with an explanation of another of the features noted by Russell in his experiments, namely that

[5] That work also contains initial investigations of what will later become known as *Stokes' drift*.

the wave breaks at a certain height: *"When the wave is treated as stationary, it is evident from the dynamics that its height can never exceed that due to the velocity of the stream in the undisturbed part; [...] When the wave is on the point of breaking, the water at the crest is moving with the velocity of the wave."*. In this last sentence we can recognise the description of what is called a *point of stagnation*.

A.1.4 Korteweg and de Vries

Even if Rayleigh certainly supports Russell's work, it must have seemed to Diederik Korteweg, one of the most well known Dutch mathematicians, and his PhD student Gustav de Vries, that such support was not definite enough, as they open their famous 1895 paper [5] in the following way: *"In such excellent treatises on hydrodynamics as those of Lamb and Basset, we find that even when friction is neglected long waves in a rectangular canal must necessarily change their form as they advance [...]. Yet, since the investigations of Boussinesq, Lord Rayleigh, and St. Venant on the solitary wave, there has been some cause to doubt the truth of this assertion. Indeed, if the reasons adduced were really decisive, it is difficult to see why the solitary wave should make an exception; but even Lord Rayleigh and McCowan, who have successfully and thoroughly treated the theory of this wave, do not directly contradict the statement in question. They are, as it seems to us, inclined to the opinion that the solitary wave is stationary only to a certain approximation. It is the desire to settle this question definitively which has led us into the somewhat tedious calculations which are to be found at the end of our paper."*. This was the motivation behind their work: To finally refute Airy's opinion that waves had to change shape when travelling, and to ultimately prove that Russell's description was accurate. In their paper what would later be known as *the KdV equation* received relatively little attention.

All things considered, the curiosity of a single man sparked a debate that included some of the most prominent mathematician of those times, leading to the creation of new scientific knowledge over an arc of sixty years.

References

[1] G.B. Airy. "Tides and Waves". In: *Encyclopaedia Metropolitana*. Vol. 5. William Clowes and Sons, 1845, pp. 241–396.

[2] J. Boussinesq. "Théorie de l'intumescence liquide appelée "onde solitaire" ou "de translation", se propageant dans un canal rectangulaire". In: *Comptes Rendus de l'Acadèmie des Sciences* 72 (1871), pp. 755–759.

[3] J. Boussinesq. "Théorie des ondes et des remous qui se propagent le long d'un canal rectangulaire horizontal, en communiquant au liquide contenu dans ce canal des vitesses sensiblement pareilles de la surface au fond". In: *J. de Mathématiques Pures et Appliquées* (1872), pp. 55–108.

[4] J. Boussinesq. "Théorie générale des mouvements, qui sont propagés dans un canal rectangulaire horizontal". In: *Comptes Rendus Acad. Sci.* 73 (1871), pp. 256–260.

[5] D. J. Korteweg and G. de Vries. "On the change of form of long waves advancing in a rectangular canal, and on a new type of long stationary waves". In: *Philosophical Magazine*. 5th ser. 39.240 (1895), pp. 422–443.

[6] Lord Rayleigh. "On Waves". In: *Phil. Mag. and J. of Science* 1.4 (1876), pp. 257–279.

[7] J.S. Russell. *Report on Waves*. Report of the Fourteenth Meeting of the British Association for the Advancement of Science. John Murray, London, 1845, pp. 311–391.

[8] G.G. Stokes. "On the Theory of Oscillatory Waves". In: *Transactions of the Cambridge Philosophical Society* 8 (1847), pp. 441–455.

[9] G.G. Stokes. "Report on Recent Researches in Hydrodynamics". In: *Report of the 16th Meetings of the British Association for the Advancement of Sciences* (1846), pp. 1–20.